EPRI | ELECTRIC POWER RESEARCH INSTITUTE

BWRVIP-194NP: BWR Vessel and Internals Project

Methodologies for Demonstrating Steam Dryer Integrity for Power Uprate

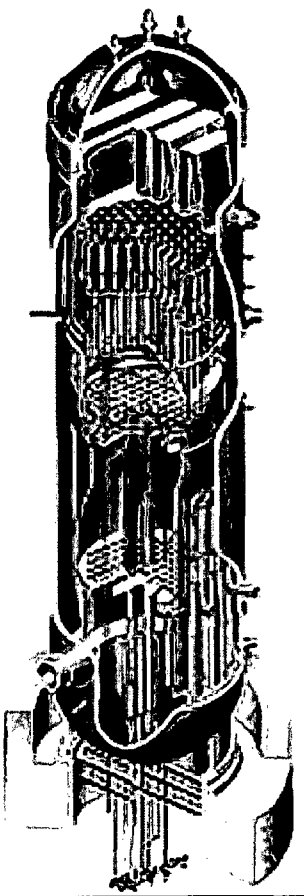

NON-PROPRIETARY INFORMATION

NOTICE: This report contains the non-proprietary information that is included in the proprietary version of this report. The proprietary version of this report contains proprietary information that is the intellectual property of BWRVIP utility members, EPRI, and Continuum Dynamics, Inc. (C.D.I.) Accordingly, the proprietary report is available only under license from C.D.I. and may not be reproduced or disclosed, wholly or in part, by any Licensee to any other person or organization.

BWRVIP-194NP: BWR Vessel and Internals Project

Methodologies for Demonstrating Steam Dryer Integrity for Power Uprate

1016578NP

Final Report, October 2008

EPRI Project Manager
J. Hosler

ELECTRIC POWER RESEARCH INSTITUTE
3420 Hillview Avenue, Palo Alto, California 94304-1338 • PO Box 10412, Palo Alto, California 94303-0813 • USA
800.313.3774 • 650.855.2121 • askepri@epri.com • www.epri.com

DISCLAIMER OF WARRANTIES AND LIMITATION OF LIABILITIES

THIS DOCUMENT WAS PREPARED BY THE ORGANIZATION(S) NAMED BELOW AS AN ACCOUNT OF WORK SPONSORED OR COSPONSORED BY THE BWR VESSEL AND INTERNALS PROJECT (BWRVIP) AND ELECTRIC POWER RESEARCH INSTITUTE, INC. (EPRI). NEITHER BWRVIP, EPRI, ANY MEMBER OF EPRI, ANY COSPONSOR, THE ORGANIZATION(S) BELOW, NOR ANY PERSON ACTING ON BEHALF OF ANY OF THEM:

(A) MAKES ANY WARRANTY OR REPRESENTATION WHATSOEVER, EXPRESS OR IMPLIED, (I) WITH RESPECT TO THE USE OF ANY INFORMATION, APPARATUS, METHOD, PROCESS, OR SIMILAR ITEM DISCLOSED IN THIS DOCUMENT, INCLUDING MERCHANTABILITY AND FITNESS FOR A PARTICULAR PURPOSE, OR (II) THAT SUCH USE DOES NOT INFRINGE ON OR INTERFERE WITH PRIVATELY OWNED RIGHTS, INCLUDING ANY PARTY'S INTELLECTUAL PROPERTY, OR (III) THAT THIS DOCUMENT IS SUITABLE TO ANY PARTICULAR USER'S CIRCUMSTANCE; OR

(B) ASSUMES RESPONSIBILITY FOR ANY DAMAGES OR OTHER LIABILITY WHATSOEVER (INCLUDING ANY CONSEQUENTIAL DAMAGES, EVEN IF BWRVIP, EPRI OR ANY EPRI REPRESENTATIVE HAS BEEN ADVISED OF THE POSSIBILITY OF SUCH DAMAGES) RESULTING FROM YOUR SELECTION OR USE OF THIS DOCUMENT OR ANY INFORMATION, APPARATUS, METHOD, PROCESS, OR SIMILAR ITEM DISCLOSED IN THIS DOCUMENT.

ORGANIZATION(S) THAT PREPARED THIS DOCUMENT

Continuum Dynamics, Inc.

NON-PROPRIETARY INFORMATION

NOTICE: This report contains non-proprietary information that is included in the proprietary version of the report. The proprietary version of this report contains proprietary information that is the intellectual property of BWRVIP utility members, EPRI, and Continuum Dynamics, Inc. (C.D.I.). Accordingly, it is available only under license from C.D.I. and may not be reproduced or disclosed, wholly or in part, by any licensee to any other person or organization.

THE WORK DESCRIBED IN THIS REPORT WAS PROCURED, REVIEWED, ACCEPTED, AND ISSUED ACCORDING TO EPRI'S QUALITY ASSURANCE PROGRAM AND PREPARED UNDER CONTINUUM DYNAMICS, INC.'S QUALITY ASSURANCE PROGRAM, BOTH OF WHICH COMPLY WITH THE REQUIREMENTS OF TITLE 10 OF THE CODE OF FEDERAL REGULATIONS, PART 50, APPENDIX B.

NOTE

For further information about EPRI, call the EPRI Customer Assistance Center at 800.313.3774 or e-mail askepri@epri.com.

CITATIONS

This report was prepared by

Continuum Dynamics, Inc.
34 Lexington Avenue
Ewing, NJ 08618

Principal Investigators:
Alan Bilanin
Alexander Boschitsch
Milton Teske

This report describes research sponsored by the Electric Power Research Institute (EPRI) and its BWRVIP participating members, and Continuum Dynamics, Inc. (C.D.I.).

The report is a corporate document that should be cited in the literature in the following manner:

BWRVIP-194NP: BWR Vessel and Internals Project, Methodologies for Demonstrating Steam Dryer Integrity for Power Uprate. EPRI, Palo Alto, CA and C.D.I., Ewing, NJ: 2008. 1016578NP.

PRODUCT DESCRIPTION

This report documents the technical basis for and validation of Continuum Dynamics, Inc. (C.D.I.) proprietary load definition and stress analysis methods that can be used to demonstrate the structural integrity of BWR steam dryers at Extended Power Uprate (EPU) conditions. The report presents screening methods for assessing the potential for acoustic excitation within BWR main steam lines (MSLs), conducting in-plant tests to define MSL fluctuating pressures using strain gages, defining acoustic and hydrodynamic fluctuating pressures on the steam dryer based on MSL pressure measurements, adjusting MSL fluctuating flow induced vibration (FIV) pressures obtained at current licensed thermal power (CLTP) to EPU power, defining the acoustic and flow loading on the steam dryer resulting from turbine stop valve (TSV) closure and main steam line break (MSLB) events, conducting ASME Code fatigue and primary stress analyses of the steam dryer, and defining MSL strain gage limit curves to support power ascension testing.

Results and Findings

The project developed and validated a suite of methods for demonstrating the structural integrity of steam dryers at power uprate conditions. These methods are intended to comply with guidance provided in BWRVIP-181 BWR Vessel and Internals Project: Steam Dryer Repair Design Criteria (EPRI report 1013403), BWRVIP-182 BWR Vessel and Internals Project: Guidance for Demonstration of Steam Dryer Integrity for Power Uprate (EPRI report 1016166), and U. S. NRC Regulatory Guide 1.20 Comprehensive Vibration Assessment Program for Reactor Internals during Preoperational and Initial Startup Testing, issued in March 2007.

Challenges and Objective(s)

In recent years, BWR plants have experienced damage to their steam dryers as a result of higher steam flows generated under power uprate conditions. Such damage is attributed to acoustic and turbulent pressure loading on the steam dryer. Validated methods for predicting pressure loading on the steam dryer at power uprate conditions due to these phenomena were needed to allow NRC approval of power uprate licenses. The purpose of this document is to provide validated generically applicable methods that can be used by utilities planning a power uprate to demonstrate the structural integrity of their steam dryer.

Applications, Values, and Use

The methods documented in this report can be applied by any BWR utility to demonstrate the structural integrity of their steam dryer under power uprate flow conditions. These methods provide a basis for evaluating the loading on and response of the steam dryer at power uprate flow conditions without need for operation of the plant above current licensed thermal power.

These methods can also inform decisions on the need for load mitigation prior to submitting an application for power uprate.

EPRI Perspective

This report provides BWR utilities with a suite of methods that can be applied with confidence to evaluate the structural integrity of their steam dryer at power uprate conditions. These methods have been validated by comparison to separate effects and full-scale, in-plant data and follow BWRVIP and NRC guidance for assessing vibratory loading on the steam dryer.

Approach

The research team developed analytical and subscale testing methods for screening for acoustic excitation in MSLs and an acoustic circuit model (ACM) for defining steam dryer fluctuating pressure loading based on MSL pressure inferred from strain gages located on the MSLs. Subscale testing can be used to adjust the MSL pressures obtained during in-plant testing at CLTP to account for higher MSL flow velocities at power uprate. The adjusted MSL pressures can be input to the ACM to define steam dryer pressure loading at power uprate. The team validated the ACM by comparing it to full-scale, in-plant tests with an instrumented steam dryer. The power uprate steam dryer pressures loading can be applied to a detailed finite element model (FEM) of the steam dryer to evaluate structural response and stresses. Structural evaluation is conducted in the frequency domain. The team developed methods for conducting an ASME code fatigue evaluation based on the FEM analysis and validated the FEM analysis methodology by comparing it to the results of shaker testing of a full-scale steam dryer. The team also developed first-principles-based methods for defining the steam dryer loading resulting from TSV closure and MSLB events and presented methods for conducting an ASME primary stress evaluation using the loads and load combinations defined in BWRVIP-181. Finally, the team devised methods for defining MSL strain gage limit curves to support power ascension testing.

Keywords

Boiling water reactor
Steam dryer
Power uprate

ACKNOWLEDGMENTS

The members of the BWRVIP Steam Dryer Focus Group listed below are acknowledged for their efforts in support of the review of this document.

Steam Dryer Focus Group Members

George Inch (Constellation), Chairman

Bob Carter (EPRI)

Guy DeBoo (Exelon)

Joseph Ferrante (Constellation)

Robert Geier (Exelon)

Roman Gesior (Exelon)

Ed Hartwig (TVA)

Steve Hammer (NMC)

Bill McCurdy (MPR Associates)

Fred Moody (XGEN)

Sam Ranganath (XGEN)

Steve Richter (Entergy Northwest)

Larry Rinaca (TVA)

Steve Scott (Entergy)

Randy Stark (EPRI)

Bruce Swoyer (PPL)

Harold Trenka (PSE&G)

Tim Wells (SNOC)

Chuck Wirtz (FENOC)

James Wolcott (TVA)

Larry Yemma (Progress Energy)

CONTENTS

LIST OF FIGURES

LIST OF TABLES

1
INTRODUCTION

1.1 Overview

The purpose of this report is to document the technical basis for and validation of Continuum Dynamics, Inc. (C.D.I.) proprietary load definition and stress analysis methods that can be used to demonstrate the structural integrity of BWR steam dryers at Extended Power Uprate (EPU) conditions. Methods are presented for:

- Screening to assess the potential for acoustic excitation within BWR main steam lines (MSLs)
- Conducting in-plant tests to define MSL fluctuating pressures using strain gages
- Eliminating extraneous noise in MSL fluctuating pressure measurements
- Defining acoustic and hydrodynamic fluctuating pressures on the steam dryer based on MSL pressure measurements
- Using subscale tests to "bump-up" MSL fluctuating pressures obtained at Current Licensed Thermal Power (CLTP) to define MSL flow induced vibration (FIV) pressures at EPU power
- Using Main Steam Isolation Valve (MSIV) closure tests to define fluctuating pressures on the steam dryer at or near EPU power
- Defining the unsteady pressure load on the steam dryer resulting from a turbine stop valve (TSV) closure event
- Defining the unsteady pressure load on the steam dryer resulting from a main steam line break (MSLB)
- Defining primary and fluctuating stresses using a detailed finite element model (FEM) of the steam dryer
- Conducting fatigue and primary stress analyses of the steam dryer using ASME Code Section 111, Subsection NG as a guide
- Defining MSL strain gage limit curves to support power ascension to EPU conditions

- Defining the pressure loading on all steam dryer surfaces based on measurements of fluctuating pressure at specific locations on the steam dryer

The steam dryer evaluation approach described herein is intended to comply with guidance provided in BWRVIP-181 "BWR Vessel and internals Project: Steam Dryer Repair Design Criteria" [1.1], BWRVIP-182 "BWR Vessel an Internals Project: Guidance for Demonstration of Steam Dryer Integrity for Power Uprate" [1.2], and U. S. NRC Regulatory Guide 1.20 "Comprehensive Vibration Assessment Program for Reactor Internals during Preoperational and Initial Startup Testing" issued in March 2007 [1.3].

The methods presented herein can be applied generically to all BWR plants considering a power uprate to demonstrate the structural integrity of the steam dryer.

This report addresses only methodologies for evaluating the structural integrity of the steam dryer. The pressure fluctuations inside the main steam lines may also have a detrimental effect on MSL instrumentation and other components such as relief valve operators. Potential detrimental effects on such components as a result of MSL vibrations at power uprate conditions should also be addressed as part of a power uprate submittal. Techniques for conducting such an assessment are beyond the scope of this report.

1.2 Implementation Requirements

In accordance with the implementation requirements of Nuclear Energy Institute (NEI) 03-08, Guideline for the Management of Materials Issues, if a BWRVIP utility choses to use the steam dryer evaluation methodologies described in this report as a basis for a power uprate submittal, Sections 3 through 11 are considered "Needed".

1.3 References

1.1 BWRVIP-181: BWR Vessel and Internals Project Steam Dryer Repair Design Criteria, December 2007. EPRI Report No. 1013403.

1.2 BWRVIP-182: BWR Vessel and Internals Project Guidance for Demonstrating Steam Dryer Integrity for Power Uprate, January 2008. EPRI Report No. 1016166.

1.3 Regulatory Guide 1.20 "Comprehensive Vibration Assessment Program for Reactor Internals during Preoperational and Initial Startup Testing, March 2007".

2
BACKGROUND

In 2002, shortly after increasing power to 117% of Original Licensed Thermal Power (OLTP), the Quad Cities Unit 2 operated by Exelon Corporation suffered a series of structural failures of its steam dryer assembly. After extensive evaluation by industry, the root cause for these failures was traced to acoustic resonances produced at the inlets to safety and relief valves attached to the main steam lines (MSLs). Such resonances can occur when the frequency of vortex shedding at the upstream lip at the entrance to piping attached to the MSLs "locks in" with the quarter-standing wave acoustic frequency of the attached piping. The frequency of vortex shedding is related to the velocity of flow in the MSLs as well as the opening diameter of the attached piping. The flow velocity in the MSLs is directly related to the operating power level in a BWR. These pressure fluctuations were found to propagate acoustically through the MSLs back to the reactor pressure vessel with the potential to damage the steam dryer.

Since that time, Continuum Dynamics, Inc. (C.D.I.), has worked with industry to develop and validate proprietary analytical and test methods for assessing the potential that such resonances may occur in a plant considering a power uprate and for defining the fluctuating pressure loading on the steam dryer surfaces based on MSL pressure measurements derived from strain gages attached to the MSLs during in-plant testing. In addition, C.D.I. has developed and validated proprietary subscale test methods for adjusting the MSL pressures obtained in the plant at the Current Licensed Thermal Power (CLTP) to Extended Power Uprate (EPU) flow conditions. This predictive capability allows the determination of steam dryer fluctuating pressure loading at EPU conditions without the need to conduct in-plant testing above CLTP.

C.D.I. has also developed proprietary analytical methods for determining the acoustic pressure and flow loading on the steam dryer resulting from the fast closure of the turbine stop valves (TSV) and from a main steam line break (MSLB).

Finally, C.D.I. has developed and validated methods for evaluating the stresses in steam dryers under the loads described above for comparison to ASME fatigue and maximum stress allowables. The stress analysis is conducted in the frequency domain, which significantly reduces data evaluation time.

3
OVERVIEW OF STEAM DRYER EVALUATION APPROACH

The overall process for evaluating the structural integrity of BWR steam dryers at power uprate follows the flowchart shown in Figure 3-1 (excerpted from BWRVIP-182). The process is described in detail as follows.

Step 1: Screening to assess the potential for acoustic excitation in MSLs up to power uprate

The process begins with analytical screening and subscale testing to assess the potential for acoustic excitation in the main steam lines (MSLs) at power levels beyond the Current Licensed Thermal Power (CLTP) level as described in Section 4.

Step 2: Assess need for acoustic load mitigation

If screening tests indicate that a potential exists for significant acoustic excitation in the MSLs, the applicant can opt to pursue acoustic load mitigation and re-screen. This approach would be expected to result in a determination that the potential acoustic excitation in the MSLs (with mitigation) is low and the applicant would follow the approach defined above for cases where MSL acoustic excitation is not expected. If mitigation is not pursued, and acoustic excitation is expected based on screening, or if acoustic excitation is not expected based on screening, in-plant tests are conducted with the MSLs instrumented using pressure transducers or strain gages to obtain MSL fluctuating pressures at power levels up to CLTP.

Step 3: Conduct in-plant tests at CLTP

Content Deleted-
Contains EPRI and Continuum Dynamics Inc. Proprietary Information

Step 4: Elimination of extraneous MSL data

Content Deleted-
Contains EPRI and Continuum Dynamics Inc. Proprietary Information

Content Deleted-
Contains EPRI and Continuum Dynamics Inc. Proprietary Information

Step 6: Determine pressure loads on the steam dryer at power uprate based on MSL pressures

Content Deleted-
Contains EPRI and Continuum Dynamics Inc. Proprietary Information

Step 7: Account for bias and uncertainties

Content Deleted-
Contains EPRI and Continuum Dynamics Inc. Proprietary Information

Step 8: Conduct structural analysis at power uprate

Content Deleted-
Contains EPRI and Continuum Dynamics Inc. Proprietary Information

Step 9: Obtain NRC approval for power uprate

Once steam dryer stress margins at power uprate are demonstrated, the applicant requests NRC to grant approval for power uprate and power ascension testing.

Step 10: Conduct power ascension testing up to power uprate

Upon NRC approval for power uprate, power ascension testing is conducted up to uprate power.

Content Deleted-
Contains EPRI and Continuum Dynamics Inc. Proprietary Information

Content Deleted-
Contains EPRI and Continuum Dynamics Inc. Proprietary Information

Figure 3-1
BWRVIP Steam Dryer Integrity Demonstration Flowchart

4
METHODS FOR SCREENING TO ASSESS THE POTENTIAL FOR MAIN STEAM LINE (MSL) ACOUSTIC EXCITATION

In accordance with guidance in BWRVIP-182, C.D.I. has developed proprietary analytical and test methods for screening to assess the potential for acoustic excitation in main steam lines at power uprate conditions. This section describes the analytical basis and validation of these methods.

4.1 Objectives and Scope

The screening process involves up to three steps:

Content Deleted-
Contains EPRI and Continuum Dynamics Inc. Proprietary Information

4.2 Acoustic Pre-Screening Method

The phenomenon of flow-excited acoustic resonance of closed side branches has been examined for many years (see as early as [4.1] and [4.2]). In this situation, acoustic resonance of the side branch is caused by feedback from the acoustic velocity of the resonant standing wave in the side branch itself.

Content Deleted-
Contains EPRI and Continuum Dynamics Inc. Proprietary Information

Content Deleted-
Contains EPRI and Continuum Dynamics Inc. Proprietary Information

Figure 4-1
Schematic of the side branch geometry

Content Deleted-
Contains EPRI and Continuum Dynamics Inc. Proprietary Information

Content Deleted-
Contains EPRI and Continuum Dynamics Inc. Proprietary Information

Figure 4-2
Strouhal number behavior, where q is the dynamic pressure ($\frac{1}{2}\rho U^2$) and ρ is the fluid density [4.6].

Content Deleted-
Contains EPRI and Continuum Dynamics Inc. Proprietary Information

Table 4-1
Pre-Screening Standpipe/Valve Parameters (QC2)

Content Deleted-
Contains EPRI and Continuum Dynamics Inc. Proprietary Information

4.3 Refined Acoustic Modeling of MSL Standpipes

Since, in the plant, the standpipe/valve combination changes area as a function of distance from the main steam line to the valve disk, a more accurate estimate of f_l is needed to include these area change effects. The combination of an accurate excitation frequency f_l and subsequent calculation of onset velocity with the appropriate Strouhal number then characterizes the behavior of the standpipe/valve combination considered.

Content Deleted-
Contains EPRI and Continuum Dynamics Inc. Proprietary Information

Table 4-2
Refined Acoustic Model predictions for Standpipe/Valve Parameters (QC2)

Content Deleted-
Contains EPRI and Continuum Dynamics Inc. Proprietary Information

4.4 One-Fifth Scale Model Testing

In accordance with BWRVIP-182, in cases where analytical predictions indicate a potential for acoustic excitation in the MSLs, a one-fifth scale single line test is conducted.

Content Deleted-
Contains EPRI and Continuum Dynamics Inc. Proprietary Information

Content Deleted-
Contains EPRI and Continuum Dynamics Inc. Proprietary Information

Content Deleted-
Contains EPRI and Continuum Dynamics Inc. Proprietary Information

Figure 4-3
Photographs of the QC2 blowdown facility: entire scaled main steam line A (top); the three standpipe locations (bottom), with the first standpipe/valve in place.

Content Deleted-
Contains EPRI and Continuum Dynamics Inc. Proprietary Information

Content Deleted-
Contains EPRI and Continuum Dynamics Inc. Proprietary Information

Figure 4-4 Content Deleted-Contains EPRI and Continuum Dynamics Inc. Proprietary Information

Content Deleted-
Contains EPRI and Continuum Dynamics Inc. Proprietary Information

Figure 4-5 Content Deleted-Contains EPRI and Continuum Dynamics Inc. Proprietary Information

Content Deleted-
Contains EPRI and Continuum Dynamics Inc. Proprietary Information

Figure 4-6 Content Deleted-Contains EPRI and Continuum Dynamics Inc. Proprietary Information

Content Deleted-
Contains EPRI and Continuum Dynamics Inc. Proprietary Information

Figure 4-7 Content Deleted-Contains EPRI and Continuum Dynamics Inc. Proprietary Information

4.5 Validation of Refined Acoustic Model and One-Fifth Scale Model Predictions of Excitation Frequency and Onset Velocity

Content Deleted-
Contains EPRI and Continuum Dynamics Inc. Proprietary Information

Table 4-3
Experimentally Determined Standpipe/Valve Parameters (QC2). The predicted excitation frequency is taken from Table 4-2.

Content Deleted-
Contains EPRI and Continuum Dynamics Inc. Proprietary Information

Table 4-4
Comparisons between predicted and measured excitation frequencies and onset velocities for the other plants analyzed using the refined model and the one-fifth scale test method.

Content Deleted-
Contains EPRI and Continuum Dynamics Inc. Proprietary Information

A typical one-fifth scale test result is shown in Figure 4-8, where normalized RMS pressure (normalized by the dynamic pressure at CLTP conditions) measured at the disk ends of the standpipe/valves is plotted against Mach number. The one-fifth scale test was conducted for Plant B on a main steam line with three standpipe/valves. The Mach numbers at CLTP and EPU conditions are shown on the figure, where it may be seen that the onset velocity measured in the one-fifth scale test is expected to occur in the plant at a velocity very close to the Bounding EPU Mach number, at a Normalized RMS Pressure of approximately Content Deleted-
Contains EPRI and Continuum Dynamics Inc. Proprietary Information.

Content Deleted-
Contains EPRI and Continuum Dynamics Inc. Proprietary Information

Figure 4-8
Normalized RMS pressure for all one-fifth scale tests of Plant B: upstream refers to the pressure at the upstream standpipe/valve; middle refers to the pressure at the middle standpipe/valve; and downstream refers to the pressure at the downstream standpipe/valve. A cubic spline curve fit to all data is shown by the green curve.

Onset may be observed from full-scale data for Plant B as shown in Figure 4-9. This figure plots the PSD of the signal recorded at the upper strain gage location on main steam line A for power levels between 100% (CLTP) and

Content Deleted-
Contains EPRI and Continuum Dynamics Inc. Proprietary Information

Content Deleted-
Contains EPRI and Continuum Dynamics Inc. Proprietary Information

Figure 4-9
PSD at the upper strain gage location on main steam line A in Plant B for various power levels as shown.

4.6 Double Vortex Mode

In most cases the normalized RMS pressure plots show a typical bell-shaped curve as shown in Figure 4-8. However, in some cases a second pressure peak may be observed, as shown in Figure 4-10 for the one-fifth scale test for Plant A. In this particular example the normalized RMS pressure peak at the double vortex occurs at a Mach number just above EPU conditions.

Content Deleted-
Contains EPRI and Continuum Dynamics Inc. Proprietary Information

Content Deleted-
Contains EPRI and Continuum Dynamics Inc. Proprietary Information

Figure 4-10
Normalized RMS pressure for all one-fifth scale tests of Plant A: upstream refers to the pressure at the upstream standpipe/valve; middle refers to the pressure at the middle standpipe/valve; and downstream refers to the pressure at the downstream standpipe/valve. A cubic spline curve fit to all data is shown by the green curve.

Content Deleted-
Contains EPRI and Continuum Dynamics Inc. Proprietary Information

Figure 4-11
Sketch showing vortex formation at the mouth of a standpipe/valve: single vortex mode (top); double vortex mode (bottom)

4.7 Criteria for Use of – Content Deleted – EPRI and Continuum Dynamics Inc. Proprietary Information

Content Deleted-
Contains EPRI and Continuum Dynamics Inc. Proprietary Information

4.8 References

4.1. Chen, Y. N. and D. Florjancic. 1975. Vortex-Induced Resonance in a Pipe System due to Branching. *Proceedings of International Conference on Vibration and Noise in Pump, Fan and Compressor Installations* 79-86. University of Southampton, England.

4.2. Baldwin, R. M. and H. R. Simmons. 1986. Flow-Induced Vibration in Safety Relief Valves. *ASME Journal of Pressure Vessel Technology* 108: 267-272.

4.3. Ziada, S. and S. Shine. 1999. Strouhal Numbers of Flow-Excited Acoustic Resonance of Closed Side Branches. *Journal of Fluids and Structures* 13: 127-142.

4.4. Ziada, S. 1994. A Flow Visualization Study of Flow Acoustic Coupling at the Mouth of a Resonant Side-Branch. *Journals of Fluids and Structures* 8: 391-416.

4.5. Graf, H. R. and S. Ziada. 1992. Flow-Induced Acoustic Resonance in Closed Side Branches: An Experimental Determination of the Excitation Source. *Proceedings of ASME International Symposium on Flow-Induced Vibration and Noise, Vol. 7: Fundamental Aspects of Fluid-Structure Interactions* (ed: M. P. Paidoussis, T. Akylas, and P. B. Abraham). AMD 51: 63-80. New York: ASME.

4.6. Weaver, D. S. and G. O. MacLeod. 1999. Entrance Port Rounding Effects on Acoustic Resonance in Safety Relief Valves. Flow-Induced Vibration: The 1999 ASME Pressure Vessels and Piping Conference. 291-298.

4.7. Bliss, D. B., T. R. Quackenbush, and M. E. Teske. 1982. Computational Simulation of High-Speed Steady Homogeneous Two-Phase Flow in Complex Piping Systems. *Transactions of the ASME Journal of Pressure Vessel Technology* 104: 272-277.

4.8. Continuum Dynamics, Inc. 2004. Plant Unique Steam Dryer Loads to Support I&E Guidelines. C.D.I. Technical Memo No. 04-14.

4.9. Continuum Dynamics, Inc. 2006. Mitigation of Pressure Oscillations in the Quad Cities Steam Delivery System: A Subscale Single Main Steam Line Investigation of Standpipe Behavior (Rev. 0). C.D.I. Report No. 06-01.

4.10. Continuum Dynamics, Inc. 2005. Onset of High Frequency Flow Induced Vibration in the Main Steam Lines at Hope Creek Unit 1: A Subscale Investigation of Standpipe Behavior (Rev. 0). C.D.I. Report No. 05-31.

4.11. Continuum Dynamics, Inc. 2005. Onset of High Frequency Flow Induced Vibration in the Main Steam Lines at Susquehanna Steam Electric Station: A Subscale Investigation of Standpipe Behavior (Rev. 0). C.D.I. Report No. 05-32.

4.12. Continuum Dynamics, Inc. 2007. Onset of High Frequency Flow Induced Vibration in the Main Steam Lines at Laguna Verde: A Subscale Investigation of Standpipe Behavior (Rev. 0). C.D.I. Report No. 07-12.

4.13. Continuum Dynamics, Inc. 2008. Onset of Flow-Induced Vibration in the Main Steam Lines at Browns Ferry Unit 1: A Subscale Investigation of Standpipe Behavior (Rev. 0). C.D.I. Report No. 08-01.

5
METHODOLOGY FOR DEFINING MSL DYNAMIC PRESSURES AND REMOVING EXTRANEOUS NOISE

Several steps are involved in defining main steam line dynamic pressure signals. These steps include locating the strain gages optimally along the MSLs, installing them at these locations with proper cable shielding, taking data with a correctly set up data acquisition system (DAS), reducing the data, and understanding the data uncertainty in the data collection. Particular care must be taken to protect the area where the gages are installed and to route strain gage instrumentation cabling away from high temperature areas and potential sources of electromagnetic interference. In addition, steps must be taken to remove extraneous noise in the MSL data.

5.1 Locating Pressure or Strain Gage Measurement Points Axially Along MSLs

Content Deleted-
Contains EPRI and Continuum Dynamics Inc. Proprietary Information

Content Deleted-
Contains EPRI and Continuum Dynamics Inc. Proprietary Information

Figure 5-1
Strain gage schematic for location analysis

Content Deleted-
Contains EPRI and Continuum Dynamics Inc. Proprietary Information

Content Deleted-
Contains EPRI and Continuum Dynamics Inc. Proprietary Information

Content Deleted-
Contains EPRI and Continuum Dynamics Inc. Proprietary Information

Figure 5-2
Strain gage locations: L1 and L2 are measured from the vessel ID along the centerline of the MSL to the upper and lower elevations, respectively, and should be at least two pipe diameters away from the elbow welds. The distance between L_1 (the upper strain gage location) and L_2 (the lower strain gage location) is ΔL.

5.2 Uncertainty Associated with Axial Measurement Locations

The acoustic circuit model (ACM) has been benchmarked with data taken by strain gages on the main steam lines of Quad Cities Unit 2 (QC2), located at average distances of

Content Deleted-
Contains EPRI and Continuum Dynamics Inc. Proprietary Information

Table 5-1
Strain gage spacing for QC2 (the actual spacing between strain gages was ΔL = 31.7 ft)

Content Deleted-
Contains EPRI and Continuum Dynamics Inc. Proprietary Information

5.3 Installation of Strain Gages around MSLs to Define Local Fluctuating Pressures

The most direct method to obtain dynamic pressure measurements is to mount pressure transducers on the piping. The orifice necessary for these instruments, however, requires a

potentially undesirable opening in the pressure boundary of the affected system. Thus, mounting the strain gages directly on the piping allows for an indirect measurement of the dynamic pressure fluctuation and eliminates the need for affecting pressure boundary integrity.

One of the challenges in performing this indirect measurement is the potential presence of significant axial strain affecting the hoop stress readings and producing signal content that is not related to the internal pressure. The pressure fluctuations are derived from the "breathing" mode of the piping; therefore, this indirect technique must be robust enough to reject the effects of other shell modes and/or bending. Several factors influence the ability to ensure that the breathing mode response can be measured. These factors include strain gage configuration options and data processing methods. The tested strain gage configurations utilized up to eight strain gages per location in an axisymmetric manner to facilitate the cancellation of any shell mode responses that may exist. Data processing strategies utilizing channel combination and filtering techniques can be applied to extract pure breathing mode data for conversion to dynamic pressure.

Strain gages should be installed at

Content Deleted-
Contains EPRI and Continuum Dynamics Inc. Proprietary Information

Content Deleted-
Contains EPRI and Continuum Dynamics Inc. Proprietary Information

Figure 5-3
Typical strain gage layout

Content Deleted-
Contains EPRI and Continuum Dynamics Inc. Proprietary Information

Figure 5-4
Strain gage orientation

5.4 Strain Gage Measurement System

A typical strain gage system is comprised of a Wheatstone Bridge (WB) as shown in Figure 5-5. In the figure, V_{in} is the DC voltage supplied to the WB circuit, V_{out} is the output voltage measured, and R_1, R_2, R_3 and R_4 are the four resistances on the four arms of the WB circuit. In order to improve the sensitivity of the SG measurements, each SG location has two similar strain gages that are connected in the places of R_1 and R_3. Since R_1 and R_3 are in close proximity, they experience similar strains. The circuit analysis will show that R_1 and R_3 in this case will be additive. Before the start of the measurements, and with no applied strain on the active gages, the compensating resistors R_2 and R_4 will be adjusted such that the output voltage V_{out} is zero, which means that the WB circuit is balanced. In the presence of applied strain, the resistances R_1 and R_3 will vary, and the output voltage consequently will change and be proportional to the applied strain.

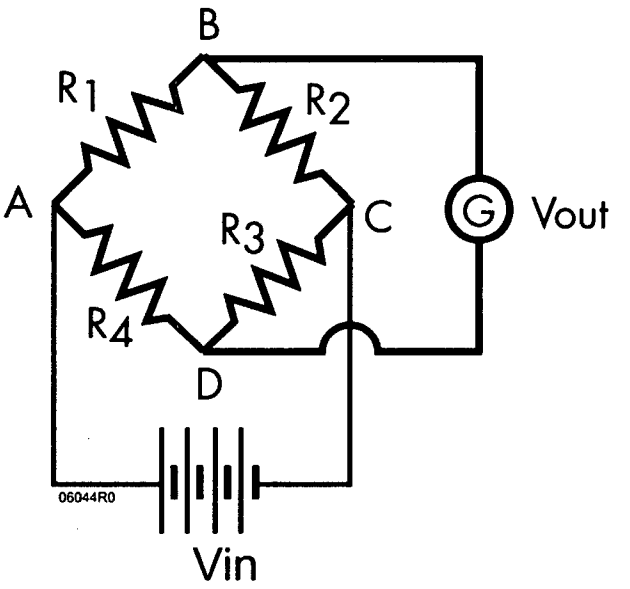

Figure 5-5
Wheatstone bridge and strain gage electrical schematic

5.5 Circuit Analysis of Wheatstone Bridge

For a given input voltage V_{in}, the currents flowing through the junctions of the WB circuit may be given as

$$V_{in} = I_{ABC}\,(R_1 + R_2) = I_{ADC}\,(R_4 + R_3) \tag{5.5.1}$$

The voltage drops between junctions A and B, and A and D, are given as

$$V_{AB} = I_{ABC}\,R_1 = \frac{V_{in}\,R_1}{R_1 + R_2} \tag{5.5.2}$$

$$V_{AD} = I_{ADC}\,R_4 = \frac{V_{in}\,R_4}{R_4 + R_3} \tag{5.5.3}$$

The output voltage V_{out} can then be obtained from

$$V_{out} = V_{AB} - V_{AD} = \frac{R_1\,R_3 - R_2\,R_4}{(R_1 + R_2)\,(R_4 + R_3)}\,V_{in} \tag{5.5.4}$$

If the bridge is initially balanced, then V_{out} is zero, which means that the numerator should be zero. Thus

$$R_1 R_3 - R_2 R_4 = 0 \qquad \text{or} \qquad R_1 R_3 = R_2 R_4 \tag{5.5.5}$$

which can rewritten as

$$\frac{R_1}{R_2} = \frac{R_4}{R_3} = \frac{1}{\gamma} \tag{5.5.6}$$

In the presence of the applied strain, the change in the output voltage may be computed from Equation (5.5.4) and may be given as

$$\Delta V_{out} = \frac{\gamma}{(1+\gamma)^2}\left(\frac{\Delta R_1}{R_1} - \frac{\Delta R_2}{R_2} + \frac{\Delta R_3}{R_3} - \frac{\Delta R_4}{R_4}\right)(1+\eta)\, V_{in} \tag{5.5.7}$$

where η is given by

$$\eta = \frac{1}{1 + \dfrac{1+\gamma}{\dfrac{\Delta R_1}{R_1} + \dfrac{\Delta R_4}{R_4} + \gamma\left(\dfrac{\Delta R_2}{R_2} + \dfrac{\Delta R_3}{R_3}\right)}} \tag{5.5.8}$$

When the resistance changes are small (less than 5%), the second-order term of η in Equation (5.5.8) may be neglected, resulting in the final relationship of

$$\Delta V_{out} \approx \frac{\gamma}{(1+\gamma)^2}\left(\frac{\Delta R_1}{R_1} - \frac{\Delta R_2}{R_2} + \frac{\Delta R_3}{R_3} - \frac{\Delta R_4}{R_4}\right) V_{in} \tag{5.5.9}$$

The coefficient $\dfrac{\gamma}{(1+\gamma)^2}$ is called the circuit efficiency. In practice, all four resistances are chosen to be nominally equal ($R_1 = R_2 = R_3 = R_4 = R$), thus making $\gamma = 1$ in Equation (5.5.9). The change in voltage then can be further simplified to

$$\Delta V_{out} \approx \left(\frac{\Delta R_1 - \Delta R_2 + \Delta R_3 - \Delta R_4}{4R}\right) V_{in} \tag{5.5.10}$$

The WB circuit arrangement with the active gage attached at R_1 and R_3 locations is called a half bridge. If only one of the arms has an active gage (either R_1 or R_3 is active), then it is termed a quarter bridge.

It is noted that during the strain measurements with a half bridge, $\Delta R_2 = \Delta R_4 = 0$ in Equation (5.5.10). In addition, the change in resistance to the strain ε is related through a factor called the Gage Factor (GF), provided by the strain gage manufacturer, namely

$$\frac{\Delta R}{R} = GF * \varepsilon \tag{5.5.11}$$

Hence, if $\Delta R_1 = \Delta R_3 = \Delta R$ and $R_1 = R_3 = R$, Equation (5.5.10) then becomes

$$\frac{\Delta V_{out}}{V_{in}} = \frac{1}{2}\frac{\Delta R}{R} = \frac{1}{2} GF \times \varepsilon \tag{5.5.12}$$

for the half-bridge configuration. Similarly, for a quarter-bridge configuration, the corresponding relationship will be

$$\frac{\Delta V_{out}}{V_{in}} = \frac{1}{4}\frac{\Delta R}{R} = \frac{1}{4} GF \times \varepsilon \tag{5.5.13}$$

5.6 Conversion of MSL Strain Gage Measurements to Local Fluctuating Pressure

Content Deleted-
Contains EPRI and Continuum Dynamics Inc. Proprietary Information

Content Deleted-
Contains EPRI and Continuum Dynamics Inc. Proprietary Information

5.7 Bias and Random Uncertainties Associated with MSL Pressure Measurements

The objective here is to determine the uncertainty in the measurement given the uncertainties in the various quantities shown in Equation (5.6.8) that relate the pressure to the measured hoop strain. The major uncertainties in the dynamic pressure estimation are:

1. Geometric uncertainties of the pipe such as the outside diameter (OD), thickness, etc.
2. Uncertainty associated with the gage factor (GF).
3. Uncertainties in the Young's Modulus of Elasticity, (E).
4. Uncertainty in the orientation of the strain gage whose contribution is generally negligibly small.

Therefore, to determine the uncertainty in the pressure measurement, the outside diameter (OD) and wall thickness need to be determined at each of the strain gage locations. Prior to installation of the strain gages, the pipe wall thickness at each strain gage location should be obtained via UT measurement. The OD is often easiest determined from a circumference measurement, and so the uncertainty in the OD measurements has to be derived from the uncertainty in the circumference.

In order to develop an expression for the relative uncertainty in the internal pressure, first the logarithm of both sides of Equation (5.6.8) is taken to yield

Content Deleted-
Contains EPRI and Continuum Dynamics Inc. Proprietary Information

Content Deleted-
Contains EPRI and Continuum Dynamics Inc. Proprietary Information

5.7.1 The Effect of Approximation in the Determination of Uncertainty

In order to determine the effect of applying the approximation

Content Deleted-
Contains EPRI and Continuum Dynamics Inc. Proprietary Information

Content Deleted-
Contains EPRI and Continuum Dynamics Inc. Proprietary Information

5.7.2 Equivalency of Uncertainty Determination to Other Methods

Content Deleted-
Contains EPRI and Continuum Dynamics Inc. Proprietary Information

Content Deleted-
Contains EPRI and Continuum Dynamics Inc. Proprietary Information

Content Deleted-
Contains EPRI and Continuum Dynamics Inc. Proprietary Information

5.8 Testing Requirements and Recommendations

The recommended minimum requirements for a data acquisition system (DAS) that will be used to monitor MS piping are now described. If the instrumentation follows the guidelines in Section 5.3, the DAS will be required to acquire to 32 channels of data simultaneously over a bandwidth of 1 to 250 Hz for a period of at least 2 minutes. A typical modern DAS will be computer-based with one or more high speed digital data acquisition cards. It is recommended that a minimum sample rate of 2500 samples/second/channel (simultaneously) be supported at a 16-bit signal amplitude resolution. It is critical that DAS be equipped with low pass anti-alias filter(s) with a sufficiently high roll-off gradient (> 24 dB/octave).

The DAS should have selectable gain settings to help resolve signals of low amplitude which are typical for the subject application. Recommended values are 1, 10, 20, 50, and 100. The data files generated are substantial in size (40 MB typical); therefore, a storage medium with a minimum of 30 GB capacity is recommended. In order to properly view the data as they are being collected, the DAS should have the capability to display the signal time history, its frequency spectrum, peak value, and root mean square (RMS) value.

Post-processing the data can involve scaling the data, combining channels, band pass filtering, notch filtering, windowing, and overlap averaging of frequency spectra, so post-processing software with such capabilities is also recommended.

5.9 Removal of Extraneous Noise from MSL Data

Content Deleted-
Contains EPRI and Continuum Dynamics Inc. Proprietary Information

Content Deleted-
Contains EPRI and Continuum Dynamics Inc. Proprietary Information

5.9.1 Noise Removal by Content Deleted-Contains EPRI and Continuum Dynamics Inc. Proprietary Information

Content Deleted-
Contains EPRI and Continuum Dynamics Inc. Proprietary Information

Content Deleted-
Contains EPRI and Continuum Dynamics Inc. Proprietary Information

Table 5-2
Confidence limits on Content Deleted-Contains EPRI and Continuum Dynamics Inc. Proprietary Information

Content Deleted-
Contains EPRI and Continuum Dynamics Inc. Proprietary Information

Figure 5-6 Content Deleted-Contains EPRI and Continuum D Inc. Proprietary Information

Content Deleted-
Contains EPRI and Continuum Dynamics Inc. Proprietary Information

Content Deleted-
Contains EPRI and Continuum Dynamics Inc. Proprietary Information

5.9.2 Noise Removal by - Content Deleted - Contains EPRI and Continuum Dynamics Inc. Proprietary Information

Content Deleted-
Contains EPRI and Continuum Dynamics Inc. Proprietary Information

Content Deleted-
Contains EPRI and Continuum Dynamics Inc. Proprietary Information

5.9.3 Noise Removal Example

The effect of the various noise removal steps may be illustrated with the data from Plant A for MSL A upper strain gage location.

Content Deleted-
Contains EPRI and Continuum Dynamics Inc. Proprietary Information

Content Deleted-
Contains EPRI and Continuum Dynamics Inc. Proprietary Information

Figure 5-7
Original pressure signals at MSL A upper strain gage location for Plant A. Content Deleted-Contains EPRI and Continuum Dynamics Inc. Proprietary Information

Content Deleted-
Contains EPRI and Continuum Dynamics Inc. Proprietary Information

Figure 5-8
Filtered pressure signals at MSL A upper strain gage location for Plant A.

Content Deleted-
Contains EPRI and Continuum Dynamics Inc. Proprietary Information

Figure 5-9 Content Deleted-Contains EPRI and Continuum Dynamics Inc. Proprietary Information

Content Deleted-
Contains EPRI and Continuum Dynamics Inc. Proprietary Information

Figure 5-10 Content Deleted-Contains EPRI and Continuum Dynamics Inc. Proprietary Information

Content Deleted-
Contains EPRI and Continuum Dynamics Inc. Proprietary Information

Figure 5-11 Content Deleted-Contains EPRI and Continuum Dynamics Inc. Proprietary Information

5.10 References

5.1 Timoshenko, S. P. and J. N. Goodier. 1970. Theory of Elasticity. McGraw-Hill.

5.2 Wheeler, A. J. and A. R. Ganji. 2004. Introduction to Engineering Experimentation (Second Edition). Pearson Education, Inc.

5.3 Bendat, J. S. and A. G. Piersol. 2000. Random Data: Analysis and Measurement Procèdures. Third Edition. John Wiley and Sons, Inc.: New York.

6
METHODOLOGY TO PREDICT STEAM DRYER FLUCTUATING PRESSURE LOADING FROM IN-PLANT MSL PRESSURE MEASUREMENTS

This section details the technical basis for and validation of a methodology for determining the fluctuating pressure loading on steam dryer surfaces resulting from acoustic sources based on measured main steam line (MSL) fluctuating pressures (inferred by circumferentially-oriented strain gages) and hydrodynamic sources within the steam dome based on **Content Deleted-Contains EPRI and Continuum Dynamics Inc. Proprietary Information.** The methodology is designated the C.D.I. Acoustic Circuit Model (ACM) Revision 4.

6.1 Overview of ACM Rev. 4 Methodology

In general, a BWR steam dryer pressure loading evaluation is split into two distinct analyses:

Content Deleted-
Contains EPRI and Continuum Dynamics Inc. Proprietary Information

The question naturally arises as to where the most significant source of acoustic pressure is located. It is now understood that SRV/ERV standpipes can be excited when the frequency of vortex shedding in the shear layer over the standpipe, which is dependent on the steam velocity in the main steam line, matches the organ pipe frequency of the standpipe. These sources are downstream of the pressures measured on the steam lines. In addition, hydrodynamic pressure loading can occur on the steam dryer surfaces resulting from Content Deleted-Contains EPRI and Continuum Dynamics Inc. Proprietary Information. Revision 4 of the ACM predicts the fluctuating pressure loading on the steam dryer due to both acoustic and hydrodynamic sources.

6.2 Acoustic Circuit Analysis

Analyses of pressure fluctuations in a single-phase compressible medium, where acoustic wavelengths are long compared to component dimensions, and in particular long compared to transverse dimensions (directions perpendicular to the primary flow directions), lend themselves to application of the acoustic circuit methodology. If the analysis is restricted to frequencies below 250 Hz, acoustic wavelengths are approximately six feet in length, and wavelengths are therefore long compared to most components of interest, such as branch junctions.

Acoustic circuit analysis

Content Deleted-
Contains EPRI and Continuum Dynamics Inc. Proprietary Information

Content Deleted-
Contains EPRI and Continuum Dynamics Inc. Proprietary Information

Figure 6-1
Schematic of the pressure measurement locations in a main steam line

During plant operation, fluctuating pressures are derived at two locations along each steam line using several circumferentially-mounted strain gages. The specific axial locations of the strain gages along the MSLs are determined using the procedure described in Section 5.1. Content Deleted-Contains EPRI and Continuum Dynamics Inc. Proprietary Information.

Content Deleted-
Contains EPRI and Continuum Dynamics Inc. Proprietary Information

6.3 Evaluation of Fluctuating Pressures on the Surface of the Steam Dryer

Steam dryer pressure loads are computed by a Content Deleted-Contains EPRI and Continuum Dynamics Inc. Proprietary Information

6.3.1 Content Deleted – Contains EPRI and Continuum Dynamics Inc. Proprietary Information

Content Deleted-
Contains EPRI and Continuum Dynamics Inc. Proprietary Information

6.3.2 Content Deleted – Contains EPRI and Continuum Dynamics Inc. Proprietary Information

Content Deleted-
Contains EPRI and Continuum Dynamics Inc. Proprietary Information

Content Deleted-
Contains EPRI and Continuum Dynamics Inc. Proprietary Information

Content Deleted-
Contains EPRI and Continuum Dynamics Inc. Proprietary Information

Content Deleted-
Contains EPRI and Continuum Dynamics Inc. Proprietary Information

Figure 6-2
Typical cross-sectional description of the steam dome and steam dryer

Content Deleted-
Contains EPRI and Continuum Dynamics Inc. Proprietary Information

Figure 6-3
Cover and base plate low resolution load pressure node locations on a typical dryer

Content Deleted-
Contains EPRI and Continuum Dynamics Inc. Proprietary Information

Figure 6-3
Top plate low resolution load pressure node locations on a typical dryer.

Content Deleted-
Contains EPRI and Continuum Dynamics Inc. Proprietary Information

Figure 6-4
Outer and inner hood low resolution load pressure nodes on a typical dryer.

Content Deleted-
Contains EPRI and Continuum Dynamics Inc. Proprietary Information

Figure 6-5
Skirt and end plate low resolution load pressure nodes on a typical dryer.

Content Deleted-
Contains EPRI and Continuum Dynamics Inc. Proprietary Information

Figure 6-6
Content Deleted-Contains EPRI and Continuum Dynamics Inc. Proprietary Information

6.3.3 Low Frequency Contribution Due to Hydrodynamic Flow over the Steam Dryer

In addition to the acoustic pressure loading on the steam dryer emanating from sources within the MSLs, a low frequency hydrodynamic pressure loading can occur on the dryer due to Content Deleted-Contains EPRI and Continuum Dynamics Inc. Proprietary Information. This hydrodynamic component of the overall fluctuating pressure loading on the steam dryer is evaluated in Revision 4 of the ACM as described below.

To evaluate the hydrodynamic contribution of the pressure loading on the steam dryer, the pressure computed from

Content Deleted-
Contains EPRI and Continuum Dynamics Inc. Proprietary Information

Content Deleted-
Contains EPRI and Continuum Dynamics Inc. Proprietary Information

Figure 6-7
Content Deleted-Contains EPRI and Continuum Dynamics Inc. Proprietary Information

Content Deleted-
Contains EPRI and Continuum Dynamics Inc. Proprietary Information

Content Deleted-
Contains EPRI and Continuum Dynamics Inc. Proprietary Information

Content Deleted-
Contains EPRI and Continuum Dynamics Inc. Proprietary Information

Figure 6-8
Sketch of a main steam line inlet from the steam dome

Content Deleted-
Contains EPRI and Continuum Dynamics Inc. Proprietary Information

Content Deleted-
Contains EPRI and Continuum Dynamics Inc. Proprietary Information

Content Deleted-
Contains EPRI and Continuum Dynamics Inc. Proprietary Information

Figure 6-9
Content Deleted-Contains EPRI and Continuum Dynamics Inc. Proprietary Information

Content Deleted-
Contains EPRI and Continuum Dynamics Inc. Proprietary Information

Content Deleted-
Contains EPRI and Continuum Dynamics Inc. Proprietary Information

Figure 6-10
Content Deleted-Contains EPRI and Continuum Dynamics Inc. Proprietary Information

Content Deleted-
Contains EPRI and Continuum Dynamics Inc. Proprietary Information

6.3.4 Combined Acoustic and Hydrodynamic Fluctuating Pressure Load Definition

Content Deleted-
Contains EPRI and Continuum Dynamics Inc. Proprietary Information

Content Deleted-
Contains EPRI and Continuum Dynamics Inc. Proprietary Information

6.4 Key Modeling Parameters

When the steam dryer geometry is defined and the physical parameters at the power level of interest are provided (such as the mean steam flow in the main steam lines), the acoustic circuit and

Content Deleted-
Contains EPRI and Continuum Dynamics Inc. Proprietary Information

Table 6-1
ACM Revision 4 locked modeling parameters

Content Deleted-
Contains EPRI and Continuum Dynamics Inc. Proprietary Information

These parameters were chosen for the following reasons:

Acoustic Speed: Content Deleted-Contains EPRI and Continuum Dynamics Inc. Proprietary Information

Acoustic Speed Damping in Steam Dome: Content Deleted-Contains EPRI and Continuum Dynamics Inc. Proprietary Information

Steam-Froth Proportionality Factor (Z_{sf}): Content Deleted-Contains EPRI and Continuum Dynamics Inc. Proprietary Information

Steam-Water Proportionality Factor (Z_{sw}): Content Deleted-Contains EPRI and Continuum Dynamics Inc. Proprietary Information

Main Steam Line Inlet Loss Coefficient: Content Deleted-Contains EPRI and Continuum Dynamics Inc. Proprietary Information

Content Deleted-
Contains EPRI and Continuum Dynamics Inc. Proprietary Information

6.5 Validation of ACM Revision 4

This section summarizes the validation process to achieve ACM Revision 4.

6.5.1 Quad Cities Unit 2 Instrumented Steam Dryer Testing

In the spring of 2005, Exelon Corporation installed a replacement steam dryer in QC2. The steam dryer was instrumented with 27 pressure transducers to measure the fluctuating pressures on the surfaces of the steam dryer and in the steam dome. A photograph of the instrumented dryer is shown in Figure 6-12. As can be seen in the photo, the pressure sensors were mounted below "hubcap" enclosures to protect them during plant operation. The pressure transducers were mounted both inside and outside the dryer as shown in Figure 6-13 to Figure 6-15 [6.3]. Sensor P19 appeared to fail during the startup but appeared to provide creditable information. Sensor P26 was located on a mast above the dryer as shown in Figure 6-15.

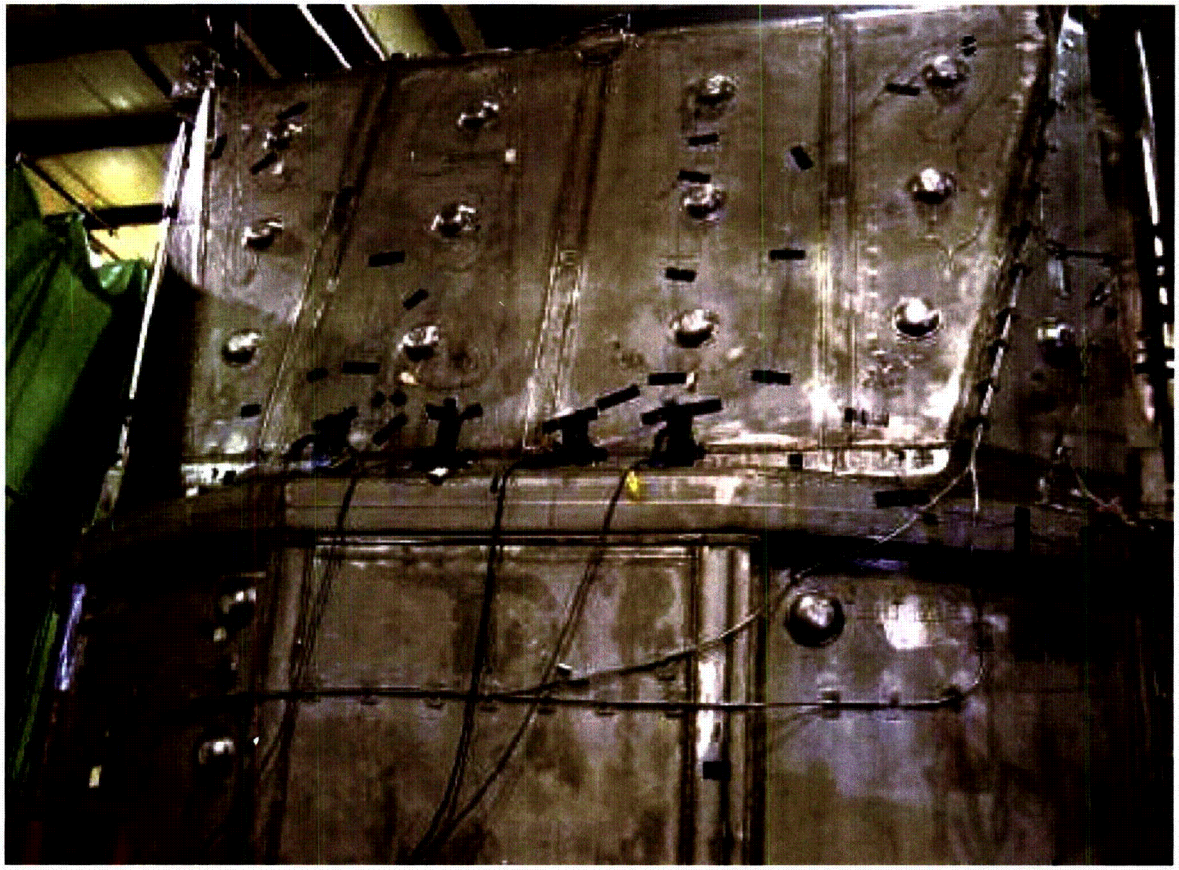

Figure 6-11
Photograph of the QC2 instrumented steam dryer

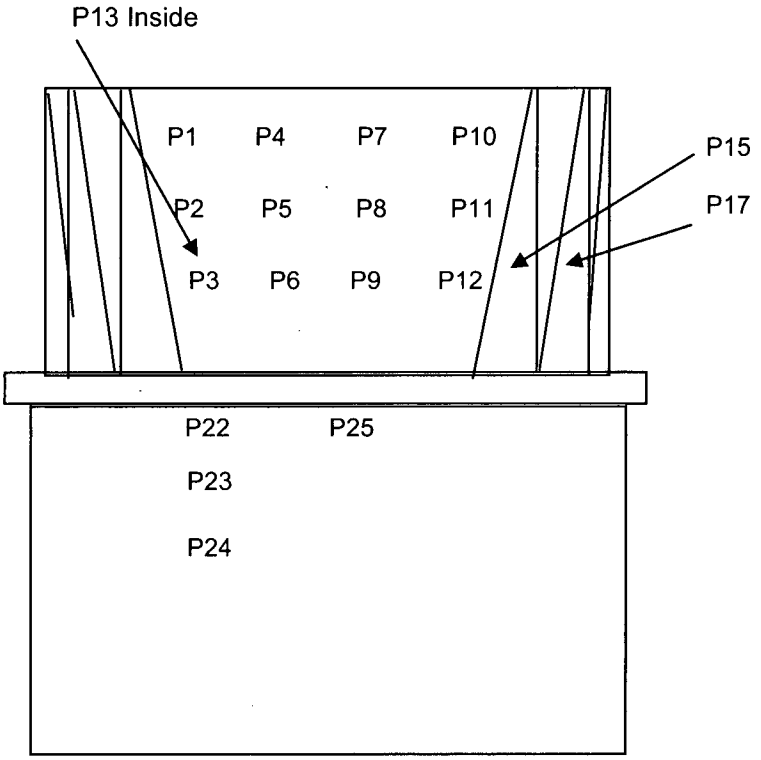

Figure 6-12
Pressure transducer locations on QC2 dryer (MSL A and B side)

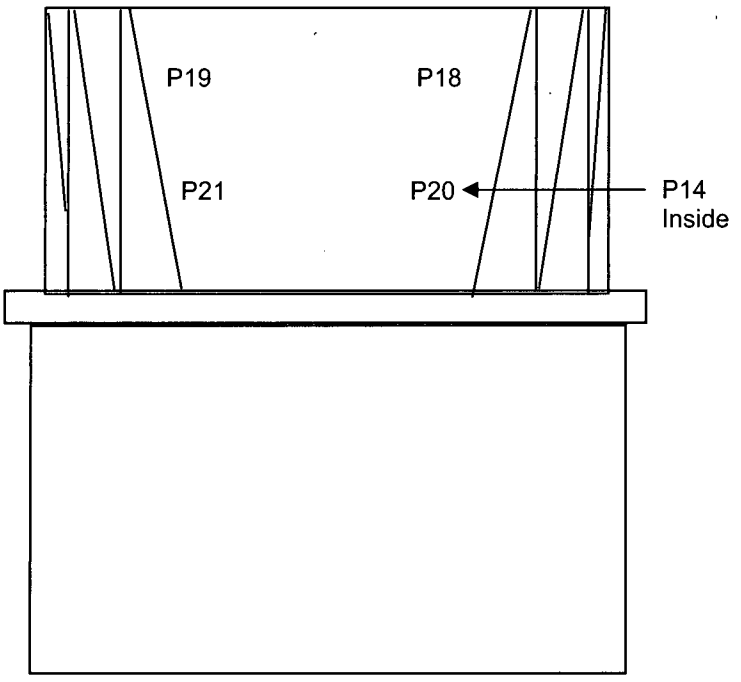

Figure 6-13
Pressure transducer locations on QC2 dryer (MSL C and D side)

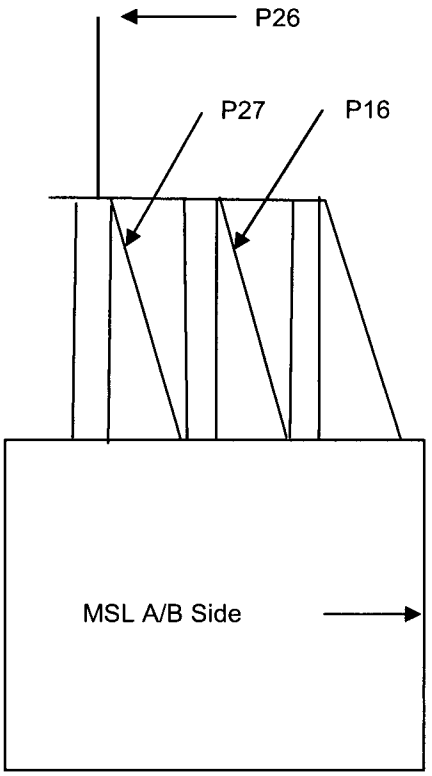

Figure 6-14
Pressure transducer locations on QC2 dryer inner hoods

6.5.1.1 Main Steam Line Instrumentation

In addition to the pressure transducers on the steam dryer, two strain gage pairs were mounted at 90° from each other at each of two locations on each of the four main steam lines, upstream of the ERV standpipes, as summarized in Table 6-2. These data proved reliable throughout the QC2 startup. The strain gage data were taken at 2000 samples/sec, while the pressure sensor data were taken at 2048 samples/sec, on different recording systems. Thus, the two data sets each included a channel for a trigger. In this way a common zero time could be established for the strain gage pairs and the pressure sensors, so as to eliminate any phasing differences. The analysis was conducted to 200 Hz.

6.5.1.2 QC2 Tests used for Model Validation

Content Deleted-
Contains EPRI and Continuum Dynamics Inc. Proprietary Information

Table 6-2
Location of strain gage pairs on main steam lines

Content Deleted-
Contains EPRI and Continuum Dynamics Inc. Proprietary Information

Table 6-3
Summary QC2 power level used to finalize key parameters and validate ACM Revision 4

Content Deleted-
Contains EPRI and Continuum Dynamics Inc. Proprietary Information

6.5.2 ACM Revision 4 Model/Data Comparisons

The development of the ACM Revision 4 predictive methodology was necessitated by two conditions: (1) the need to include a low frequency contribution beyond that provided by the acoustic load alone, and (2) the desire to reduce uncertainty levels when comparing model predictions with QC2 data, as compared to those for previous revisions of the methodology.

Content Deleted-
Contains EPRI and Continuum Dynamics Inc. Proprietary Information

Content Deleted-
Contains EPRI and Continuum Dynamics Inc. Proprietary Information

Figure 6-15
ACM Revision 4 predictions at 790 MWe at the dryer pressure sensors: peak minimum (top) and peak maximum (bottom) pressure levels, with data (blue) and predictions (red).

Content Deleted-
Contains EPRI and Continuum Dynamics Inc. Proprietary Information

Figure 6-16
PSD comparison for 790 MWe for pressure sensor data (blue curves) and ACM Revision 4 prediction (red curves), for sensor P20: PSD scale is logarithmic (top); PSD scale is linear (bottom).

Content Deleted-
Contains EPRI and Continuum Dynamics Inc. Proprietary Information

Figure 6-17
PSD comparison for 790 MWe for pressure sensor data (blue curves) and ACM Revision 4 prediction (red curves), for sensor P21: PSD scale is logarithmic (top); PSD scale is linear (bottom).

6.5.3 Evaluation of ACM Revision 4 Prediction Bias and Uncertainty

Once predictions have been made with ACM Revision 4, those predictions can be compared with the QC2 data to determine bias and uncertainty levels.

6.5.3.1 Data used for Evaluation of Bias and Uncertainty

As shown in this section, model comparisons with data demonstrate the high degree of correlation found in the application of the acoustic circuit methodology Revision 4 to the QC2 steam dryer, steam dome, and main steam lines. It is natural then to ask about the applicable range of the model and where model uncertainty is anticipated.

The approach taken for bias and uncertainty is

Content Deleted-
Contains EPRI and Continuum Dynamics Inc. Proprietary Information

Content Deleted-
Contains EPRI and Continuum Dynamics Inc. Proprietary Information

Figure 6-18
Modified bounding pressure comparisons (790 MWe) at the six averaged pressure sensors: P1, P2, and P3 (top); P4, P5, and P6 (bottom): data (blue curves), model predictions (red curves).

Content Deleted-
Contains EPRI and Continuum Dynamics Inc. Proprietary Information

Figure 6-19
Modified bounding pressure comparisons (790 MWe) at the six averaged pressure sensors: P7, P8, and P9 (top); P10, P11, and P12 (bottom): data (blue curves), model predictions (red curves).

Content Deleted-
Contains EPRI and Continuum Dynamics Inc. Proprietary Information

Figure 6-20
Modified bounding pressure comparisons (790 MWe) at the six averaged pressure sensors: P19 and P21 (top); P18 and P20 (bottom): data (blue curves), model predictions (red curves).

6.5.3.2 Bias and Uncertainty Evaluation

Bias is computed by taking the difference between the measured and predicted RMS pressure values for the six "averaged pressures" group, and dividing the mean of this difference by the mean of the predicted RMS. RMS is computed by integrating the PSD across the frequency range of interest and taking the square root

$$\text{BIAS} = \frac{\frac{1}{N}\sum(\text{RMS}_{\text{measured}} - \text{RMS}_{\text{predicted}})}{\frac{1}{N}\sum \text{RMS}_{\text{predicted}}} \qquad (6.5.1)$$

where $\text{RMS}_{\text{measured}}$ is the RMS of the measured data and $\text{RMS}_{\text{predicted}}$ is the RMS of the predicted data. Summations are over the number of "averaged pressures", or N = 6.

Uncertainty is defined as the fraction computed by the standard deviation

$$\text{UNCERTAINTY} = \frac{\sqrt{\frac{1}{N}\sum(\text{RMS}_{\text{measured}} - \text{RMS}_{\text{predicted}})^2}}{\frac{1}{N}\sum \text{RMS}_{\text{predicted}}} \qquad (6.5.2)$$

ACM bias and uncertainty summary results are compiled for specified frequency ranges of interest and summarized in Table 6-4. The bias and uncertainty values within ±2 Hz of each of the three standpipe frequencies at QC2 (discussed in Section 4) are shown in Table 6-5. The values for Dresser 6×8, Electromatic, and Target Rock are computed from Equations (6.5.1) and (6.5.2) across the frequency intervals shown for each valve type.

Table 6-4
QC2 bias and uncertainty values for specified frequency intervals

Content Deleted-
Contains EPRI and Continuum Dynamics Inc. Proprietary Information

Table 6-5
QC2 bias and uncertainty values at standpipe resonances

Content Deleted-
Contains EPRI and Continuum Dynamics Inc. Proprietary Information

6.5.3.3 Revised Bias and Uncertainty Values at Acoustic Excitation Frequencies

Content Deleted-
Contains EPRI and Continuum Dynamics Inc. Proprietary Information

Table 6-6
QC2 bias and uncertainty values at standpipe resonances with optimal axial strain gage spacing

Content Deleted-
Contains EPRI and Continuum Dynamics Inc. Proprietary Information

6.5.4 Blind Benchmark

To provide further confidence in the adequacy of the ACM Revision 4 model, an additional comparison was made to another QC2 data set at power conditions above OLTP, corresponding to Content Deleted-Contains EPRI and Continuum Dynamics Inc. Proprietary Information.

Table 6-7
QC2 blind benchmark test conditions

Content Deleted-
Contains EPRI and Continuum Dynamics Inc. Proprietary Information

A comparison of ACM Revision 4 model predictions of maximum and minimum peak pressures to those measured at 820 MWe are shown in Figure 6-22. It should be noted that sensors P13 and P14 are positioned on the inner side of the outer bank hoods (aligned opposite P3 and P20, respectively), P16 and P27 are positioned on the outside of inner bank hoods, P26 is on a mast above the dryer, and P19 is considered inoperative by GE. Predictions of minimum and maximum peak pressures bound the QC2 dryer data except for sensors P14, P16, and P27.

Content Deleted-
Contains EPRI and Continuum Dynamics Inc. Proprietary Information

Content Deleted-
Contains EPRI and Continuum Dynamics Inc. Proprietary Information

Figure 6-21
ACM Revision 4 predictions at 820 MWe at the dryer pressure sensors: peak minimum (top) and peak maximum (bottom) pressure levels, with data (blue) and predictions (red).

Content Deleted-
Contains EPRI and Continuum Dynamics Inc. Proprietary Information

Figure 6-22
Modified bounding pressure comparisons (820 MWe) at the six averaged pressure sensors: P1, P2, and P3 (top); P4, P5, and P6 (bottom): data (blue curves), model predictions (red curves).

Content Deleted-
Contains EPRI and Continuum Dynamics Inc. Proprietary Information

Figure 6-23
Modified bounding pressure comparisons (820 MWe) at the six averaged pressure sensors: P7, P8, and P9 (top); P10, P11, and P12 (bottom): data (blue curves), model predictions (red curves).

Content Deleted-
Contains EPRI and Continuum Dynamics Inc. Proprietary Information

Figure 6-24
Modified bounding pressure comparisons (820 MWe) at the six averaged pressure sensors: P19 and P21 (top); P18 and P20 (bottom): data (blue curves), model predictions (red curves).

A comparison of bias and uncertainty values computed for the 790 MWe case to those computed for the 820 MWe case are summarized in Table 6-8.

Table 6-8
ACM Revision 4 bias and uncertainty comparison

Content Deleted-
Contains EPRI and Continuum Dynamics Inc. Proprietary Information

As shown in Table 6-8, the ACM Revision 4 predictive ability is determined to be essentially the same based on benchmarking using QC2 data obtained at two different plant power levels.

6.6 Overall Bias and Uncertainty in ACM Revision 4

The bias and uncertainty values identified in Table 6-8 are added together to compute an overall uncertainty that multiplies up the predicted pressure loading on the dryer to account for the model not identically predicting the QC2 data. Besides the model comparison with data, there are several sources of additional bias and uncertainty values that must be taken into account as well. These additional bias and uncertainty values arise from two sources: (1) the accuracy of the strain gage measurements on the main steam lines (detailed in Section 5.7), and (2) the accuracy of the pressure measurements on the QC2 steam dryer.

Content Deleted-
Contains EPRI and Continuum Dynamics Inc. Proprietary Information

Table 6-9
Overall uncertainty on ACM Revision 4 predictions at 790 and 820 MWe

Content Deleted-
Contains EPRI and Continuum Dynamics Inc. Proprietary Information

Another way of plotting the model comparison shown in Figure 6-16 and Figure 6-22 is to plot the measured peak pressures on the horizontal scale and the predicted peak pressures on the vertical scale. Figure 6-26 plots the 790 MWe data from Figure 6-16, while Figure 6-27 plots the 790 MWe data with multiplication by the overall uncertainty given in the second column of Table 6-9. Figure 6-28 plots the 820 MWe data from Figure 6-22, while Figure 6-29 plots the 820 MWe data with multiplication by the overall uncertainty given in the last column of Table 6-9.

Content Deleted-
Contains EPRI and Continuum Dynamics Inc. Proprietary Information

Content Deleted-
Contains EPRI and Continuum Dynamics Inc. Proprietary Information

Figure 6-25
Comparison between measured and predicted peak pressures at the 27 pressure sensors in QC2 at 790 MWe. The line is the one-to-one boundary.

Content Deleted-
Contains EPRI and Continuum Dynamics Inc. Proprietary Information

Figure 6-26
Comparison between measured and predicted peak pressures at the 27 pressure sensors in QC2 at 790 MWe with overall uncertainty added to the predicted load. The line is the one-to-one boundary.

Content Deleted-
Contains EPRI and Continuum Dynamics Inc. Proprietary Information

Figure 6-27
Comparison between measured and predicted peak pressures at the 27 pressure sensors in QC2 at 820 MWe. The line is the one-to-one boundary.

Content Deleted-
Contains EPRI and Continuum Dynamics Inc. Proprietary Information

Figure 6-28
Comparison between measured and predicted peak pressures at the 27 pressure sensors in QC2 at 820 MWe with overall uncertainty added to the predicted load. The line is the one-to-one boundary.

6.7 Conclusions

The model evaluation presented herein confirms the adequacy of the C.D.I. acoustic circuit model ACM Revision 4 for use with in-plant strain gage data collected on main steam lines. The model with "locked" modeling parameters can be used with other steam dryer geometries and other main steam line configurations to provide a representative pressure loading on the steam dryer.

Content Deleted-
Contains EPRI and Continuum Dynamics Inc. Proprietary Information

An alternative evaluation approach, based on pressure transducer measurements on the steam dryer, is discussed in Appendix F.

6.8 References

6.1. Indiana University Chemistry Department / Babcock and Wilcox Co. Fossil Generation Division. Subprograms of 1967 ASME Steam Tables. Quantum Chemistry Program Exchange Program No. SPHF006.

6.2. Bliss, D. B., T. R. Quackenbush, and M. E. Teske. 1982. Computational Simulation of High-Speed Steady Homogeneous Two-Phase Flow in Complex Piping Systems. *Transactions of the ASME Journal of Pressure Vessel Technology* 104: 272-277.

6.3. General Electric Company (C. Hinds). 2005. Dryer Sensor Locations. Letter Report No. GE-ENG-DRY-087. Dated 18 May 2005.

6.4. Communication from Enrico Betti. 2006. Excerpts from Entergy Calculation VYC-3001 (Rev. 3), EPU Steam Dryer Acceptance Criteria, Attachment I: VYNPS Steam Dryer Load Uncertainty (Proprietary).

6.5. Structural Integrity Associates, Inc. 2005. Quad Cities Strain Gage Evaluation. Calculation Package File No. EXLN-20Q-301 (Rev. 0). Project No. EXLN-20Q.

6.6. Exelon Nuclear Generating Co. 2005. An Assessment of the Effects of Uncertainty in the Application of Acoustic Circuit Model Predictions to the Calculation of Stresses in the Replacement Quad Cities Units 1 and 2 Steam Dryers (Rev. 0). Document No. AM-2005-008.

7
MSIV CLOSURE TESTING

In accordance with guidance in BWRVIP-182, C.D.I. has developed a conservative analytical method for constructing a composite dryer load from main steam line strain gage data when one of the main steam line stop valves is closed. MSIV closure serves as an alternative way to obtain EPU power level dryer loads, rather than through the use of one-eighth scale testing (to be discussed in Section 8). This section describes the approach and its potential for predicting pressure loads at EPU power when the plant is running at below CLTP conditions. This approach can also be used as a means of screening for MSL acoustic excitation.

7.1 Testing Objectives

An MSIV closure test would enable the following:

1. Computation of a conservative EPU pressure load on a dryer, based on full-scale in-plant MSL data, which can then be used to predict the conservative stresses that will likely exist at EPU conditions.
2. Verification of the approach with the development of a conservative CLTP pressure load, based on full-scale data with one MSIV closed, that could be checked against full-scale data taken at CLTP conditions with all MSIVs open.
3. Screen for potential acoustic excitation at full scale at EPU conditions, without going to EPU conditions.

7.2 Testing Approach

Content Deleted-
Contains EPRI and Continuum Dynamics Inc. Proprietary Information

Content Deleted-
Contains EPRI and Continuum Dynamics Inc. Proprietary Information

Content Deleted-
Contains EPRI and Continuum Dynamics Inc. Proprietary Information

Figure 7-1
Schematic of top view of steam dome and four main steam lines: A, B, C, and D.

Content Deleted-
Contains EPRI and Continuum Dynamics Inc. Proprietary Information

Content Deleted-
Contains EPRI and Continuum Dynamics Inc. Proprietary Information

Content Deleted-
Contains EPRI and Continuum Dynamics Inc. Proprietary Information

Figure 7-2
PSD comparisons of MSL pressures on main steam line A at 75% power (upper locations, top; lower locations, bottom), comparing the signals with MSIV D closed (blue curves) and MSIV C closed (red curves).

Content Deleted-
Contains EPRI and Continuum Dynamics Inc. Proprietary Information

Figure 7-3
PSD comparisons of MSL pressures on main steam line B at 75% power (upper locations, top; lower locations, bottom), comparing the signals with MSIV D closed (blue curves) and MSIV C closed (red curves).

Content Deleted-
Contains EPRI and Continuum Dynamics Inc. Proprietary Information

Figure 7-4
PSD comparisons of MSL pressures on main steam line C at 75% power (upper locations, top; lower locations, bottom), comparing the signals with MSIV B closed (blue curves) and MSIV A closed (red curves).

Content Deleted-
Contains EPRI and Continuum Dynamics Inc. Proprietary Information

Figure 7-5
PSD comparisons of MSL pressures on main steam line D at 75% power (upper locations, top; lower locations, bottom), comparing the signals with MSIV B closed (blue curves) and MSIV A closed (red curves).

Content Deleted-
Contains EPRI and Continuum Dynamics Inc. Proprietary Information

Figure 7-6
Time history comparisons of MSL pressures on the upper locations of main steam line A and D at 75% power (top) and lower locations (bottom). The MSL A signal is obtained for MSIV D closed (blue curves), while the MSL D signal is obtain for MSIV A closed (red curves).

7.3 Testing Results

Content Deleted-
Contains EPRI and Continuum Dynamics Inc. Proprietary Information

Content Deleted-
Contains EPRI and Continuum Dynamics Inc. Proprietary Information

Figure 7-7
Comparisons of low resolution loads at CLTP power level from CLTP conditions (100% power level) and 75% power conditions (100% composite).

7.4 Testing Conclusions

The comparison shown in Figure 7-7 is encouraging, and suggests that MSIV closure is a viable way of conservatively estimating dryer loads at power levels above CLTP conditions.

8
METHODOLOGY FOR PREDICTING THE EFFECT OF MSL FLOW RATE ON MSL PRESSURES (WHEN ACOUSTIC EXCITATION IS PRESENT)

In accordance with guidance in BWRVIP-182, C.D.I. has developed proprietary analytical and test methods for measuring at subscale the effects of possible acoustic excitation in the main steam lines caused by the standpipe/valves. This section describes the test procedure and expected results, particularly with regard to **Content Deleted-Contains EPRI and Continuum Dynamics Inc. Proprietary Information**

8.1 Objectives and Scope

Construction of a nominal one-eighth scale model of the complete steam delivery system at a plant, from the steam dome to the turbine, is done so as to achieve the following:

1. Measure the excitation frequency and amplitudes of the as-built standpipe/valve configuration (encompassing all four main steam lines), and determine the behavior of the system at CLTP and EPU conditions.

2. Provide subscale main steam line pressure data to **Content Deleted-Contains EPRI and Continuum Dynamics Inc. Proprietary Information**

8.2 One-Eighth Scale Testing Approach

A one-eighth scale four-line test facility is proposed as a means of measuring the effect of standpipes on the anticipated acoustic signal to the steam dome. The one-eighth scale model test includes a **Content Deleted-Contains EPRI and Continuum Dynamics Inc. Proprietary Information**

Content Deleted-
Contains EPRI and Continuum Dynamics Inc. Proprietary Information

Content Deleted-
Contains EPRI and Continuum Dynamics Inc. Proprietary Information

Figure 8-1
One-eighth scale model of the QC2 reactor vessel

Content Deleted-
Contains EPRI and Continuum Dynamics Inc. Proprietary Information

Figure 8-2
One-eighth scale model of a steam dryer

Content Deleted-
Contains EPRI and Continuum Dynamics Inc. Proprietary Information

Figure 8-3
Reactor vessel

Content Deleted-
Contains EPRI and Continuum Dynamics Inc. Proprietary Information

Figure 8-4
Stepping back shows the D-ring and turbine control valve assembly (resting on the table on the center left of the picture)

Content Deleted-
Contains EPRI and Continuum Dynamics Inc. Proprietary Information

Figure 8-5
A view of the D-ring and the piping leading to the turbine control valves and out the turbine. From top to bottom, MSLs are identified as B, A, D, and C.

Content Deleted-
Contains EPRI and Continuum Dynamics Inc. Proprietary Information

Figure 8-6
A view from the turbine end of the test rig. The four MSLs are the correctly scaled lengths.

8.3 One-Eighth Scale Test System Description

The purpose of the testing effort is to measure the excitation frequency and amplitudes of the as-built standpipe/valve configuration, and determine its behavior at CLTP and EPU conditions. To do so, a one-eighth scale test facility is constructed that represents the full-scale steam delivery system.

The scaling basis for one-eighth scale follows exactly as the scaling basis for one-fifth scale, and is found in Section 4.4.

In the subscale tests summarized herein for QC2, the main steam lines at the safety valves are 1.0/7.83 scale and the reactor dome and steam dryer are 1.0/8.04. This slight difference in scale results from commercially available hemispherical vessel heads and readily available piping.

The line geometry upstream of the valves is geometrically scaled on all four main steam lines so that the valve standpipes see a prototypical flow profile. Downstream of the standpipes, the scaled main steam lines each end at their turbine location with a test initiation full bore ball valve and an orifice plate that sets the test Mach number.

A schematic of the typical setup of the steam delivery system is shown in Figure 8-7. **Content Deleted-Contains EPRI and Continuum Dynamics Inc. Proprietary Information**

Content Deleted-
Contains EPRI and Continuum Dynamics Inc. Proprietary Information

Figure 8-7
Schematic of a typical steam delivery system. Segment lengths marked 1 to 11 connect the steam dome to the turbine. Typically, the standpipe/valves are positioned on segment 5, and a steam header is placed along segment 8, while the main steam turbine stop valve is located between segment 10 and 11 in the plant.

Content Deleted-
Contains EPRI and Continuum Dynamics Inc. Proprietary Information

Content Deleted-
Contains EPRI and Continuum Dynamics Inc. Proprietary Information

Content Deleted-
Contains EPRI and Continuum Dynamics Inc. Proprietary Information

Figure 8-8
Behavior of the inlet Mach number and the Mach number immediately upstream of the orifice plates, as a function of the ratio of the orifice area A_a to the pipe area A, for a typical one-eighth scale test.

Content Deleted-
Contains EPRI and Continuum Dynamics Inc. Proprietary Information

Figure 8-9
Normalized RMS pressure (RMS pressure normalized by the dynamic pressure at CLTP conditions) for the pressure transducer at the end of a standpipe/valve, as a function of inlet and orifice Mach numbers. The two curves illustrate the shift in Mach number from the use of the inlet Mach number (blue points) to the use of the Mach number immediately upstream of the orifice (red points). CLTP and EPU Mach numbers are shown for this plant.

8.4 Validation of One-Eighth Scale Test System

One of the objectives of subscale testing is to develop **Content Deleted-Contains EPRI and Continuum Dynamics Inc. Proprietary Information** that relate unsteady steam dryer loads at CLTP conditions to those anticipated at EPU conditions. **Content Deleted-Contains EPRI and Continuum Dynamics Inc. Proprietary Information** would then be applied to full-scale CLTP strain gage data collected on the main steam lines to obtain a conservative estimate of the full-scale EPU strain gage data. The EPU strain gage data would then be used to estimate steam dryer stresses at EPU power.

As discussed previously, Exelon recorded pressure data on its replacement QC2 steam dryer at several power levels, including OLTP and EPU [8.4]. These two data sets, at 790 MWe (used in Section 6.5 for ACM validation) and 930 MWe, respectively, provide the data needed to validate the use of **Content Deleted-Contains EPRI and Continuum Dynamics Inc. Proprietary Information** methodology with the subscale test results from a one-eighth scale test [8.3].

Content Deleted-
Contains EPRI and Continuum Dynamics Inc. Proprietary Information

Content Deleted-
Contains EPRI and Continuum Dynamics Inc. Proprietary Information

Figure 8-10
Content Deleted-Contains EPRI and Continuum Dynamics Inc. Proprietary Information generated from QC2 main steam line data between OLTP and EPU power levels. The separate curves identify the strain gage locations on the main steam lines. The standpipe excitation frequencies of 115 Hz (Target Rock), 135 Hz (Electromatic), and 155 Hz (Dresser 6x8) are clearly seen in the plot.

Content Deleted-
Contains EPRI and Continuum Dynamics Inc. Proprietary Information

Content Deleted-
Contains EPRI and Continuum Dynamics Inc. Proprietary Information

Content Deleted-
Contains EPRI and Continuum Dynamics Inc. Proprietary Information

Figure 8-11
Normalized PSD for Test qc2-2: as-built configuration at a Mach number = OLTP. PD1: MSL A upstream strain gage location; PD2: MSL A downstream strain gage location; and PD11: Target Rock standpipe/valve end.

Content Deleted-
Contains EPRI and Continuum Dynamics Inc. Proprietary Information

Figure 8-12
Normalized PSD for Test qc2-2: as-built configuration at a Mach number = OLTP. PD3: MSL B upstream strain gage location; PD4: MSL B downstream strain gage location.

Content Deleted-
Contains EPRI and Continuum Dynamics Inc. Proprietary Information

Figure 8-13
Normalized PSD for Test qc2-2: as-built configuration at a Mach number = OLTP. PD5: MSL C upstream strain gage location; PD6: MSL C downstream strain gage location

Content Deleted-
Contains EPRI and Continuum Dynamics Inc. Proprietary Information

Figure 8-14
Normalized PSD for Test qc2-2: as-built configuration at a Mach number = OLTP. PD7: MSL D upstream strain gage location; PD8: MSL D downstream strain gage location.

Content Deleted-
Contains EPRI and Continuum Dynamics Inc. Proprietary Information

Figure 8-15
Normalized PSD for Test qc2-8: as-built configuration at a Mach number = EPU. PD1: MSL A upstream strain gage location; PD2: MSL A downstream strain gage location; and PD11: Target Rock standpipe/valve end.

Content Deleted-
Contains EPRI and Continuum Dynamics Inc. Proprietary Information

Figure 8-16
Normalized PSD for Test qc2-8: as-built configuration at a Mach number = EPU. PD3: MSL B upstream strain gage location; PD4: MSL B downstream strain gage location.

Content Deleted-
Contains EPRI and Continuum Dynamics Inc. Proprietary Information

Figure 8-17
Normalized PSD for Test qc2-8: as-built configuration at a Mach number = EPU. PD5: MSL C upstream strain gage location; PD6: MSL C downstream strain gage location.

\Cntent Deleted-
Contains EPRI and Continuum Dynamics Inc. Proprietary Information

Figure 8-18
Normalized PSD for Test qc2-8: as-built configuration at a Mach number = EPU. PD7: MSL D upstream strain gage location; PD8: MSL D downstream strain gage location.

Content Deleted-
Contains EPRI and Continuum Dynamics Inc. Proprietary Information

Figure 8-19
Normalized PSD for Test qc2-12: as-built configuration at a Mach number = EPU. PD1: MSL A upstream strain gage location; PD2: MSL A downstream strain gage location; and PD11: Target Rock standpipe/valve end.

Content Deleted-
Contains EPRI and Continuum Dynamics Inc. Proprietary Information

Figure 8-20
Normalized PSD for Test qc2-12: as-built configuration at a Mach number = EPU. PD3: MSL B upstream strain gage location; PD4: MSL B downstream strain gage location.

Content Deleted-
Contains EPRI and Continuum Dynamics Inc. Proprietary Information

Figure 8-21
Normalized PSD for Test qc2-12: as-built configuration at a Mach number = EPU. PD5: MSL C upstream strain gage location; PD6: MSL C downstream strain gage location.

Content Deleted-
Contains EPRI and Continuum Dynamics Inc. Proprietary Information

Figure 8-22
Normalized PSD for Test qc2-12: as-built configuration at a Mach number = EPU. PD7: MSL D upstream strain gage location; PD8: MSL D downstream strain gage location.

Content Deleted-
Contains EPRI and Continuum Dynamics Inc. Proprietary Information

Figure 8-23
Content Deleted-Contains EPRI and Continuum Dynamics Inc. Proprietary Information generated from subscale data qc2-2 (OLTP) and qc2-8 (EPU). The separate curves identify the strain gage locations on the main steam lines.

Content Deleted-
Contains EPRI and Continuum Dynamics Inc. Proprietary Information

Figure 8-24
Content Deleted-Contains EPRI and Continuum Information generated Dynamics Inc. Proprietary **from subscale data qc2-2 (OLTP) and qc2-12 (EPU). The separate curves identify the strain gage locations on the main steam lines.**

Content Deleted-
Contains EPRI and Continuum Dynamics Inc. Proprietary Information

Figure 8-25
ACM Revision 4 predictions at 930 MWe at the dryer pressure sensors: peak minimum (top) and peak maximum (bottom) pressure levels, with data (blue) and predictions for subscale data #1 (red) and subscale data #2 (green).

Content Deleted-
Contains EPRI and Continuum Dynamics Inc. Proprietary Information

Figure 8-26
Modified bounding pressure comparisons (930 MWe) at the six averaged pressure sensors: P1, P2, and P3 (top); P4, P5, and P6 (bottom): data (blue curves), model predictions with subscale data #1 (red curves) and subscale data #2 (green curves).

Content Deleted-
Contains EPRI and Continuum Dynamics Inc. Proprietary Information

Figure 8-27
Modified bounding pressure comparisons (930 MWe) at the six averaged pressure sensors: P7, P8, and P9 (top); P10, P11, and P12 (bottom): data (blue curves), model predictions with subscale data #1 (red curves) and subscale data #2 (green curves).

Content Deleted-
Contains EPRI and Continuum Dynamics Inc. Proprietary Information

Figure 8-28
Modified bounding pressure comparisons (790 MWe) at the six averaged pressure sensors: P19 and P21 (top); P18 and P20 (bottom): data (blue curves), model predictions with subscale data #1 (red curves) and subscale data #2 (green curves).

8.5 Bias and Uncertainty Associated with Prediction of MSL Flow Rate Effects on MSL Pressure Amplitudes

The averaged predicted pressures at EPU may then be used to generate the bias and uncertainty with respect to the EPU data and compare the results with the bias and uncertainty for the QC2 data at OLTP conditions. This approach, as discussed previously in Section 6.5, results in the

comparisons shown in Table 8-1 **Content Deleted-Contains EPRI and Continuum Dynamics Inc. Proprietary Information.**

Table 8-1
Composite ACM Bias and Uncertainty Based on QC2 EPU Data with the First Bump-Up Factor (Subscale Data #1) Applied to QC2 OLTP Data

Content Deleted-
Contains EPRI and Continuum Dynamics Inc. Proprietary Information

Table 8-2
Composite ACM Bias and Uncertainty Based on QC2 EPU Data with the Second Bump-Up Factor (Subscale Data #2) Applied to QC2 OLTP Data

Content Deleted-
Contains EPRI and Continuum Dynamics Inc. Proprietary Information

Content Deleted-
Contains EPRI and Continuum Dynamics Inc. Proprietary Information

Figure 8-29
Comparison between measured and predicted peak pressures at the 27 pressure sensors in QC2 at 930 MWe for subscale data #1. The line is the one-to-one boundary.

Content Deleted-
Contains EPRI and Continuum Dynamics Inc. Proprietary Information

Figure 8-30
Comparison between measured and predicted peak pressures at the 27 pressure sensors in QC2 at 930 MWe for subscale data #1 with overall uncertainty added to the predicted load. The line is the one-to-one boundary.

Content Deleted-
Contains EPRI and Continuum Dynamics Inc. Proprietary Information

Figure 8-31
Comparison between measured and predicted peak pressures at the 27 pressure sensors in QC2 at 930 MWe for subscale data #2. The line is the one-to-one boundary.

Content Deleted-
Contains EPRI and Continuum Dynamics Inc. Proprietary Information

Figure 8-32
Comparison between measured and predicted peak pressures at the 27 pressure sensors in QC2 at 930 MWe for subscale data #2 with overall uncertainty added to the predicted load. The line is the one-to-one boundary.

8.6 References

8.1 Shapiro, A. H. 1953. The Dynamics and Thermodynamics of Compressible Fluid Flow. Volume I. John Wiley and Sons: New York, NY. Chapter 4.

8.2 Kayser, J. C. and R. L. Shambaugh. 1991. Discharge Coefficients for Compressible Flow through Small-Diameter Orifices and Convergent Nozzles. *Chemical Engineering Science* 46: 1697-1711.

8.3. Continuum Dynamics, Inc. 2006. Mitigation of Pressure Oscillations in the Quad Cities Unit 2 Steam Delivery System: A Subscale Four Main Steam Line Investigation of Standpipe Behavior (Rev. 0). C.D.I. Report 06-08.

8.4. Continuum Dynamics, Inc. 2007. Bounding Methodology to Predict Full Scale Steam Dryer Loads from In-Plant Measurements (Rev. 4). C.D.I. Report No. 05-28.

9
STRESS ANALYSIS METHODOLOGY

The purpose of this section is to define the methodology for performing a stress analysis of the steam dryer at extended power uprate (EPU) operating conditions. This section provides a general overview of the methodology used to predict the structural response to flow induced vibration loading, followed by a detailed description of the processes, assumptions, and bases of the structural finite element analysis performed for the steam dryer.

9.1 Overview

The steam dryer stress analysis includes primary stress (P) and fatigue evaluations (P+Q+F) consistent with the intent of the American Society of Mechanical Engineers Boiler and Pressure Vessel Code (ASME B&PV Code). Although the steam dryer is not a Code component, the methods and allowable stress intensities contained within the ASME B&PV Code, Section III, Subsection NG [9.1] are used as guidelines for this evaluation. Further, the approach described in this section follows guidance provided in BWRVIP-181 "Steam Dryer Repair Design Criteria" [9.2]. Note that the secondary loads experienced by the steam dryer are insignificant; therefore, primary plus secondary (P+Q) stress checks are not applicable to this component. The primary stress check is performed using all relevant loads as defined in the plant Final Safety Analysis Report (FSAR). In the absence of loads and load combination guidance in the plant FSAR, this document provides recommendations on appropriate loads and load combinations. A fatigue evaluation is performed considering the range of alternating stresses produced in the steam dryer components from the fluctuating pressure loads contributed by normal operation Flow Induced Vibration (FIV). Development of the flow induced vibration loads are discussed in Section 6.0.

The structural analysis is performed in the frequency domain, which confers several significant computational advantages, in terms of storage and central processing unit (CPU) time, over transient or time-domain approaches. These advantages include:

- Order of magnitude reductions in computer storage and calculation time;
- Ability to impose a constant 1% damping at all frequencies;
- Elimination of the initial startup transient response (real transients due to acoustic load variations are captured);
- Ability to reanalyze the dryer for different loads (e.g., CLTP, EPU and/or frequency-shifted loads) without performing additional finite element analyses;
- Easier and faster finite element calculation restart options following computer outage; and

- The opportunity to monitor the stress intensities at a select subset of finite element nodes (100 to 200 nodes) in real- or near real-time during power ascension.

These advantages are realized through the use of "unit" solutions representing the stress distribution resulting from the application of a unit fluctuating pressure at a MSL at a particular frequency. The solutions are summed over the four main steam lines and all frequencies in the frequency band of interest.

In addition to a complete structural stress assessment, the methodology allows

Content Deleted-
Contains EPRI and Continuum Dynamics Inc. Proprietary Information

9.1.1 Application of FIV Loads to Finite Element Model (FEM)

Content Deleted-
Contains EPRI and Continuum Dynamics Inc. Proprietary Information

Content Deleted-
Contains EPRI and Continuum Dynamics Inc. Proprietary Information

Figure 9-1
The mesh interpolation sequence. The pressure differences, rather than pressures, are interpolated to prevent errors associated with interpolating pressure jumps across thin plates. The process involves: (i) interpolating the pressure jumps over surfaces, (ii) assigning pressure differences to adjacent lattice points, and (iii) spreading these values to farther neighbors.

9.1.2 Formulation of Structural Solution for FIV Loading

This steam dryer structural FEM is constructed using the commercial ANSYS finite element software [9.3] and consists of a combination of shell and solid elements. The fluctuating pressure solution described in Section 6 is applied to the structural FEM as a force per unit area. The harmonic nodal displacements $\mathbf{q}_n(\omega)$ are obtained by performing a harmonic analysis and solving the equation

Content Deleted-
Contains EPRI and Continuum Dynamics Inc. Proprietary Information

Content Deleted-
Contains EPRI and Continuum Dynamics Inc. Proprietary Information

Comparisons of stress results from a harmonic analysis based approach and a direct integration transient analysis approach have been performed for a typical steam dryer in order to demonstrate the adequacy of the harmonic methodology. These comparisons are summarized in Appendix E.2 and confirm that the harmonic method accurately recovers the steady state response with both amplitude and phase information intact.

9.1.3 Frequency Shifting to Account for FEM Uncertainties

The harmonic stress solutions can also be used to assess the effects of frequency shifts in the applied loads. The sensitivity of the stress results to modeling approximations and perturbations

Content Deleted-
Contains EPRI and Continuum Dynamics Inc. Proprietary Information

9.1.4 Application to Real-Time Power Ascension Testing

Equations (9.1.2) and (9.1.3) can be applied to individual nodes. When performing a complete stress analysis, every node on the dryer is processed for a given MSL pressure spectrum by first computing the stress harmonics from Equation (9.1.2), then converting the harmonic solution to

Content Deleted-
Contains EPRI and Continuum Dynamics Inc. Proprietary Information

9.1.5 Compensation for Additional FEM Bias and Uncertainty

An extensive vibration test was performed on a spare Boiling Water Reactor (BWR) steam dryer (See Appendix E.4). The dryer was subjected to shaker excitation at eight different locations and the dryer responses measured using accelerometers at various points on the dryer for peak forcing frequencies in the range 0 – 250 Hz. The measured response data was compared against response predictions obtained with an ANSYS finite element model and the differences between measured and computed responses used to develop an estimate of the bias and uncertainty associated with approximations, mesh discretization, and modeling idealizations in the finite element model. These approximations produce an overall uncertainty of

Content Deleted-
Contains EPRI and Continuum Dynamics Inc. Proprietary Information

9.1.6 Computational Considerations

Content Deleted-
Contains EPRI and Continuum Dynamics Inc. Proprietary Information

Content Deleted-
Contains EPRI and Continuum Dynamics Inc. Proprietary Information

9.1.7 Solution Management

Upon completion of each frequency calculation, ANSYS is instructed to export the stresses stored in text files.

Content Deleted-
Contains EPRI and Continuum Dynamics Inc. Proprietary Information

9.1.8 Calculation of Stress Intensities

Content Deleted-
Contains EPRI and Continuum Dynamics Inc. Proprietary Information

Content Deleted-
Contains EPRI and Continuum Dynamics Inc. Proprietary Information

9.1.9 Consideration of Steam Dryer Cracking

The structural analysis methodology described in this report contains the inherent assumption that the steam dryer components are uncracked. It is impractical to postulate cracking of different sizes in each steam dryer component and assess the relative effect that these cracks have on the results of the stress analysis; therefore, any cracking identified during a dryer

inspection must be evaluated on a plant specific basis. An evaluation of observed cracking should include the following two considerations:

1. Potential for additional crack growth as a result of the suspected initiation mechanism and all relevant propagation mechanisms (IGSCC, Fatigue); and
2. Effect of observed cracking on dynamic characteristics of the steam dryer.

The normal modes of a structure are generally not significantly affected by cracking unless there are a large number of cracks distributed throughout the structure or a crack is very large; nevertheless, a plant specific evaluation is considered appropriate to identify if the existence of cracking must be included in the stress analysis. The output of this evaluation will assist the utility in determining whether a repair must be applied.

9.2 Finite Element Model Description

This section describes the modeling methodology, assumptions, geometry, material properties, and boundary conditions applied to the steam dryer structural FEM. Loads and Load combinations are discussed separately in Section 9.3.

9.2.1 Steam Dryer Geometry

The analytical steam dryer geometry is built from available steam dryer design and as-built drawings. The model includes any modifications made to the dryer since fabrication. A completed model for a typical steam dryer is shown in Figure 9-2.

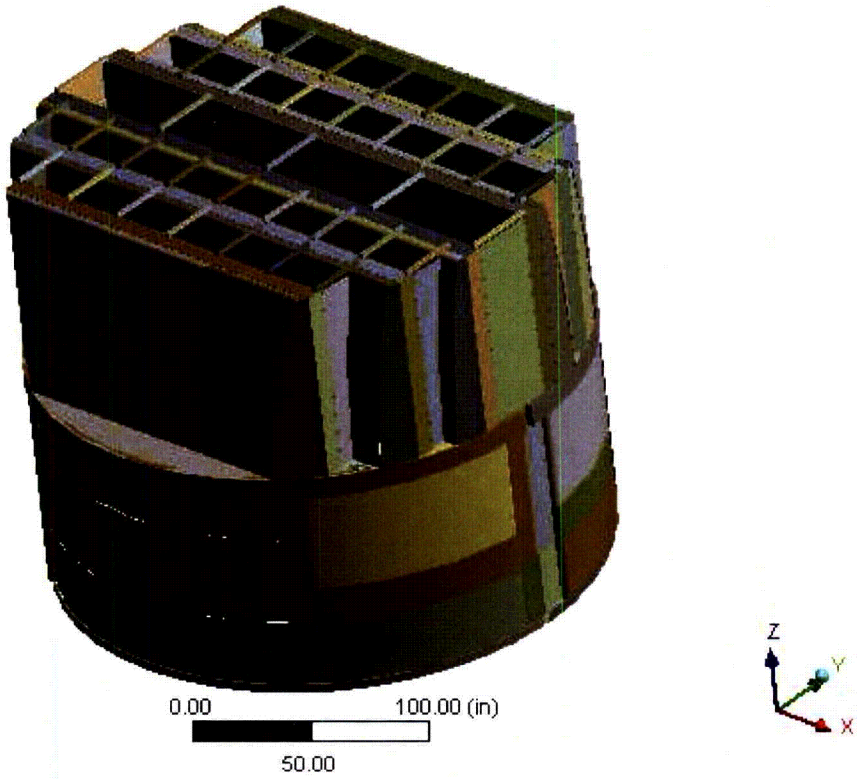

Figure 9-2
Overall geometry of a typical steam dryer ANSYS model.

9.2.2 Material Properties

The steam dryer is constructed from Type 304 stainless steel and has an operating temperature of 550°F. Material properties for a plant specific analysis are obtained from the ASME B&PV Code of Construction. Typical material properties are summarized in Table 9-1.

Content Deleted-
Contains EPRI and Continuum Dynamics Inc. Proprietary Information

Table 9-1
Typical Material Properties

Content Deleted-
Contains EPRI and Continuum Dynamics Inc. Proprietary Information

9.2.3 Model Simplifications

The following simplifications are made to achieve reasonable model size while maintaining good modeling fidelity for key structural properties:

Content Deleted-
Contains EPRI and Continuum Dynamics Inc. Proprietary Information

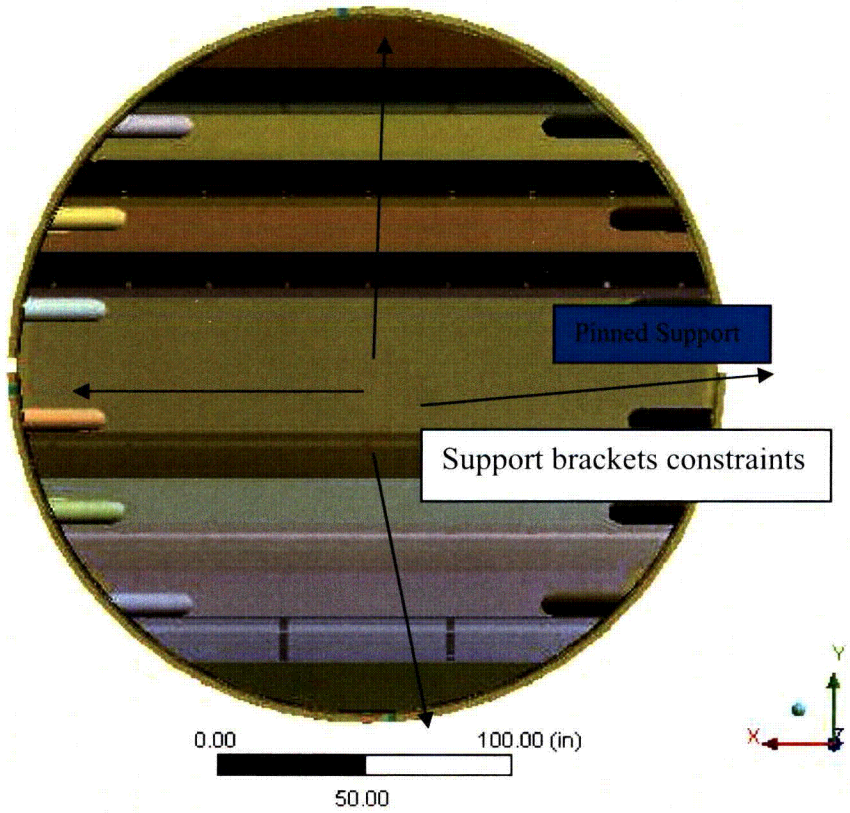

Figure 9-3
Pinned support constraints for typical steam dryer

9.2.3.1 Perforated Plate Model

Content Deleted-
Contains EPRI and Continuum Dynamics Inc. Proprietary Information

Content Deleted-
Contains EPRI and Continuum Dynamics Inc. Proprietary Information

9.2.3.2 Vane Bank Model

The vane bank assemblies consist of many vertical angled plates that are computationally expensive to model explicitly, since a prohibitive number of elements would be required. These parts have significant weight which is transmitted through the surrounding structure, so it is important to capture their gross inertial properties. Here the vane banks are modeled as a collection of point masses located at the center of mass for each vane bank section (see Figure 9-4).

Content Deleted-
Contains EPRI and Continuum Dynamics Inc. Proprietary Information

Content Deleted-
Contains EPRI and Continuum Dynamics Inc. Proprietary Information

Figure 9-4
Point masses representing the vanes. The pink shading represents where constraint equations between nodes are applied in the point mass implementation.

9.2.3.3 Water Inertia Effect on Submerged Panels

Water inertia (hydrodynamic mass) is modeled by an increase in density of the submerged structure. This added mass is determined by a separate hydrodynamic analysis and is included in the ANSYS model by modifying the density of the submerged structural elements when computing harmonic response. This additional density is given by

Content Deleted-
Contains EPRI and Continuum Dynamics Inc. Proprietary Information

9.2.3.4 Connections between Structural Components

Most connections between parts are modeled as node-to-node connections. This modeling is the correct manner of joining elements in a finite element model. At joints between shells, this approach omits the additional stiffness provided by the extra weld material. Also, locally 3D effects are more pronounced. The latter effect is accounted for using weld factors in the fatigue evaluation. The deviation in stiffness due to weld material is negligible, since weld dimensions are on the order of the shell thickness. The consequences upon modal frequencies and amplitude are, to first order, proportional to t/L, where t is the thickness and L a characteristic shell length. The errors introduced by ignoring additional weld stiffness are thus small and readily compensated for by performing frequency shifts as described in Section 9.1.3.

Content Deleted-
Contains EPRI and Continuum Dynamics Inc. Proprietary Information

Content Deleted-
Contains EPRI and Continuum Dynamics Inc. Proprietary Information

Content Deleted-
Contains EPRI and Continuum Dynamics Inc. Proprietary Information

Figure 9-5
Face to face shell to solid connection.

Content Deleted-
Contains EPRI and Continuum Dynamics Inc. Proprietary Information

Figure 9-5
Shell edge-to-solid face connection.

9.2.4 Damping in the FEM

This section describes the damping included in the ANSYS FEM for structural analyses of the steam dryer.

9.2.4.1 Structural Damping

Structural damping is defined as 1% of critical damping for all frequencies. This damping is consistent with guidance given on page 10 of NRC RG-1.20 [9.7], and is implemented in the ANSYS model by setting the damping matrix **C** in Equation (9.1.1) to

$$\mathbf{C} = \frac{2z}{\omega}\mathbf{K} \qquad (9.2.3)$$

where **K** is the stiffness matrix and ω is the forcing frequency. While this representation does not exactly enforce a constant damping ratio, the response peaks obtained with both models are identical. Moreover, one can show that for the low 1% damping considered here, the maximum difference between the response functions for the harmonic damping model above with z = 1% and a damped oscillator with constant damping ratio ζ = 1% is less than 0.5% at all frequencies.

9.2.4.2 Content Deleted-Contains EPRI and Continuum Dynamics Inc. Proprietary Information

Content Deleted-
Contains EPRI and Continuum Dynamics Inc. Proprietary Information

9.2.5 Mesh Details and Element Types

ANSYS linear SHELL63 elements are used to model the skirt, hoods, perforated plates, side and end plates, trough bottom plates, reinforcements, base plates, and cover plates. This element models bending and membrane stresses, but omits transverse shear. SHELL181 elements are used to model submerged parts of the drain channels, as fewer elements are needed to adequately resolve the curved regions; also, more accurate stresses are computed as considerable shear components develop in these areas. The use of shell elements is appropriate for most of the structure, where the characteristic thickness is small compared to the other plate dimensions.

Quadratic SOLID186 elements are used for the upper and lower support rings and tie bars as well as other components where strongly 3D stress fields can be expected. The SURF154 element is used to assure proper application of pressure loading to the structure.

Typical mesh details and element types are shown in Table 9-2 and Table 9-3.

The mesh is generated automatically by ANSYS with adaptive refinement near edges. The maximum allowable mesh spacing is specified by the user. A 3-inch maximum allowable spacing is specified everywhere except in the following areas:

- Drain pipes (2 inch maximum spacing);
- Base plates (2.75 inches);
- Perforated plates (2 inches);
- Top tie rods (0.75 inches); and
- Curved portions of the drain channels (1.5 inches).

Details of a typical steam dryer finite element mesh are shown in Figure 9-7 through Figure 9-9.

An assessment of the error due to the use of finite mesh size and modeling idealizations in ANSYS upon the response peak frequencies was performed by comparing computed modal frequencies against known analytical solutions for simple structures (see Appendix E.1). The

uncertainties determined from this study are very small and well within the range of frequency variation (±10%) used in conducting the FEM evaluations of steam dryer structural response. A more comprehensive comparison between the analytical and experimental frequency response of an actual steam dryer was performed in a full scale "shaker" test as discussed in Appendix E.4.

Table 9-2
Typical FE Model Summary

Description	Quantity
Total Nodes	90,000
Total Elements	125,000
Element Types	5
Materials	3

Table 9-3
Listing of Typical Element Types

Generic Element Type Name	Element Name	ANSYS Name
20-Node Quadratic Hexahedron	SOLID186	20-Node Hexahedral Structural Solid
4-Node Elastic Shell	SHELL63	4-Node Elastic Shell
4-Node Linear Quadrilateral Shell	SHELL181	4-Node Finite Strain Shell
Mass Element	MASS21	Structural Mass
Pressure Surface Definition	SURF154	3D Structural Surface Effect

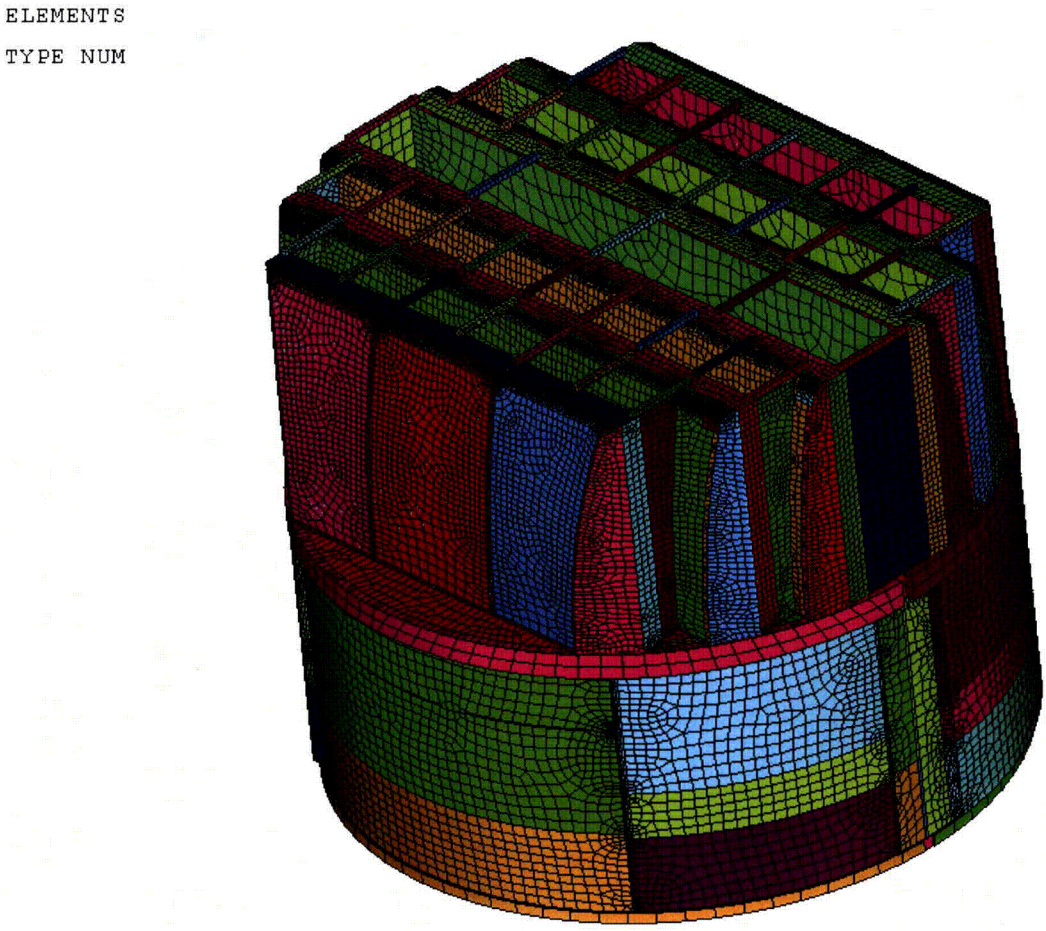

Figure 9-6
Typical FEM mesh overview. The colors emphasize structural component.

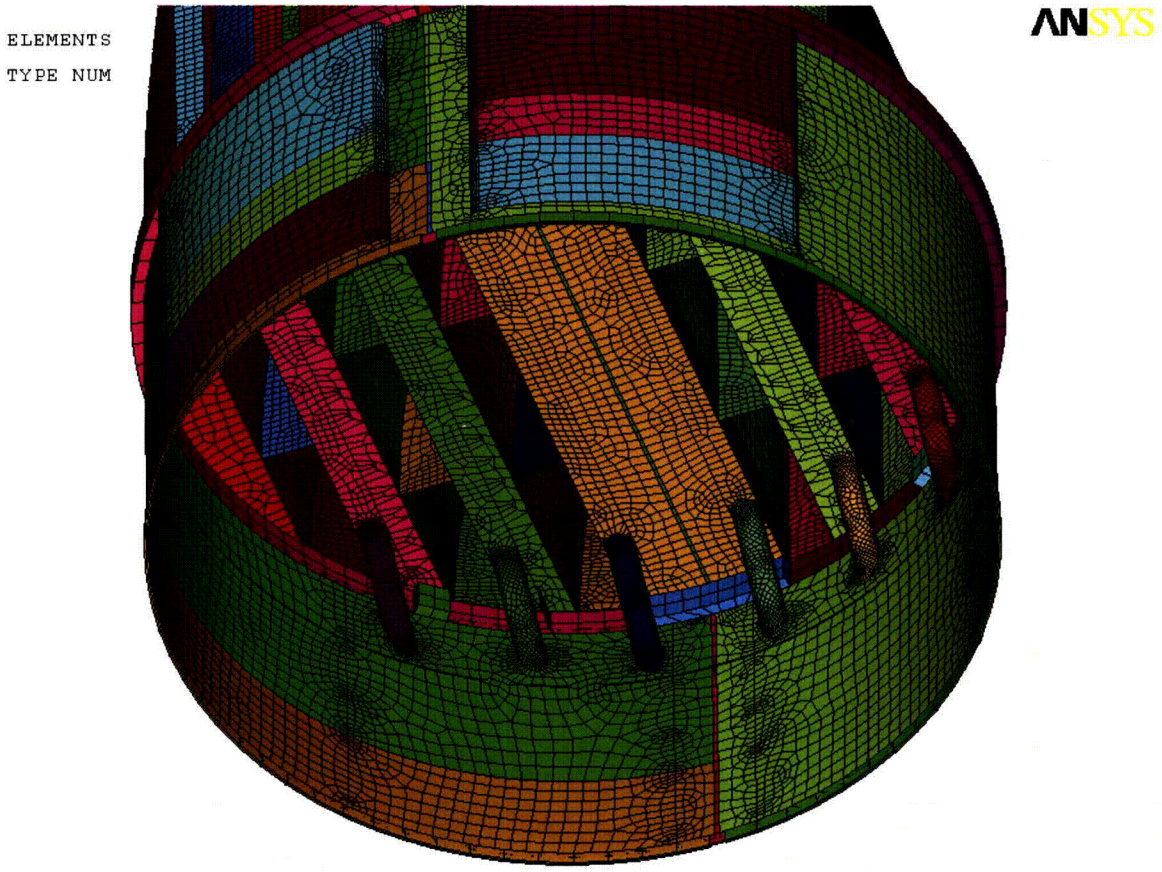

Figure 9-7
Close-up of typical mesh showing drain pipes and hood supports. The colors emphasize structural component.

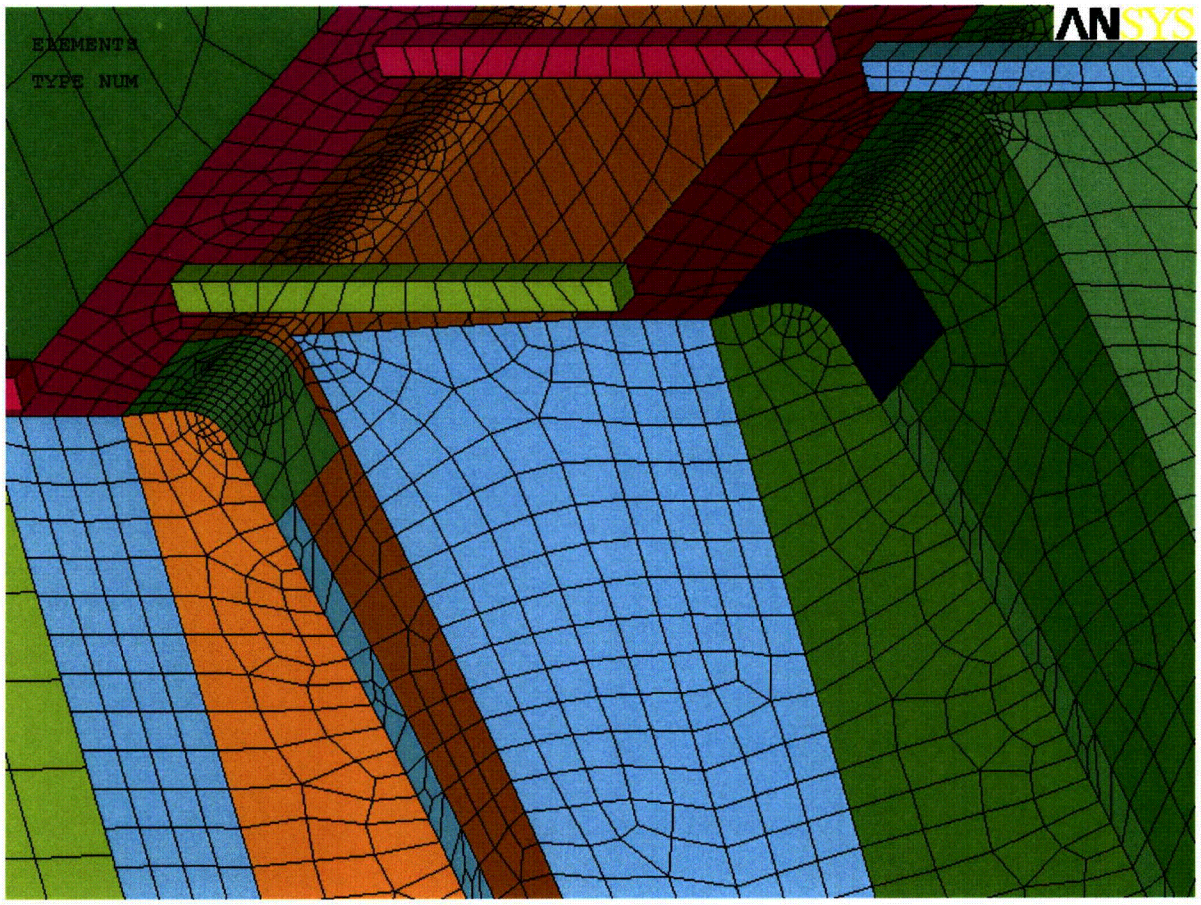

Figure 9-8
Close-up of typical mesh showing node-to-node connections between closure panels, end plates, and hoods. The colors emphasize structural component.

9.3 Loads and Load Combinations

This report documents methods for predicting:

1. FIV pressure loads on the steam dryer at EPU conditions resulting from acoustic excitation in the main steam lines and turbulent flow over the dryer at power uprate (FIV - Section 6)

2. Acoustic load on the dryer resulting from closure of the turbine stop valves (TSV_A – Section 12)

3. Flow loading on the steam dryer resulting from closure of the turbine stop valves (TSV_F – Section 12)

4. Acoustic load due to main steam line break (MSLB) outside containment, at the rated power and core flow condition ($MSLB_{A1}$ – Section 12)

5. Acoustic load due to main steam line break (MSLB) outside containment, at the low power/high core flow condition ($MSLB_{A2}$ - Section 12).

In addition, the effect of deadweight of the dryer is evaluated during the FEM analysis. To the extent that other loads specified in the tables below require evaluation, the licensee is responsible for providing the EPU load as input to the steam dryer stress analysis.

In accordance with BWRVIP-181 [9.2], stresses at EPU conditions are evaluated and compared to applicable allowable stress intensities for Service Levels A through D. A description of these Service Levels and the associated loads and load combinations, as excerpted from BWRVIP-181, is provided below.

9.3.1 Service Levels

This section summarizes the different Service Levels for which loads are defined for steam dryer analysis.

9.3.1.1 Service Level A (Normal Operating Conditions)

Service Level A loads include the combination of all sustained loads that are anticipated during normal plant/system operation. These loads include deadweight of all supported components, differential pressures, and thermal-hydraulic loads (including FIV).

9.3.1.2 Service Level B (Upset Conditions)

Service Level B loads include loads due to anticipated operational occurrences that have the potential to increase the loads acting on the reactor internals components above those experienced during normal operation. Typical events include normal operation loads plus

system operating transients (SOT). The SOTs shown on the RPV thermal cycle diagram should be used to determine the applicable transient conditions. Also, the combination of normal loads plus OBE loads is considered an upset event.

9.3.1.3 Service Level C (Emergency Conditions)

Service Level C loads include the combination of all sustained normal operation loads in conjunction with loads from the design basis pipe break (DBPB). The DBPB includes all postulated pipe breaks other than a LOCA, MSLB, or feedwater pipe break. These loads include postulated pipe breaks in Class 1 branch lines that result in the loss of reactor coolant at a rate less than or equal to the capability of the reactor coolant makeup system.

9.3.1.4 Service Level D (Faulted Conditions)

Service Level D loads include the combination of all sustained loads in conjunction with several combinations of design basis events. These combinations include the DBPB, MSLB/feedwater pipe break, or LOCA and the SSE (where applicable per the plant specific design basis). All components of these loads should be considered.

For plants that use systems for injection (e.g., jet pumps for LPCI injection and core spray injection), the loads associated with the injection are treated as a faulted condition. This assumption is acceptable provided that the system functional requirements for delivery of coolant under long term DBA conditions are ensured.

Because the MSLB is the most significant of all of the pipe breaks and since it is categorized as a Level D event, the Level C load combinations are not considered further for steam dryer analyses.

9.3.2 Load Combinations

The load combinations used in the evaluation should be consistent with the requirements of the plant SAR or related licensing basis documentation. Typically, Section 3.9 of the SAR contains the necessary information on loads including, for some plants, hydrodynamic loads (i.e., "new loads") and/or AP loads. However, steam dryer loads are not typically included in the SAR. Loads and load combinations are recommended in this document in the event that adequate definition of load combinations is not contained in the plant licensing basis documentation.

Load combinations used to analyze reactor internals vary, depending on the plant vintage. There are two major categories of plants: those with Mark II or Mark III containments where hydrodynamic events cause vessel internals loads, and those with Mark I containments where hydrodynamic effects in the torus do not cause significant loads on the vessel internals. Even for the Mark II and Mark III containments, loading on the steam dryer is bounded by the main steam line break (MSLB). Owners may eliminate any load combinations if the decision can be justified technically, e.g., demonstrate that some combinations are bounded by other loads or load combinations.

9.3.2.1 Mark I Plants

For the purposes of providing a general guideline in the event that load combinations are not specified in the SAR, the set of load combinations shown in Table 9-4 may be used.

9.3.2.2 Mark II and III Plants

For Mark II and III plants, the method for load combination was specified at the time that the loads caused by hydrodynamic events were defined and labeled "new loads". A recommended set of load combinations to be considered, in absence of plant specific documentation, is shown in Table 9-5. Load term definitions are summarized in Table 9-6.

Table 9-4
Load Combinations for Mark I Plants

Load Case	Service Conditions	Operating Condition	Load Combination[1,2,3,4,5,6,]
A	Normal	Normal Operation	$DW + DP_N + FIV$
B-1	Upset	Turbine Stop Valve Closure (Acoustic Load)	$DW + DP_N + (TSV_A^2 + FIV^2)^{1/2}$
B-2	Upset	Turbine Stop Valve Closure (Flow Reversal Load)	$DW + DP_N + TSV_F$
B-3[7]	Upset	Operating Basis Earthquake	$DW + DP_N + OBE + FIV$
B-4	Upset	Upset DP	$DW + DP_U + FIV$
C-1	Emergency	Emergency DP	$DW + DP_E + FIV$
D-1	Faulted	Main Steam Line Break plus SSE (High Power)	$DW + DP_N + (MSLB_{A1}^2 + SSE^2 + FIV^2)^{1/2}$
D-2	Faulted	Main Steam Line Break plus SSE (High Power)	$DW + MSLB_{DP1} + SSE$
D-3	Faulted	Main Steam Line Break (Under Critical Conditions – interlock)	$DW + DP_N + (MSLB_{A2}^2 + FIV^2)^{1/2}$
D-4	Faulted	Main Steam Line Break (Under Critical Conditions – interlock)	$DW + MSLB_{DP2}$

Notes:

1. The intention of considering a number of load combinations is to help determine the most conservative load condition. Owners may eliminate load combinations that can be technically justified to be bounded by other load combinations.
2. For definitions of terms see Table 9-6.
3. FIV loads are for the normal operating condition. FIV loads could be higher at some particular steam line velocities other than the normal steam line velocity. Accordingly, dwelling for extended periods of time at such flow velocities is to be avoided.
4. For plants that do not combine MSLB (limiting DBA) with SSE, MSLB may be considered separately from an SSE.
5. These load combinations are based on MSLB bounding other pipe break loads for the Steam Dryer. If other pipe break loads are bounding, they should used in-place of the MSLB loads.
6. Thermal, pressure and seismic anchor displacements can result in localized loads on the dryer. If these loads are not determined to be negligible (BWRVIP-181 Sections 7.1.6 and 7.1.9) they must be addressed in addition to the load combinations listed here.
7. SRSS can be used to combine OBE and FIV provided with plant specific justification.

Table 9-5
Load Combinations for Mark II and Mark III Plants

Load Case	Service Conditions	Operating Condition	Load Combination (1,2,3,4,5,6,)
A	Normal	Normal Operation	$DW + DP_N + FIV$
B-1	Upset	SRV Opening	$DW + DP_N + SRV$
B-2	Upset	Single SRV Opening	$DW + DP_N + (SRV_1^2 + FIV^2)^{1/2}$
B-3(7)	Upset	Operating Basis Earthquake	$DW + DP_N + OBE + FIV$
B-4	Upset	Upset DP	$DW + DP_U + FIV$
B-5	Upset	Turbine Stop Valve Closure (Acoustic Load)	$DW + DP_N + (TSV_A^2 + FIV^2)^{1/2}$
B-6	Upset	Turbine Stop Valve Closure (Flow Reversal Load)	$DW + DP_N + TSV_F$
C-1	Emergency	Emergency Depressurization	$DW + DP_N + SRV_{ADS}$
C-2	Emergency	Emergency DP	$DW + DP_E + FIV$
D-1	Faulted	SSE plus SRV Valves Actuate	$DW + DP_N + (SSE^2 + SRV^2)$
D-2	Faulted	Single SRV opening with SSE	$DW + DP_N + FIV + (SSE^2 + SRV_1^2)^{1/2}$
D-3	Faulted	Main Steam Line Break plus SSE Under Rated Power Conditions	$DW + DP_N + (MSLB_{A1}^2 + SSE^2 + FIV^2)^{1/2}$
D-4	Faulted	Main Steam Line Break plus SSE Under Rated Power Conditions	$DW + MSLB_{DP1} + SSE$

Notes:

1. The intention of considering a number of load combinations is to help determine the most conservative load condition. Owners may eliminate load combinations that can be technically justified to be bounded by other load combinations.
2. For definitions of terms see Table 9-6.
3. FIV loads are for the normal operating condition. FIV loads could be higher at some particular steam line velocities other than the normal steam line velocity. Accordingly, dwelling for extended periods of time at such flow velocities is to be avoided.
4. For plants that do not combine MSLB (limiting DBA) with SSE, MSLB may be considered separately from an SSE.
5. These load combinations are based on MSLB bounding other pipe break loads for the Steam Dryer. If other pipe break loads are bounding, they should used in-place of the MSLB loads.
6. Thermal, pressure and seismic anchor displacements can result in localized loads on the dryer. If these loads are not determined to be negligible (BWRVIP-181 Sections 7.1.6 and 7.1.9) they must be addressed in addition to the load combinations listed here.
7. SRSS can be used to combine OBE and FIV provided with plant specific justification.

Table 9-6
Load Term Definitions for Table 9-4 and Table 9-5

Loading Term	Description [1]
DW	Deadweight
DP	Differential pressure loading (Subscripts refer to N = Normal , U = Upset , E = Emergency
FIV	Flow induced vibration loads at power uprate
$MSLB_{DP1}$	Differential pressure load in the faulted condition, due to main steam line break outside containment at the rated power and core flow condition
$MSLB_{DP2}$	Differential pressure load in the faulted condition, due to main steam line break outside containment at the low power/high core flow condition
$MSLB_{A1}$	Acoustic load due to main steam line break (MSLB) outside containment, at the rated power and core flow condition
$MSLB_{A2}$	Acoustic load due to main steam line break (MSLB) outside containment, at the low power/high core flow condition.
OBE	Combination of all OBE induced loads
SSE	Combination of all SSE induced loads
SRV	Highest Load from either All safety relief valves open or asymmetric safety relief valves open
SRV_{ADS}	Load from opening of automatic depressurization system valves
TSV_A	Acoustic load caused by closure of turbine stop valve
TSV_F	Flow impingement load caused by closure of turbine stop valve

Note:

1. Unless otherwise specified, pressures and temperatures that are applicable to the conditions associated with the operating condition and postulated event.

9.4 ASME B&PV Code Section III Stress Analysis Procedure

The structural integrity of each steam dryer was originally evaluated for OLTP flow conditions in accordance with the design basis of the specific plant using load combinations defined in the plant Safety Evaluation Report (SAR). These analyses did not generally include fluctuating pressure loading. In cases where specific quasi-steady and or transient loads used in the original stress evaluation could potentially increase as a result of the higher main steam line flows at power uprate conditions, this evaluation needs to be revised to reflect the potentially higher quasi-steady and/or transient loads at power uprate. Revised seismic loading also needs to be included in cases where the design/weight of the dryer has changed since the original evaluation. Further, such analyses should be revised to include (where applicable) the stresses produced at EPU as a result of FIV loading.

The structural analysis of a steam dryer includes:

- An ASME Section III, Subsection NG, primary stress evaluation that includes all loading types and combinations considered in the original design basis of the plant, adjusted as appropriate to account for the higher steam flow velocities at EPU in combination with the FIV loads where applicable. Note that no loads defined for the steam dryer will produce secondary stresses; therefore, no primary plus secondary (P+Q) stress intensity check is performed.
- An ASME Section III, subsection NG, fatigue analysis, considering only fluctuating pressure loading (FIV) due to both turbulent flow over the steam dryer surfaces and acoustic pressure loads from sources within the main steam lines.

9.4.1 ASME Code Stress Allowable Values

Table 9-7 and Table 9-8 summarize the ASME B&PV Code allowable stress intensities applicable to this evaluation. The allowable stress intensity values for type 304 stainless steel at an operating temperature of 550°F are taken from the appropriate section of the ASME B&PV Code. The calculation for different stress categories is performed in accordance with Figure NG-3221-1 of Division I, Section III, subsection NG.

Table 9-7
ASME Code Allowable Stress Intensity Limits

Categories	Levels A and B (Normal & Upset)	Level C (Emergency)	Level D[(1)] (Faulted)
P_m	S_m	$1.5S_m$	min of 2.4 S_m and 0.7S_u
$P_m + P_b$	$1.5S_m$	$2.25S_m$	1.5 P_m Limit
FIV Stresses	S_a	n/a	n/a

Notes: 1. Level D uses Section III Appendix F criteria.
2. n/a: not applicable

Table 9-8
ASME Code Allowable Stress Intensity Values

Categories	Levels A and B (Design, Normal & Upset), ksi	Level C (Emergency), ksi	Level D (Faulted), ksi
P_m	16.9 [(1)]	25.3 [(1)]	min(40.5,44.38) = 40.5
$P_m + P_b$	25.3 [(1)]	38.0 [(1)]	60.8
FIV Stresses	S_a[(2)]=13.6	n/a	n/a

Notes: 1. Use S_m at 550 °F.
2. See Figure I-9.2.2, Figure 1-9.2.3 and Table I-9.2.2 of Appendices of Section III.
3. n/a: not applicable

9.4.2 Primary Stress Evaluation Procedure

A static stress analysis is performed for all load cases except for the FIV load case. Stresses and deflections from all static loads and the static equivalent of all transient loads (other than FIV) are evaluated and stored for later combination with those resulting from fluctuating pressure loading (FIV). The stress results from all load cases are combined at each node either directly or by square root of sums of squares as shown in the load combination tables, Table 9-4 and Table 9-5.

The classification of stresses as membrane or membrane plus bending is made according to the location where the stress intensity was calculated; namely, general membrane, P_m, for middle surface of shell element, and membrane plus bending, $P_m + P_b$, for other locations. For solid elements the most conservative, general membrane, P_m, allowable is used, as it is compared to a lower allowable for stress evaluation.

The calculated stress intensities are compared to the allowable stress intensity at each node location. Locations where the stresses exceed allowable levels will have stress ratios less than unity. Computation of stress intensities and associated stress ratios is performed using a separate FORTRAN code. Specifically, the following quantities are computed at every node:

1. Primary membrane stress intensity P_m (evaluated at the mid-thickness location for shells);
2. Primary membrane plus bending stress intensity P_m+P_b (conservatively taken as the largest of the stress intensity values at the bottom, top, and mid thickness locations, for shells);
3. Stress ratio assuming the node lies on a non-weld location. Note that this ratio is the minimum ratio obtained considering P_m and P_m+P_b limits: SR-P = min$\{S_m/P_m, 1.5 \times S_m/(P_m+P_b)\}$.
4. The same as 3, but assuming the node lies on a weld: SR-P(w)=SR-P(nw) $\times$ 0.55. This value is 0.55 times the value at a non-weld (S_m), which is the origin of the 0.55 factor in the expression for the stress ratio.

Content Deleted-
Contains EPRI and Continuum Dynamics Inc. Proprietary Information

Content Deleted-
Contains EPRI and Continuum Dynamics Inc. Proprietary Information

9.4.3 Fatigue Analysis Procedure

A fatigue analysis is conducted with FIV loads only. Consistent with ASME B&PV Code, Section III, Subsection NG-3216.2, the following procedure is established to calculate alternating stress intensities:

Content Deleted-
Contains EPRI and Continuum Dynamics Inc. Proprietary Information

Content Deleted-
Contains EPRI and Continuum Dynamics Inc. Proprietary Information

9.4.3.1 Weld Fatigue Strength Reduction Factor

For locations on welds, the calculated range of alternating stress intensity is multiplied by a weld fatigue strength reduction factor of

Content Deleted-
Contains EPRI and Continuum Dynamics Inc. Proprietary Information

9.4.3.2 Comparison to Allowable Range of Alternating Stress Intensity S_a

For the fatigue evaluation the range of alternating stress intensity, S_{alt}, at each node is taken as the maximum alternating stress intensity predicted at any point through the thickness of the FEM element (top, middle, or bottom).

The fatigue evaluation is carried out by computing alternating stress intensity ratios (SR-a) between the computed alternating stress intensities and the allowable level from Table 9-7 and Table 9-8. The stress ratio is defined as the alternating stress intensity allowable divided by the

predicted alternating stress intensity at that location. SR-a values are evaluated both at welds, [SR-a(w)], and away from welds, [SR-a(nw)].

Locations where any of the stresses exceed allowable levels will have stress ratios less than unity.

Content Deleted-
Contains EPRI and Continuum Dynamics Inc. Proprietary Information

9.4.3.3 FEA Sub-Modeling at Welds

In order to keep computational costs at a feasible level, the steam dryer model is predominantly comprised of shell elements. These elements are well suited for structures, such as the steam dryer, consisting of shell-like components and tend to produce conservative estimates of the stresses. In some cases, however, such as welded junctions involving multiple components, shell element models can overestimate the nominal stress intensities in the vicinity of the junctions. In such cases a more refined analysis, using solid elements to capture the 3-D stress distribution is warranted. Therefore, to efficiently analyze complex structures such as steam dryers, a standard engineering practice is to first analyze the structure using a shell-based model. Then, if any locations with high stresses are identified, these regions are examined in greater detail using 3D solid elements to obtain a more accurate stress prediction.

Content Deleted-
Contains EPRI and Continuum Dynamics Inc. Proprietary Information

Content Deleted-
Contains EPRI and Continuum Dynamics Inc. Proprietary Information

9.4.4 Presentation of Stress Analysis Results

Results of both the stress and fatigue evaluations are summarized in tabular form as shown in Table 9-9.

Table 9-9
Typical Stress Analysis Results Table

Stress Type	Weld Y or N	Location	% Freq. Shift	Location (in.)			node	Stress Intensity (psi)			Stress Ratio	
				x	y	z		Pm	Pm+Pb	S_{alt}	SR-P	SR-a
SR-P												
SR-a												
"												
SR-P												
"												
"												
"												
"												
SR-a												
"												
"												
"												
"												

9.5 References

9.1. ASME Boiler and Pressure Vessel Code, Section II & Section III, Subsection NG.

9.2. BWRVIP-181. December 2007. Steam Dryer Repair Design Criteria.

9.3. ANSYS Release 10.0. URL http://www.ansys.com. Documentation: ANSYS 10.0 Complete User's Manual Set.

9.4. Press, W. H., S. A. Teukolsky, W. T. Vetterling, and B. P. Flannery. 1992. Numerical Recipes. Cambridge University Press.

9.5. O'Donnell, W. J. 1973. Effective Elastic Constants For the Bending of Thin Perforated Plates With Triangular and Square Penetration Patterns. *ASME Journal of Engineering for Industry* 95: 121-128.

9.6. Fritz, R. J. and E. Kiss. 1966. The Vibration Response of a Cantilevered Cylinder Surrounded by an Annular Fluid. Knolls Atomic Power Laboratory Report No. KAPL M-6539.

9.7. U.S. Nuclear Regulatory Commission. March 2007. Regulatory Guide 1.20: Comprehensive Vibration Assessment Program for Reactor Internals During Preoperational and Initial Startup Testing.

9.8. GE-NE-0000-0053-7413-R4-NP. August 2006.

9.9. WRC Bulletin 432. 1998. Fatigue Strength Reduction and Stress Concentration Factors For Welds In Pressure Vessels and Piping. WRC, NY, p.32.

9.10. WRC Bulletin 474. 2002. Master S-N Curve Method for Fatigue Evaluation of Welded Components. WRC, NY, p.35.

9.11. Pilkey, W. D. 1997. Peterson's Stress Concentration Factors, 2nd ed., John Wiley, NY, p. 139.

9.12. Lawrence, F. V., N.-J. Ho, and P. K. Mazumdar P.K. 1981. Predicting the Fatigue Resistance of Welds. *Annual Reviews of Material Science* 11: 401-425.

10
APPLICATION OF COMBINED BIAS AND UNCERTAINTY

Each step in the process, from strain gage data collection on the main steam lines to construction of an ANSYS structural model of the steam dryer, contains the potential for error and approximation, and hence the addition of bias and uncertainty to the dryer stress margins that are eventually used to determine the acceptability of the steam dryer to acoustic loading. These several factors – ultimately, all adding conservatism to the prediction process – are collected here and discussed in greater detail.

10.1 Sources of Bias and Uncertainty

Bias and uncertainty enter the solution process at the following steps:

Content Deleted-
Contains EPRI and Continuum Dynamics Inc. Proprietary Information

Content Deleted-
Contains EPRI and Continuum Dynamics Inc. Proprietary Information

An overall model uncertainty is developed by use of the following equation

$$\text{Overall Uncertainty} = \Sigma\,[\text{Bias}] + \text{SRSS}\,[\text{Uncertainty}] \qquad (10.1.1)$$

where Equation (10.1.1) is evaluated for each frequency interval shown in Table 10-1. The various bias values are added together and then added to an SRSS of all of the uncertainty in that frequency interval. Table 10-2 summarizes the bias and uncertainty values added to the ACM model prediction beyond that of the model comparison with data.

Table 10-1
Frequency-dependent bias and uncertainty for the ACM Revision 4. A negative bias indicates that the ACM overpredicts the QC2 data in that interval. The excitation frequency interval is ±2 Hz, and is based on the Electromatic bias and uncertainty at QC2.

Content Deleted-
Contains EPRI and Continuum Dynamics Inc. Proprietary Information

Table 10-2
Bias and uncertainty contributions to total uncertainty.

Content Deleted-
Contains EPRI and Continuum Dynamics Inc. Proprietary Information

10.2 Example

Equation (10.1.1) provides the equation to compute the overall uncertainty within each of the frequency intervals. For example, for the frequency interval from 20 to 40 Hz, the overall uncertainty would be computed as follows (assuming the average pressure measurement uncertainty and using the data in Table 10-1 and

Content Deleted-
Contains EPRI and Continuum Dynamics Inc. Proprietary Information

Table 10-2):

Overall Uncertainty =

Content Deleted-
Contains EPRI and Continuum Dynamics Inc. Proprietary Information

10.3 References

10.1 Exelon Nuclear Generating LLC. 2005. An Assessment of the Effects of Uncertainty in the Application of Acoustic Circuit Model Predictions to the Calculation of Stresses in the Replacement Quad Cities Units 1 and 2 Steam Dryers (Revision 0). Document No. AM-21005-008.

10.2 Continuum Dynamics, Inc. 2007. Finite Element Modeling Bias and Uncertainty Estimates Derived from the Hope Creek Unit 2 Dryer Shaker Test (Rev. 0). C.D.I. Report No. 07-27.

10.3 NRC Request for Additional Information on the Hope Creek Generating Station, Extended Power Uprate. 2007. RAI No. 14.79.

10.4 NRC Request for Additional Information on the Hope Creek Generating Station, Extended Power Uprate. 2007. RAI No. 14.110.

11
METHODOLOGY FOR MONITORING STEAM DRYER STRESSES DURING POWER ASCENSION TESTING

During power ascension testing from CLTP to EPU power, each utility is required to monitor and evaluate MSL strain measurements to ensure that steam dryer stresses do not exceed ASME fatigue allowables. To facilitate this evaluation, MSL limit curves are generated prior to power ascension testing. Limit curves provide an upper bound safeguard to ensure that dryer stress levels do not exceed allowables, by estimating the not-to-be-exceeded main steam line pressure (strain) levels.

11.1 Approach

Two levels of steam dryer performance criteria are described: (1) a Level 1 pressure level based on ensuring that the ASME allowable alternating stress value on the dryer is not exceeded, and (2) a Level 2 pressure level based on ensuring that 80% of the allowable alternating stress value on the dryer is not exceeded. Should Level 2 be reached or exceeded (under the rules discussed below), reactor power ascension is to be suspended until an engineering evaluation concludes that further power ascension is justified. Should Level 1 be reached or exceeded, reactor power is returned to a previously acceptable power level while an engineering evaluation is undertaken.

To develop the Level 1 and Level 2 limit curves, the stress levels in the dryer corresponding to the current plant (CLTP) MSL acoustic signature are first determined (as discussed in Sections 5, 6, 9, and 10) and then the factor by which the MSL acoustic signatures can be increased to reach the 13,600 psi stress fatigue limit is determined. Specifically, the Level 1 limit curve is constructed by scaling up each of the current plant (CLTP) MSL acoustic signatures at all points along the frequency spectrum by this overall factor. A Level 2 limit curve is produced in the same manner except at 80% of the fatigue limit, or 10,880 psi.

Steam dryer data and evaluations are performed in accordance with plant specific EPU power ascension plans.

11.2 Sample Implementation

The methodology for monitoring steam dryer stresses during power ascension will be discussed by way of a sample implementation.

11.2.1 CLTP Stress Analysis

The finite element analysis using the CLTP data from Plant A results in a lowest/minimum alternating stress ratio (fatigue allowable stress/maximum predicted stress) of 3.11, as summarized in Table 11-1. The minimum stress ratio includes the model bias and uncertainties for specific frequency ranges as defined in Section 6 and summarized in Table 11-2. Note that for this sample plant,

Content Deleted-
Contains EPRI and Continuum Dynamics Inc. Proprietary Information

Table 11-1
Alternating Stress Limit Summary for Plant A

Content Deleted-
Contains EPRI and Continuum Dynamics Inc. Proprietary Information

Table 11-2
Bias and Uncertainty for ACM Revision 4

Content Deleted-
Contains EPRI and Continuum Dynamics Inc. Proprietary Information

Table 11-3
Additional Bias and Uncertainty for Plant A

Content Deleted-
Contains EPRI and Continuum Dynamics Inc. Proprietary Information

Table 11-4
Total Uncertainty for Plant A

Content Deleted-
Contains EPRI and Continuum Dynamics Inc. Proprietary Information

11.2.2 Limit Curve Generation

Limit curves are generated from the in-plant CLTP strain gage data collected for Plant A. These data are filtered across the frequency range of interest to remove noise and extraneous signal content, as described in Section 5. The resulting PSD curve for each of the eight strain gage locations is then used to develop the limit curves, shown in Figure 11-1 to Figure 11-4. Level 1 limit curves are found by multiplying

Content Deleted-
Contains EPRI and Continuum Dynamics Inc. Proprietary Information

Content Deleted-
Contains EPRI and Continuum Dynamics Inc. Proprietary Information

Figure 11-1
Level 1 (black) and Level 2 (red) limit curves for main steam line A, compared against the base curves (blue) over the frequency range of interest: A upper strain gage location (top); A lower strain gage location (bottom).

Content Deleted-
Contains EPRI and Continuum Dynamics Inc. Proprietary Information

Figure 11-2
Level 1 (black) and Level 2 (red) limit curves for main steam line B, compared against the base curves (blue) over the frequency range of interest: B upper strain gage location (top); B lower strain gage location (bottom).

Content Deleted-
Contains EPRI and Continuum Dynamics Inc. Proprietary Information

Figure 11-3
Level 1 (black) and Level 2 (red) limit curves for main steam line C, compared against the base curves (blue) over the frequency range of interest: C upper strain gage location (top); C lower strain gage location (bottom).

Content Deleted-
Contains EPRI and Continuum Dynamics Inc. Proprietary Information

Figure 11-4
Level 1 (black) and Level 2 (red) limit curves for main steam line D, compared against the base curves (blue) over the frequency range of interest: D upper strain gage location (top); D lower strain gage location (bottom).

11.3 Analysis of Data During Power Ascension Testing

The MSL strain measurements are monitored closely during power ascension to ensure that no Level 1 or Level 2 limit curves are exceeded at any frequency.

If a Level 1 limit is reached or exceeded, power is reduced immediately to a previously acceptable level at or below the Level 2 limit.

If a Level 2 limit is reached or exceeded, power ascension is paused and a reanalysis of dryer stresses is conducted using the MSL data obtained at the new power level to allow determination of a revised margin to the fatigue allowable stress. The new margin is applied to the new MSL data as described in Section 11.2 to define new Level 1 and Level 2 limit curves. This process is repeated as necessary during power ascension testing until the target EPU power level is reached, or the margin to the fatigue allowable is reduced to zero, whichever comes first.

Content Deleted-
Contains EPRI and Continuum Dynamics Inc. Proprietary Information

12
METHOD FOR DEFINING TURBINE STOP VALVE CLOSURE AND MAIN STEAM LINE BREAK LOADS

LATER

A
EVALUATION OF-- CONTENT DELETED-CONTAINS EPRI AND CONTINUUM DYNAMICS INC. PROPRIETARY INFORMATION

Content Deleted-
Contains EPRI and Continuum Dynamics Inc. Proprietary Information

\

Content Deleted-
Contains EPRI and Continuum Dynamics Inc. Proprietary Information

Content Deleted-
Contains EPRI and Continuum Dynamics Inc. Proprietary Information

Content Deleted-
Contains EPRI and Continuum Dynamics Inc. Proprietary Information

Content Deleted-
Contains EPRI and Continuum Dynamics Inc. Proprietary Information

Content Deleted-
Contains EPRI and Continuum Dynamics Inc. Proprietary Information

B
MECHANISM FOR—CONTENT DELETED-CONTAINS EPRI AND CONTINUUM DYNAMICS INC. PROPRIETARY INFORMATION

Content Deleted-
Contains EPRI and Continuum Dynamics Inc. Proprietary Information

Content Deleted-
Contains EPRI and Continuum Dynamics Inc. Proprietary Information

Content Deleted-
Contains EPRI and Continuum Dynamics Inc. Proprietary Information

Content Deleted-
Contains EPRI and Continuum Dynamics Inc. Proprietary Information

Content Deleted-
Contains EPRI and Continuum Dynamics Inc. Proprietary Information

Content Deleted-
Contains EPRI and Continuum Dynamics Inc. Proprietary Information

Content Deleted-
Contains EPRI and Continuum Dynamics Inc. Proprietary Information

Content Deleted-
Contains EPRI and Continuum Dynamics Inc. Proprietary Information

C
ACM REVISION 4 COMPARISONS TO QUAD CITIES UNIT 2 790 MWE TEST DATA

This appendix provides the comparison of QC2 data collected at 790 MWe with ACM Revision 4 model predictions.

Figure C-1 and Figure C-2 plot the main steam line data, while Figure C-3 to Figure C-16 plot the comparisons between model predictions and data at each of the 27 pressure transducer locations on the dryer.

Content Deleted-
Contains EPRI and Continuum Dynamics Inc. Proprietary Information

Figure C-1
PSDs of pressure data at 790 MWe on main steam lines A (top) and B (bottom): upper strain gage locations (blue curves), lower strain gage locations (red curves).

Content Deleted-
Contains EPRI and Continuum Dynamics Inc. Proprietary Information

Figure C-2
PSDs of pressure data at 790 MWe on main steam lines C (top) and D (bottom): upper strain gage locations (blue curves), lower strain gage locations (red curves).

Content Deleted-
Contains EPRI and Continuum Dynamics Inc. Proprietary Information

Figure C-3
PSD comparison at 790 MWe for pressure sensor data (blue curves) and Rev. 4 model prediction (red curves), for P1 (top) and P2 (bottom).

Content Deleted-
Contains EPRI and Continuum Dynamics Inc. Proprietary Information

Figure C-4
PSD comparison at 790 MWe for pressure sensor data (blue curves) and Rev. 4 model prediction (red curves), for P3 (top) and P4 (bottom).

Content Deleted-
Contains EPRI and Continuum Dynamics Inc. Proprietary Information

Figure C-5
PSD comparison at 790 MWe for pressure sensor data (blue curves) and Rev. 4 model prediction (red curves), for P5 (top) and P6 (bottom).

Content Deleted-
Contains EPRI and Continuum Dynamics Inc. Proprietary Information

Figure C-6
PSD comparison at 790 MWe for pressure sensor data (blue curves) and Rev. 4 model prediction (red curves), for P7 (top) and P8 (bottom).

Content Deleted-
Contains EPRI and Continuum Dynamics Inc. Proprietary Information

Figure C-7
PSD comparison at 790 MWe for pressure sensor data (blue curves) and Rev. 4 model prediction (red curves), for P9 (top) and P10 (bottom).

Content Deleted-
Contains EPRI and Continuum Dynamics Inc. Proprietary Information

Figure C-8
PSD comparison at 790 MWe for pressure sensor data (blue curves) and Rev. 4 model prediction (red curves), for P11 (top) and P12 (bottom).

Content Deleted-
Contains EPRI and Continuum Dynamics Inc. Proprietary Information

Figure C-9
PSD comparison at 790 MWe for pressure sensor data (blue curves) and Rev. 4 model prediction (red curves), for P13 (top) and P14 (bottom).

Content Deleted-
Contains EPRI and Continuum Dynamics Inc. Proprietary Information

Figure C-10
PSD comparison at 790 MWe for pressure sensor data (blue curves) and Rev. 4 model prediction (red curves), for P15 (top) and P16 (bottom).

Content Deleted-
Contains EPRI and Continuum Dynamics Inc. Proprietary Information

Figure C-11
PSD comparison at 790 MWe for pressure sensor data (blue curves) and Rev. 4 model prediction (red curves), for P17 (top) and P18 (bottom).

Content Deleted-
Contains EPRI and Continuum Dynamics Inc. Proprietary Information

Figure C-12
PSD comparison at 790 MWe for pressure sensor data (blue curves) and Rev. 4 model prediction (red curves), for P19 (top) and P20 (bottom).

Content Deleted-
Contains EPRI and Continuum Dynamics Inc. Proprietary Information

Figure C-13
PSD comparison at 790 MWe for pressure sensor data (blue curves) and Rev. 4 model prediction (red curves), for P21 (top) and P22 (bottom).

Content Deleted-
Contains EPRI and Continuum Dynamics Inc. Proprietary Information

Figure C-14
PSD comparison at 790 MWe for pressure sensor data (blue curves) and Rev. 4 model prediction (red curves), for P23 (top) and P24 (bottom).

Content Deleted-
Contains EPRI and Continuum Dynamics Inc. Proprietary Information

Figure C-15
PSD comparison at 790 MWe for pressure sensor data (blue curves) and Rev. 4 model prediction (red curves), for P25 (top) and P26 (bottom).

Content Deleted-
Contains EPRI and Continuum Dynamics Inc. Proprietary Information

Figure C-16
PSD comparison at 790 MWe for pressure sensor data (blue curves) and Rev. 4 model prediction (red curves), for P27

D
ACM REVISION 4 COMPARISONS TO QUAD CITIES UNIT 2 820 MWE TEST DATA

This appendix provides the comparison of QC2 data collected at 820 MWe with ACM Revision 4 model predictions.

Figure D-1 and Figure D-2 plot the main steam line data, while Figure D-3 to Figure D-16 plot the comparisons between model predictions and data at each of the 27 pressure transducer locations on the dryer.

Content Deleted-
Contains EPRI and Continuum Dynamics Inc. Proprietary Information

Figure D-1
PSDs of pressure data at 820 MWe on main steam lines A (top) and B (bottom): upper strain gage locations (blue curves), lower strain gage locations (red curves).

Content Deleted-
Contains EPRI and Continuum Dynamics Inc. Proprietary Information

Figure D-2
PSDs of pressure data at 820 MWe on main steam lines C (top) and D (bottom): upper strain gage locations (blue curves), lower strain gage locations (red curves).

Content Deleted-
Contains EPRI and Continuum Dynamics Inc. Proprietary Information

Figure D-3
PSD comparison at 820 MWe for pressure sensor data (blue curves) and Rev. 4 model prediction (red curves), for P1 (top) and P2 (bottom).

Content Deleted-
Contains EPRI and Continuum Dynamics Inc. Proprietary Information

Figure D-4
PSD comparison at 820 MWe for pressure sensor data (blue curves) and Rev. 4 model prediction (red curves), for P3 (top) and P4 (bottom).

Content Deleted-
Contains EPRI and Continuum Dynamics Inc. Proprietary Information

Figure D-5
PSD comparison at 820 MWe for pressure sensor data (blue curves) and Rev. 4 model prediction (red curves), for P5 (top) and P6 (bottom).

Content Deleted-
Contains EPRI and Continuum Dynamics Inc. Proprietary Information

Figure D-6
PSD comparison at 820 MWe for pressure sensor data (blue curves) and Rev. 4 model prediction (red curves), for P7 (top) and P8 (bottom).

Content Deleted-
Contains EPRI and Continuum Dynamics Inc. Proprietary Information

Figure D-7
PSD comparison at 820 MWe for pressure sensor data (blue curves) and Rev. 4 model prediction (red curves), for P9 (top) and P10 (bottom).

Content Deleted-
Contains EPRI and Continuum Dynamics Inc. Proprietary Information

Figure D-8
PSD comparison at 820 MWe for pressure sensor data (blue curves) and Rev. 4 model prediction (red curves), for P11 (top) and P12 (bottom).

Content Deleted-
Contains EPRI and Continuum Dynamics Inc. Proprietary Information

Figure D-9
PSD comparison at 820 MWe for pressure sensor data (blue curves) and Rev. 4 model prediction (red curves), for P13 (top) and P14 (bottom).

Content Deleted-
Contains EPRI and Continuum Dynamics Inc. Proprietary Information

Figure D-10
PSD comparison at 820 MWe for pressure sensor data (blue curves) and Rev. 4 model prediction (red curves), for P15 (top) and P16 (bottom).

Content Deleted-
Contains EPRI and Continuum Dynamics Inc. Proprietary Information

Figure D-11
PSD comparison at 820 MWe for pressure sensor data (blue curves) and Rev. 4 model prediction (red curves), for P17 (top) and P18 (bottom).

Content Deleted-
Contains EPRI and Continuum Dynamics Inc. Proprietary Information

Figure D-12
PSD comparison at 820 MWe for pressure sensor data (blue curves) and Rev. 4 model prediction (red curves), for P19 (top) and P20 (bottom).

Content Deleted-
Contains EPRI and Continuum Dynamics Inc. Proprietary Information

Figure D-13
PSD comparison at 820 MWe for pressure sensor data (blue curves) and Rev. 4 model prediction (red curves), for P21 (top) and P22 (bottom).

Content Deleted-
Contains EPRI and Continuum Dynamics Inc. Proprietary Information

Figure D-14
PSD comparison at 820 MWe for pressure sensor data (blue curves) and Rev. 4 model prediction (red curves), for P23 (top) and P24 (bottom).

Content Deleted-
Contains EPRI and Continuum Dynamics Inc. Proprietary Information

Figure D-15
PSD comparison at 820 MWe for pressure sensor data (blue curves) and Rev. 4 model prediction (red curves), for P25 (top) and P26 (bottom).

Content Deleted-
Contains EPRI and Continuum Dynamics Inc. Proprietary Information

Figure D-16
PSD comparison at 820 MWe for pressure sensor data (blue curves) and Rev. 4 model prediction (red curves), for P27.

E
VALIDATION OF STRESS ANALYSIS METHODOLOGY

This appendix summarizes validation activities completed to demonstrate the adequacy of the stress analysis methods used to evaluate the structural integrity of steam dryers. Section E.1 compares the frequency response of a cantilevered flat plate predicted by ANSYS 10.0 to known analytical solutions. Section E.2 compares predicted structural response and stresses in a typical steam dryer using time integration to those using harmonic techniques. Section E.3 summarizes the results of an experimental program carried out to validate the method employed for modeling the structural damping of perforated plates. Section E.4 describes an experimental program conducted to assess the bias and random uncertainties associated with ANSYS 10.0 modeling of a typical BWR steam dryer. Section E.5 summarizes the results of a test program conducted to **Content Deleted-Contains EPRI and Continuum Dynamics Inc. Proprietary Information.** Finally, Section E.6 summarizes the errors in stress prediction due to use of finite mesh size in the FE model.

E.1 Comparison of ANSYS Frequency Predictions against Analytical Formulas for Flat Plates

The computed modal masses affect the response amplitude, and while these masses can be computed using the ANSYS finite element (FE) software, there are no modal mass measurements or analytical solutions they can be compared against. One approach for assessing bias errors and uncertainties is to consider a geometrically simple structure (e.g., a flat plate) for which analytical solutions for the modal amplitudes, masses, and responses are available. Predictions of these properties using an ANSYS FE model having the same elements and connections present in the steam dryer model can then be compared against these analytical results, thus allowing one to estimate the errors in frequency as a function of response frequency.

Content Deleted-
Contains EPRI and Continuum Dynamics Inc. Proprietary Information

Content Deleted-
Contains EPRI and Continuum Dynamics Inc. Proprietary Information

E.1.1 Simply Supported Plate

Analytical eigenfrequencies for a plate that is simply supported on all sides is given by [E.1] as

$$f_{mn} = \frac{\pi}{2}\sqrt{\frac{D}{\rho h}}\left(\frac{m^2}{a^2}+\frac{n^2}{b^2}\right) \qquad \text{(E.1.1)}$$

where $D = \frac{Eh^3}{12(1-\nu^2)}$, E is the Young's modulus, ρ is the density, h is the plate thickness, a and b denote the plate dimensions, and m and n are modal numbers. **Content Deleted-Contains EPRI and Continuum Dynamics Inc. Proprietary Information.**

Table E-1
Comparison of analytical and ANSYS predictions of natural frequencies for simply supported plates (m and n are modal numbers)

Content Deleted-
Contains EPRI and Continuum Dynamics Inc. Proprietary Information

Thus, the errors in computed frequencies are less than 1% and are due to mesh resolution.

E.1.2 Clamped Plate

The middle hood is modeled with a plate, clamped on all sides and of thickness h = 0.125 in and side lengths a = 17.92 in and b = 44.8 in. This corresponds to the section of plate immediately adjacent to the location of high stress in an EPU calculation with a +10% frequency shift. At this aspect ratio, b/a = 2.5, the analytical eigenfrequencies are given by [E.2] as

$$f_{ij} = \frac{\lambda_{ij}^2}{2\pi b^2}\sqrt{\frac{D}{\rho h}} \qquad \text{(E.1.2)}$$

where D = 516.32 Nm and the coefficients λ_{ij}^2, the lowest frequencies, and relative errors are shown in the Table E-2.

Table E-2
Comparison of analytical and ANSYS predictions of natural frequencies for clamped plates (i and j are modal numbers)

Content Deleted-
Contains EPRI and Continuum Dynamics Inc. Proprietary Information

The mesh used to calculate plate eigenfrequencies and the mesh on the steam dryer model are shown in Figure E-1.

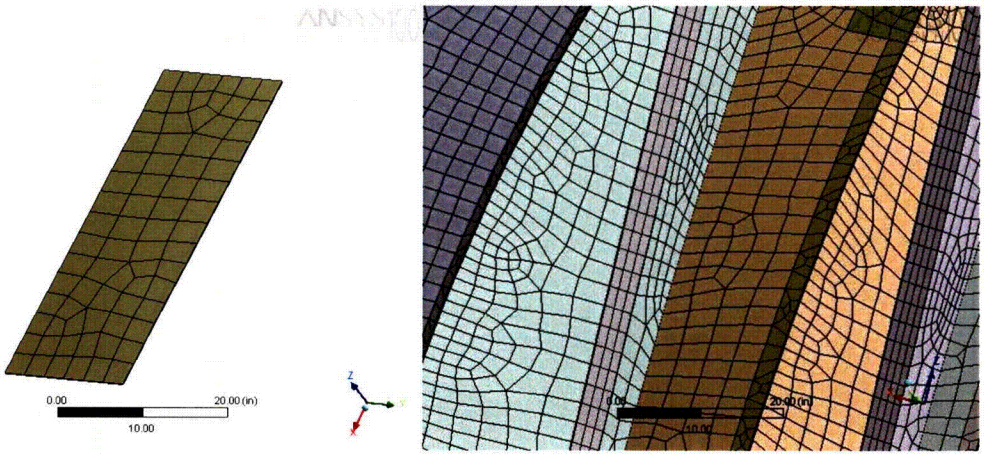

Figure E-1
Left: mesh on the flat plate model for eigenvalue comparison calculations; right: mesh on an actual steam dryer FE model. The size of elements in both models is kept similar.

E.1.3 Summary and Conclusions

As shown in **Content Deleted-Contains EPRI and Continuum Dynamics Inc. Proprietary Information.**

Table E-1 and Table E-2, the relative error in prediction of frequencies using the ANSYS code is small and well within the range of frequency shift used in evaluating BWR steam dryers (±10%).

E.2 Comparison of Transient and Harmonic Simulations for a Typical Steam Dryer

A comparison between the harmonic and time-domain methods is performed for a complete steam dryer subjected to a multi-frequency acoustic load. The primary objective of this comparison is to establish agreement between the time-domain and harmonic approaches for a full steam dryer model subjected to a complicated time- and spatially varying loading, and thereby validate the ability of the newer harmonic analysis model to reproduce the stress predictions of previously used time-domain methods. While the underlying theory of the harmonic and time domain approaches is not in question, i.e., the mathematical soundness of the approach and theoretical agreement (at infinite spatial and temporal resolution, etc.) between the two approaches is accepted, it is important to demonstrate that the implementation of the harmonic method and its software embodiment is correct and shows good agreement with time-domain solutions.

The second objective is to evaluate the effect of using two different damping models, specifically a Rayleigh damping model and one that enforces 1% critical damping at all frequencies. Unless a complete modal decomposition is performed, then the time domain method can only employ the Rayleigh damping model where 1% damping is enforced at two "pin" frequencies. Between these frequencies the damping is less than specified (and therefore overly conservative); elsewhere the damping is higher. The harmonic method can enforce 1% damping over the entire frequency range.

The main challenge in comparing the time-domain and harmonic responses for a complete steam dryer over the typical 0 - 200 Hz frequency range is the time required to perform the time-domain calculation. The costs amount to multiple weeks of parallel computing time, terabytes of storage and susceptibility to power interruption. These computational costs motivated a modified approach that retains complexity for the applied loading in both space and time.

Content Deleted-
Contains EPRI and Continuum Dynamics Inc. Proprietary Information

Content Deleted-
Contains EPRI and Continuum Dynamics Inc. Proprietary Information

Content Deleted-
Contains EPRI and Continuum Dynamics Inc. Proprietary Information

Content Deleted-
Contains EPRI and Continuum Dynamics Inc. Proprietary Information

E.2.1 Effects of Damping

The influence of the damping model on the computed stresses is assessed by comparing the harmonic responses at selected nodes. Specifically, the calculations (1) and (2) described above are compared

Content Deleted-
Contains EPRI and Continuum Dynamics Inc. Proprietary Information

Table E-3
Stress and error measures at selected nodes for different damping models

Content Deleted-
Contains EPRI and Continuum Dynamics Inc. Proprietary Information

Content Deleted-
Contains EPRI and Continuum Dynamics Inc. Proprietary Information

Figure E-2
Comparison of harmonic solutions with Raleigh damping and flat 1% of critical damping: dashed red line – Rayleigh damping; solid blue line – 1% flat damping. Nodes 82290 and 86424.

Content Deleted-
Contains EPRI and Continuum Dynamics Inc. Proprietary Information

Figure E-3
Comparison of harmonic solutions with Raleigh damping and flat 1% of critical damping: dashed red line – Rayleigh damping; solid blue line – 1% flat damping. Nodes 82652 and 88325.

Content Deleted-
Contains EPRI and Continuum Dynamics Inc. Proprietary Information

Figure E-4
Comparison of harmonic solutions with Raleigh damping and flat 1% of critical damping: dashed red line – Rayleigh damping; solid blue line – 1% flat damping. Node 88252.

E.2.2 Comparison of Harmonic and Time-Domain Predictions of Steady State Stresses

The next comparison examines the responses obtained with the same damping model (Rayleigh damping), but using different prediction methods – the transient or time marching approach and the harmonic analysis. In the transient analysis, the initial conditions (displacements and velocities) are set from the harmonic analysis results in order to minimize the presence of transients in the response. Mathematically, identical responses are expected and the goal here is to verify whether this is reflected in the computational implementation.

Content Deleted-
Contains EPRI and Continuum Dynamics Inc. Proprietary Information

Content Deleted-
Contains EPRI and Continuum Dynamics Inc. Proprietary Information

Table E-4
Comparison of harmonic and transient calculations: index 1 corresponds to harmonic solution; index 4 corresponds to transient calculation with adjusted initial conditions.

Content Deleted-
Contains EPRI and Continuum Dynamics Inc. Proprietary Information

Content Deleted-
Contains EPRI and Continuum Dynamics Inc. Proprietary Information

Figure E-5
Comparison of harmonic and transient solutions with adjusted initial conditions: dashed red line – transient; solid blue line – harmonic. Nodes 82290 and 86424.

Content Deleted-
Contains EPRI and Continuum Dynamics Inc. Proprietary Information

Figure E-6
Comparison of harmonic and transient solutions with adjusted initial conditions: dashed red line – transient; solid blue line – harmonic. Nodes 82652 and 88325.

Content Deleted-
Contains EPRI and Continuum Dynamics Inc. Proprietary Information

Figure E-7
Comparison of harmonic and transient solutions with adjusted initial conditions: dashed red line – transient; solid blue line – harmonic. Node 88252.

E.2.3 Influence of Initial Startup Transients

The last comparison examines the differences in the responses obtained when starting the calculation at rest and when initializing the calculation with deflections and velocities designed to eliminate all startup transients. Put another way, this compares responses obtained with and without start up transients.

Content Deleted-
Contains EPRI and Continuum Dynamics Inc. Proprietary Information

Table E-5
Comparison of transient calculations with different initial conditions: index 3 corresponds to zero initial conditions; index 4 corresponds to transient calculation with adjusted initial conditions.

Content Deleted-
Contains EPRI and Continuum Dynamics Inc. Proprietary Information

Content Deleted-
Contains EPRI and Continuum Dynamics Inc. Proprietary Information

Figure E-8
Comparison of transient calculations with zero initial conditions (IC) and initial conditions calculated from harmonic solution: solid blue line – zero IC; dashed red line – adjusted (or non-zero) IC. Nodes 82290 and 86424.

Content Deleted-
Contains EPRI and Continuum Dynamics Inc. Proprietary Information

Figure E-9
Comparison of transient calculations with zero initial conditions (IC) and initial conditions calculated from harmonic solution: solid blue line – zero IC; dashed red line – adjusted (or non-zero) IC. Nodes 82652 and 88325.

Content Deleted-
Contains EPRI and Continuum Dynamics Inc. Proprietary Information

Figure E-10
Comparison of transient calculations with zero initial conditions (IC) and initial conditions calculated from harmonic solution: solid blue line – zero IC; dashed red line – adjusted (or non-zero) IC. Node 88252.

E.2.4 PSD comparison

The power spectral density (PSD) of stress component σ_{xx} is calculated for

Content Deleted-
Contains EPRI and Continuum Dynamics Inc. Proprietary Information

Content Deleted-
Contains EPRI and Continuum Dynamics Inc. Proprietary Information

Figure E-11
PSD comparison of the harmonic solutions obtained with Rayleigh damping and constant 1% critical damping: dashed red line – Rayleigh damping; solid blue line – 1% flat damping. Node 82290.

Content Deleted-
Contains EPRI and Continuum Dynamics Inc. Proprietary Information

Figure E-12
PSD comparison of the harmonic and transient solutions with adjusted initial conditions: dashed red line – transient; solid blue line – harmonic. Node 82290.

Content Deleted-
Contains EPRI and Continuum Dynamics Inc. Proprietary Information

Figure E-13
PSD comparison of the transient solutions with zero initial conditions (IC) and initial conditions calculated from the harmonic solution: solid blue line – zero IC; dashed red line – adjusted (or non-zero) IC. Node 82290.

Content Deleted-
Contains EPRI and Continuum Dynamics Inc. Proprietary Information

Figure E-14
PSD comparison of the harmonic solutions obtained with Rayleigh damping and constant 1% critical damping: dashed red line – Rayleigh damping; solid blue line – 1% flat damping. Node 88252.

Content Deleted-
Contains EPRI and Continuum Dynamics Inc. Proprietary Information

Figure E-15
PSD comparison of the harmonic and transient solutions with adjusted initial conditions: dashed red line – transient; solid blue line – harmonic. Node 88252.

Content Deleted-
Contains EPRI and Continuum Dynamics Inc. Proprietary Information

Figure E-16
PSD comparison of the transient solutions with zero initial conditions (IC) and initial conditions calculated from the harmonic solution: solid blue line – zero IC; dashed red line – adjusted (or non-zero) IC. Node 88252.

E.2.5 Summary

The comparisons carried out above have shown that:

- The effects of damping (Rayleigh vs. constant 1% damping) upon the periodic response behave as expected. In this case the Rayleigh damping model results in over-predictions of the stress response due to lower effective damping.
- Excellent agreement is achieved when comparing the harmonic and transient responses obtained for identical steam dryer models and damping models. This agreement is demonstrated for a load that is complex in both space and time and is established for both amplitude and phase. Remaining discrepancies can be attributed to discretization error in the time integration scheme and/or frequency schedule discretization.
- Transients can produce **Content Deleted-**
  Contains EPRI and Continuum Dynamics Inc. Proprietary Information.

Content Deleted-
Contains EPRI and Continuum Dynamics Inc. Proprietary Information

E.3 Structural Modeling of Perforated Plates

Modeling the perforated plates in the steam dryer assembly explicitly is computationally prohibitive, and an alternative approach is adopted where the plates are characterized by modified material properties adjusted to match the key static and dynamic behavior. This portion of this appendix summarizes the modeling method employed and its verification against measurements.

E.3.1 Overview

The perforated plates used in the steam dryer assembly are very thin, i.e. the ratio of thickness and pitch of perforation is less than unity, so that the effective properties provided in ASME Code [E.5], for thick perforated plates cannot be used. Therefore, to model the steam dryer, the effective material properties reported by O'Donnell [E.6], that directly apply to the bending of thin plates, are adopted. In his work the effective properties are calculated by equating an average stress field over the periodicity cell in a perforated plate. Thus, for a given static loading the solid plate with the effective or modified material properties will yield a similar stress field as the perforated plate with original material properties. Comparisons are made against the values provided in ASME Code [E.5], as well as to experimental data, where good agreement is obtained.

In order to apply these results to the steam dryer analysis, the staggered 45° perforation (typical of BWR steam dryer bank perforated plates) was approximated by an equilateral staggered 60° perforation. The difference was judged insignificant for modeling purposes. The effective properties were inferred from Figure 8 (Young's modulus) and Figure 9 (Poisson's ratio) of [E.6].

E.3.2 Verification

To estimate how well the dynamic properties of the plates are reproduced, simple hammer test experiments were performed upon both solid and perforated cantilevered plates. In the first case, a steel solid plate of length a = 10 in, width b = 6 in, and thickness h = 0.08 in, clamped on one of the shorter edges, was excited, and the response recorded.

Content Deleted-
Contains EPRI and Continuum Dynamics Inc. Proprietary Information

Content Deleted-
Contains EPRI and Continuum Dynamics Inc. Proprietary Information

Figure E-17
Measured response to hammer test for solid plate.

Next, the same experiment was conducted with a perforated plate having length a = 15 in, width b = 6.125 in, and thickness h = 0.125 in; again the plate is clamped on a shorter edge. The perforation pattern was triangular with pitch (distance between hole centers) P = 0.375 in and hole diameter D = 0.25 in, which corresponds to a 40% open area. This plate therefore displays the same characteristics as some of the perforated plates used in steam dryer assembly (namely, those at the steam entry top location of the vane banks). The natural frequency estimated from the experimental time history (shown below in Figure E-18) is **Content Deleted-Contains EPRI and Continuum Dynamics Inc. Proprietary Information.**

Content Deleted-
Contains EPRI and Continuum Dynamics Inc. Proprietary Information

Figure E-18
Measured response for perforated plate.

For natural frequency calculations the same material properties and formula are used as for a solid plate. For this perforation pattern the ligament efficiency, (P–D)/P = 0.33 and the thickness ratio, h/P = 0.33. Using these values, the correction factors for the elastic constants from [E.6] are E_{eff}/E = 0.31 and ν_{eff} = 0.35. The density of the effective solid plate is ρ_{eff}/ρ = 0.6. Using the effective values, the calculated natural frequency of the perforated plate is **Content Deleted-Contains EPRI and Continuum Dynamics Inc. Proprietary Information.**

E.4 Finite Element Modeling and Uncertainty Estimates Derived from Shaker Testing of a Typical Full Scale Steam Dryer

A shaker test of a spare Hope Creek Unit 2 steam dryer was performed and the results compared against predictions obtained with the ANSYS 10.0 finite element analysis (FEA) to quantify the bias and uncertainty of the FEA model associated with the prediction of response peak amplitudes. Details of this test program and model data comparisons can be found in [E.7] and [E.8].

E.4.1 Summary

The spare Hope Creek Unit 2 dryer was suspended by four support rods and forced horizontally by a shaker unit at eight different locations: three on the upper support ring, two on the lower support ring, and three on the tie bars on the top of the dryer. For each shaker location, up to 20 accelerometers were placed on the dryer at locations predicted (with the ANSYS FEA) to produce the highest response over the 0 – 250 Hz frequency range. The pre-test FEA predictions also provided discrete frequencies where the response exhibited a peak. The test then proceeded to record the response at the accelerometers resulting from harmonic shaker forcing at frequencies in the vicinity of the predicted peak frequencies. These measured accelerations were then compared to the FEA predictions.

At each measured frequency peak for each shaker location, the comparison between the measured and predicted response was originally made by adjusting both the structural damping in the FEA model and shifting the forcing frequency by ±10% until the combined absolute value of bias plus uncertainty was minimized. The bias and uncertainty were then evaluated at the optimal damping and frequency shift values.

Content Deleted-
Contains EPRI and Continuum Dynamics Inc. Proprietary Information

Table E-6
|Bias|+Uncertainty obtained with various damping optimization methods

Content Deleted-
Contains EPRI and Continuum Dynamics Inc. Proprietary Information

The mean |bias| + uncertainty of 21.51% is the recommended value for use in the steam dryer analysis. Since the bias is virtually zero, this value is expressed as an uncertainty. Moreover, because the combined (|bias| + uncertainty) does not change significantly over the range considered (0 to 250 Hz), a single value can be used over the entire frequency range when performing operational steam dryer stress assessment.

E.4.2 Introduction

A shaker test of a spare Hope Creek Unit 2 dryer was performed to validate and compute biases and uncertainties of a finite element analysis used in steam dryer qualification for extended power uprate (EPU) operation. The dryer was suspended by lifting rods and subjected to shaker-induced forces at eight specified locations. Figure E-19 shows the shaker locations and directions of forcing during testing. The forcing locations were selected on the basis of several considerations, including reasonable access by a shaker rod, sufficient strength to support a 100 lb force amplitude (this precluded, for example, the skirt and hoods as suitable excitation locations; it also ensured that the maximum response location was likely to be away from the shaker location), and potential of exciting significant response at points on the dryer that experienced high stresses in the operational Unit 1 dryer (e.g., drain channels, skirt, and hood structures).

For each shaker location, finite element analysis (FEA) using the harmonic analysis in ANSYS 10.0 was carried out over a series of frequencies in the 0 – 250 Hz range. Peak frequencies were estimated with the objective of ensuring, where possible, at least three peaks per 25 Hz frequency band. From this information, locations for up to 20 accelerometers were identified on the dryer for each shaker location (Figure E-20 to Figure E-33). Acceleration data were then collected with these accelerometers at frequency peaks identified within specified frequency bands. These acceleration data were transmitted to C.D.I. and compared against the predicted displacement responses.

Content Deleted-
Contains EPRI and Continuum Dynamics Inc. Proprietary Information

Figure E-19
Shaker Locations and Forcing Directions

Content Deleted-
Contains EPRI and Continuum Dynamics Inc. Proprietary Information

Figure E-20
Accelerometer Locations for Shaker 1

Content Deleted-
Contains EPRI and Continuum Dynamics Inc. Proprietary Information

Figure E-21
Accelerometer Locations for Shaker 1

Content Deleted-
Contains EPRI and Continuum Dynamics Inc. Proprietary Information

Figure E-22
Accelerometer Locations for Shaker 2

Content Deleted-
Contains EPRI and Continuum Dynamics Inc. Proprietary Information

Figure E-23
Accelerometer Locations for Shaker 2

Content Deleted-
Contains EPRI and Continuum Dynamics Inc. Proprietary Information

Figure E-24
Accelerometer Locations for Shaker 3

Content Deleted-
Contains EPRI and Continuum Dynamics Inc. Proprietary Information

Figure E-25
Accelerometer Locations for Shaker 3

Content Deleted-
Contains EPRI and Continuum Dynamics Inc. Proprietary Information

Figure E-26
Accelerometer Locations for Shaker 4

Content Deleted-
Contains EPRI and Continuum Dynamics Inc. Proprietary Information

Figure E-27
Accelerometer Locations for Shaker 5

Content Deleted-
Contains EPRI and Continuum Dynamics Inc. Proprietary Information

Figure E-28
Accelerometer Locations for Shaker 5

Content Deleted-
Contains EPRI and Continuum Dynamics Inc. Proprietary Information

Figure E-29
Accelerometer Locations for Shaker 6

Content Deleted-
Contains EPRI and Continuum Dynamics Inc. Proprietary Information

Figure E-30
Accelerometer Locations for Shaker 7

Content Deleted-
Contains EPRI and Continuum Dynamics Inc. Proprietary Information

Figure E-31
Accelerometer Locations for Shaker 7

Content Deleted-
Contains EPRI and Continuum Dynamics Inc. Proprietary Information

Figure E-32
Accelerometer Locations for Shaker 8

Content Deleted-
Contains EPRI and Continuum Dynamics Inc. Proprietary Information

Figure E-33
Accelerometer Locations for Shaker 8

Content Deleted-
Contains EPRI and Continuum Dynamics Inc. Proprietary Information

Content Deleted-
Contains EPRI and Continuum Dynamics Inc. Proprietary Information

In the following sections, a brief review is given of the frequency selection and accelerometer placement procedures. This review is followed by an explanation of the comparison method and means for estimating bias and uncertainty. Finally, the biases and uncertainties are presented.

E.4.3 ANSYS 10.0 FEA of Spare Hope Creek Unit 2 Dryer

Content Deleted-
Contains EPRI and Continuum Dynamics Inc. Proprietary Information

Content Deleted-
Contains EPRI and Continuum Dynamics Inc. Proprietary Information

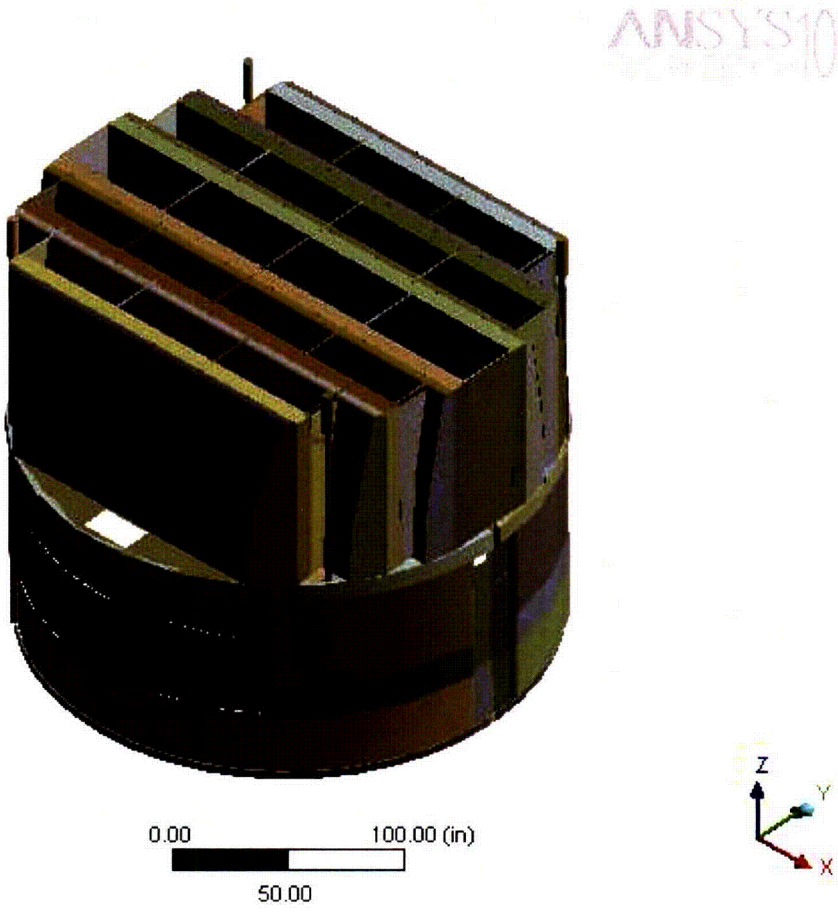

Figure E-34
Hope Creek steam dryer Unit 2 geometry overview

Content Deleted-
Contains EPRI and Continuum Dynamics Inc. Proprietary Information

Figure E-35
Boundary conditions applied to the model

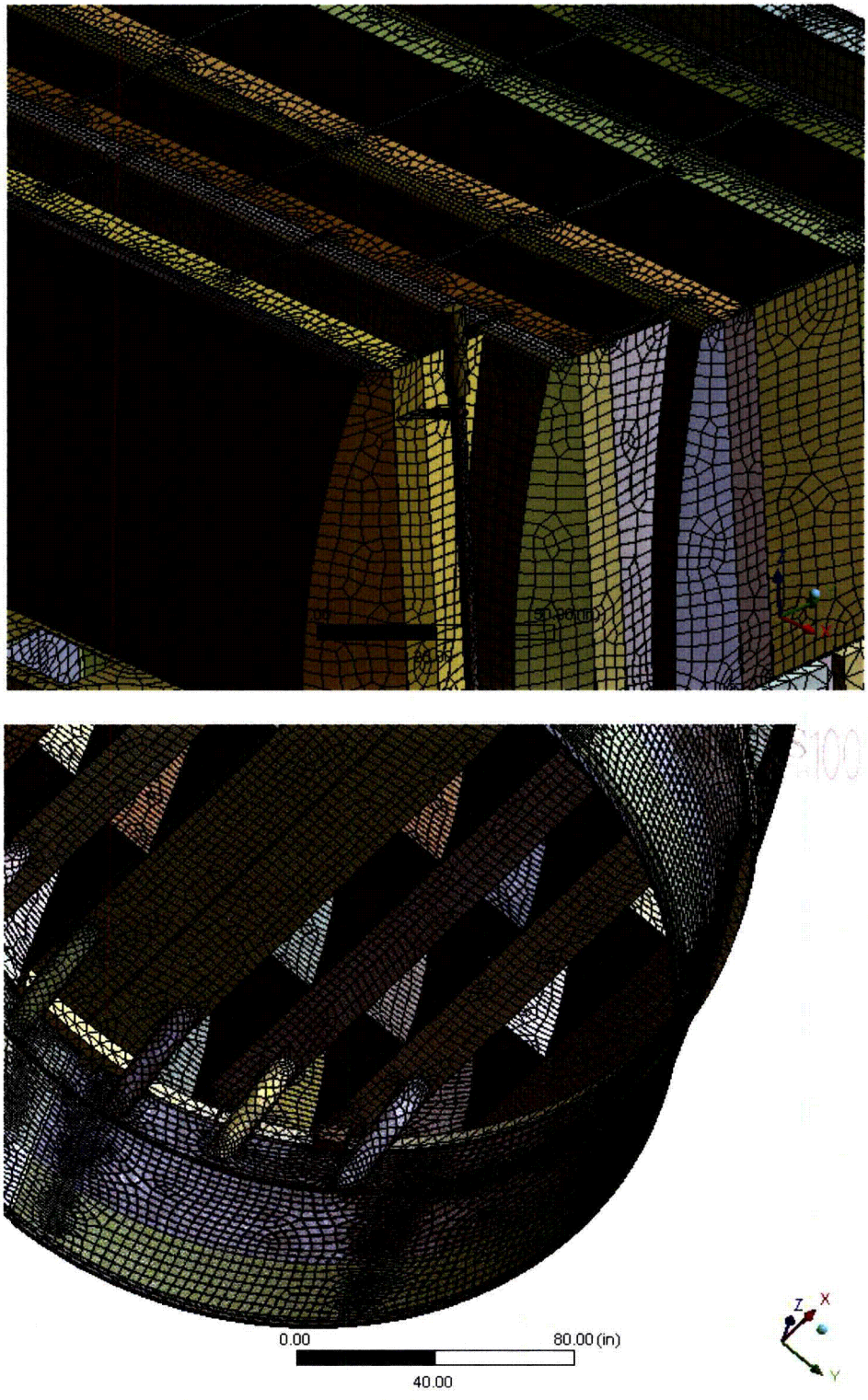

Figure E-36
Mesh overview

E.4.4 Analysis

Content Deleted-
Contains EPRI and Continuum Dynamics Inc. Proprietary Information

Content Deleted-
Contains EPRI and Continuum Dynamics Inc. Proprietary Information

E.4.4.1 Selection of Accelerometer Locations

Content Deleted-
Contains EPRI and Continuum Dynamics Inc. Proprietary Information

Content Deleted-
Contains EPRI and Continuum Dynamics Inc. Proprietary Information

E.4.4.2 Comparison Procedure

For each shaker location and measured peak frequency, a comparison between the computed and measured displacements at the accelerometer locations is performed

Content Deleted-
Contains EPRI and Continuum Dynamics Inc. Proprietary Information

Content Deleted-
Contains EPRI and Continuum Dynamics Inc. Proprietary Information

Content Deleted-
Contains EPRI and Continuum Dynamics Inc. Proprietary Information

Content Deleted-
Contains EPRI and Continuum Dynamics Inc. Proprietary Information

Figure E-37
Surface plot of J_{bu} as a function of frequency and damping for low and high frequency case.

Algorithm 1

Content Deleted-
Contains EPRI and Continuum Dynamics Inc. Proprietary Information

Content Deleted-
Contains EPRI and Continuum Dynamics Inc. Proprietary Information

Algorithm 2

Content Deleted-
Contains EPRI and Continuum Dynamics Inc. Proprietary Information

Content Deleted-
Contains EPRI and Continuum Dynamics Inc. Proprietary Information

E.4.4.3 Comparison between Algorithms 1 and 2

Content Deleted-
Contains EPRI and Continuum Dynamics Inc. Proprietary Information

Content Deleted-
Contains EPRI and Continuum Dynamics Inc. Proprietary Information

Table E-7
Summary of the J_{bu}=(|bias| + uncertainty) obtained using harmonic calculations

Content Deleted-
Contains EPRI and Continuum Dynamics Inc. Proprietary Information

Content Deleted-
Contains EPRI and Continuum Dynamics Inc. Proprietary Information

Figure E-38
Comparisons of predicted and measured accelerations at accelerometer locations for shaker location 4.

Content Deleted-
Contains EPRI and Continuum Dynamics Inc. Proprietary Information

Figure E-39
Comparisons of predicted and measured accelerations at accelerometer locations for shaker location 5.

Content Deleted-
Contains EPRI and Continuum Dynamics Inc. Proprietary Information

Figure E-40
Comparisons of predicted and measured accelerations at accelerometer locations for shaker location 8.

E.4.5 Results

Comparisons between measured and predicted responses were performed for all measured response peaks for all shaker locations. Also, all accelerometers were included in the comparisons.

Content Deleted-
Contains EPRI and Continuum Dynamics Inc. Proprietary Information

Content Deleted-
Contains EPRI and Continuum Dynamics Inc. Proprietary Information

Content Deleted-
Contains EPRI and Continuum Dynamics Inc. Proprietary Information

Figure E-41
Computed J_{bu} = |bias| + uncertainty plotted as a function of forcing frequency.

Content Deleted-
Contains EPRI and Continuum Dynamics Inc. Proprietary Information

Figure E-42
Comparison of predicted and measured responses for the two cases yielding the highest values of J_{bu}.

Table E-8
Statistics of error J_{bu} bias and uncertainty

Content Deleted-
Contains EPRI and Continuum Dynamics Inc. Proprietary Information

Content Deleted-
Contains EPRI and Continuum Dynamics Inc. Proprietary Information

Figure E-43
Computed J_{bu} = |bias| + uncertainty plotted as a function of shaker location.

Content Deleted-
Contains EPRI and Continuum Dynamics Inc. Proprietary Information

Figure E-44
Comparison of measured and predicted accelerations for shaker location 1. Note that for this shaker location, data were only collected at forcing frequencies above 100 Hz because coherence between the forcing and accelerometer responses was low below 100 Hz.

Content Deleted-
Contains EPRI and Continuum Dynamics Inc. Proprietary Information

Figure E-45
Comparison of measured and predicted accelerations for shaker location 2.

Content Deleted-
Contains EPRI and Continuum Dynamics Inc. Proprietary Information

Figure E-46
Comparison of measured and predicted accelerations for shaker location 3.

Content Deleted-
Contains EPRI and Continuum Dynamics Inc. Proprietary Information

Figure E-47
Comparison of measured and predicted accelerations for shaker location 3.

Content Deleted-
Contains EPRI and Continuum Dynamics Inc. Proprietary Information

Figure E-48
Comparison of measured and predicted accelerations for shaker location 5.

Content Deleted-
Contains EPRI and Continuum Dynamics Inc. Proprietary Information

Figure E-49
Comparison of measured and predicted accelerations for shaker location 6.

Content Deleted-
Contains EPRI and Continuum Dynamics Inc. Proprietary Information

Figure E-50
Comparison of measured and predicted accelerations for shaker location 7.

Content Deleted-
Contains EPRI and Continuum Dynamics Inc. Proprietary Information

Figure E-51
Comparison of measured and predicted accelerations for shaker location 8.

Content Deleted-
Contains EPRI and Continuum Dynamics Inc. Proprietary Information

Table E-9
Statistics of the predicted damping ratios ζ

Content Deleted-
Contains EPRI and Continuum Dynamics Inc. Proprietary Information

E.4.6 Results for Fixed and Limited Range Damping Values

Content Deleted-
Contains EPRI and Continuum Dynamics Inc. Proprietary Information

Table E-10
Damping set to 0.051%

Content Deleted-
Contains EPRI and Continuum Dynamics Inc. Proprietary Information

Table E-11
Damping optimized within 0.051% ± 37%

Content Deleted-
Contains EPRI and Continuum Dynamics Inc. Proprietary Information

E.4.7 Conclusions

The combined J_{bu} = (|bias| + uncertainty) associated with the calculation of peak responses using a FEA model, has been computed by comparing peak response predictions against measurements. The measurements consisted of accelerometer readings taken at selected peak frequencies and resulting from shaker-driven force inputs. Eight different shaker locations were considered and for each shaker location up to 20 accelerometers were placed on the dryer. Measurements were taken at approximately 40 different peak frequencies in the 10 – 250 Hz range. Both peak frequencies and accelerometer locations were selected using pre-test FEA. The collected data were compared against predictions by varying the damping in the FEA model and adjusting the forcing frequency ±10% about each measured peak frequency. The resulting error, J_{bu} = (absolute value of bias) + (uncertainty), was recorded for each measured peak frequency and statistics of J_{bu} on a per shaker location basis and for all shaker locations developed.

Content Deleted-
Contains EPRI and Continuum Dynamics Inc. Proprietary Information

Content Deleted-
Contains EPRI and Continuum Dynamics Inc. Proprietary Information

E.5 Test Program to Define Content Deleted-Contains EPRI and Continuum Dynamics Inc. Proprietary Information

A laboratory study was conducted to Content Deleted-Contains EPRI and Continuum Dynamics Inc. Proprietary Information. This portion of Appendix E details this study.

E.5.1 Executive Summary

Content Deleted-
Contains EPRI and Continuum Dynamics Inc. Proprietary Information

E.5.2 Objective

Content Deleted-
Contains EPRI and Continuum Dynamics Inc. Proprietary Information

E.5.3 Theory

Content Deleted-
Contains EPRI and Continuum Dynamics Inc. Proprietary Information

Content Deleted-
Contains EPRI and Continuum Dynamics Inc. Proprietary Information

Figure E-52
Schematic of Content Deleted-Contains EPRI and Continuum Dynamics Inc. Proprietary Information

The force per unit area on the plate as a function of time is to be estimated. The variables that contribute to this force/unit area (p) are tabulated in Table E-12 below along with their units.

Table E-12
Variables and Units

Content Deleted-
Contains EPRI and Continuum Dynamics Inc. Proprietary Information

Content Deleted-
Contains EPRI and Continuum Dynamics Inc. Proprietary Information

Content Deleted-
Contains EPRI and Continuum Dynamics Inc. Proprietary Information

Content Deleted-
Contains EPRI and Continuum Dynamics Inc. Proprietary Information

Content Deleted-
Contains EPRI and Continuum Dynamics Inc. Proprietary Information

Figure E-53
Schematic of apparatus used to determine Content Deleted-Contains EPRI and Continuum Dynamic Inc. Proprietary Information

Content Deleted-
Contains EPRI and Continuum Dynamics Inc. Proprietary Information

E.5.4 Facility Description

Content Deleted-
Contains EPRI and Continuum Dynamics Inc. Proprietary Information

Content Deleted-
Contains EPRI and Continuum Dynamics Inc. Proprietary Information

Figure E-54
Schematic of the test rig

Content Deleted-
Contains EPRI and Continuum Dynamics Inc. Proprietary Information

Figure E-55
Schematic of Content Deleted-Contains EPRI and Continuum Dynamics Inc Proprietary Information

Content Deleted-
Contains EPRI and Continuum Dynamics Inc. Proprietary Information

Figure E-56
Photograph of test setup: Content Deleted-Contains EPRI and Continuum Dynamics Inc. Proprietary Information

Figure E-57
Photographs of Content Deleted-Contains EPRI and Continuum Dynamics Inc. Proprietary Information

E.5.5 Instrumentation

The purpose of the test program was to quantify

Content Deleted-
Contains EPRI and Continuum Dynamics Inc. Proprietary Information

Table E-13 summarizes the instrument specifications.

Table E-13
Content Deleted-Contains EPRI and Contiuum Dynamics Inc. Proprietary Information

Content Deleted-
Contains EPRI and Continuum Dynamics Inc. Proprietary Information

E.5.6 Test Matrix

Content Deleted-
Contains EPRI and Continuum Dynamics Inc. Proprietary Information

Table E-14
Content Deleted-Contains EPRI and Continuum Dynamics Inc. Proprietary Information

Content Deleted-
Contains EPRI and Continuum Dynamics Inc. Proprietary Information

E.5.7 Test Procedure

For each test the instrumentation and test setup were first verified and recorded.

Content Deleted-
Contains EPRI and Continuum Dynamics Inc. Proprietary Information

Content Deleted-
Contains EPRI and Continuum Dynamics Inc. Proprietary Information

E.5.8 Test Results

Content Deleted-
Contains EPRI and Continuum Dynamics Inc. Proprietary Information

Content Deleted-
Contains EPRI and Continuum Dynamics Inc. Proprietary Information

Figure E-58 Content Deleted-Contains EPRI and Continuum Dynamics Inc. Proprietary Information

Content Deleted-
Contains EPRI and Continuum Dynamics Inc. Proprietary Information

Figure E-9 Content Deleted-Contains EPRI and Continuum Dynamics Inc. Proprietary Information

Content Deleted-
Contains EPRI and Continuum Dynamics Inc. Proprietary Information

Content Deleted-
Contains EPRI and Continuum Dynamics Inc. Proprietary Information

Figure E-59
Curve fit through data for Content Deleted-Contains EPRI and Continuum Dynamics Inc. Proprietary Information

Content Deleted-
Contains EPRI and Continuum Dynamics Inc. Proprietary Information

Figure E-60
Curve fits through data for Content Deleted-Contains EPRI and Continuum Dynamics Inc. Proprietary Information

Content Deleted-
Contains EPRI and Continuum Dynamics Inc. Proprietary Information

Figure E-61
Curve fits through data for Content Deleted-Contains EPRI and Continuum Dynamics Inc. Proprietary Information

Content Deleted-
Contains EPRI and Continuum Dynamics Inc. Proprietary Information

Figure E-62
Curve fits through data for Content Deleted-Contains EPRI and Continuum Dynamics Inc. Proprietary Information

Content Deleted-
Contains EPRI and Continuum Dynamics Inc. Proprietary Information

Figure E-63
Curve fits through data for Content Deleted-Contains EPRI and Continuum Dynamics Inc. Proprietary Information

E.5.9 Data Analysis

The collected data were then analyzed as follows.

E.5.9.1 Overview

The test results provide estimates of

Content Deleted-
Contains EPRI and Continuum Dynamics Inc. Proprietary Information

E.5.9.2 Theoretical damping coefficient calculation

Content Deleted-
Contains EPRI and Continuum Dynamics Inc. Proprietary Information

E.5.9.3 Experimental Content Deleted-Contains EPRI and Continuum Dynamics Inc. Proprietary Information

Content Deleted-
Contains EPRI and Continuum Dynamics Inc. Proprietary Information

Content Deleted-
Contains EPRI and Continuum Dynamics Inc. Proprietary Information

E.5.9.4 Analysis for Content Deleted-Contains EPRI and Continuum Dynamics Inc. Proprietary Information

Content Deleted-
Contains EPRI and Continuum Dynamics Inc. Proprietary Information

Table E-15 Content Deleted-Contains EPRI and Continuum Dynamics Inc. Proprietary Information

Table E-16
Summary of Content Deleted-Contains EPRI and Continuum Dynamics Inc. Proprietary Information

Content Deleted-
Contains EPRI and Continuum Dynamics Inc. Proprietary Information

Content Deleted-
Contains EPRI and Continuum Dynamics Inc. Proprietary Information

Content Deleted-
Contains EPRI and Continuum Dynamics Inc. Proprietary Information

Figure E-64
Experimental Content Deleted-Contains EPRI and Continuum Dynamics Inc. Proprietary Information

E.5.9.5 Content Deleted-Contains EPRI and Continuum Dynamics Inc. Proprietary Information

Content Deleted-
Contains EPRI and Continuum Dynamics Inc. Proprietary Information

Table E-17 Content Deleted-Contains EPRI and Continuum Dynamics Inc. Proprietary Information

Content Deleted-
Contains EPRI and Continuum Dynamics Inc. Proprietary Information

Table E-18
Summary of Content Deleted-Contains EPRI and Continuum Dynamics Inc. Proprietary Information

Content Deleted-
Contains EPRI and Continuum Dynamics Inc. Proprietary Information

Figure E-65
Experimental Content Deleted-Contains EPRI and Continuum Dynamics Inc. Proprietary Information

Content Deleted-
Contains EPRI and Continuum Dynamics Inc. Proprietary Information

Content Deleted-
Contains EPRI and Continuum Dynamics Inc. Proprietary Information

Figure E-66
Comparison of Content Deleted-Contains EPRI and Continuum Dynamics Inc. Proprietary Information

E.5.9.6 Implementation of Content Deleted-Contains EPRI and Continuum Dynamics Inc. Proprietary Information

Content Deleted-
Contains EPRI and Continuum Dynamics Inc. Proprietary Information

Content Deleted-
Contains EPRI and Continuum Dynamics Inc. Proprietary Information

Content Deleted-
Contains EPRI and Continuum Dynamics Inc. Proprietary Information

E.5.9.7 Content Deleted-Contains EPRI and Continuum Dynamics Inc. Proprietary Information

Content Deleted-
Contains EPRI and Continuum Dynamics Inc. Proprietary Information

Table E-19
Characteristics of Content Deleted-Contains EPRI and Continuum Dynamics Inc. Proprietary Information

Content Deleted-
Contains EPRI and Continuum Dynamics Inc. Proprietary Information

E.5.9.8 Conclusions

A test program has been conducted

Content Deleted-
Contains EPRI and Continuum Dynamics Inc. Proprietary Information

Content Deleted-
Contains EPRI and Continuum Dynamics Inc. Proprietary Information

E.6 Stress Prediction Error Due to Finite Element Discretization

Mesh refinement tests were conducted on a structure excised from the

Content Deleted-
Contains EPRI and Continuum Dynamics Inc. Proprietary Information

Content Deleted-
Contains EPRI and Continuum Dynamics Inc. Proprietary Information

Figure E-67
Substructure of a steam dryer used for mesh convergence tests. Blue lines indicate cantilevered support, red lines denote free edges, and black lines show connections between parts.

The elements used in the analysis are of the same type as those used in the steam dryer calculations, namely SHELL63 in ANSYS notation. This quadrilateral shell element utilizes Discrete Kirchoff Triangles (DKT) technology, providing cubic interpolation order in the

displacement component normal to the shell surface along the edges, and, therefore, quadratic stress variation. Note that contour plots produced by ANSYS are linear over the elements and, thus, are only approximately representative of the stress and displacement variation supported by this element.

The structure in Figure E-67 was subjected to loadings characteristic of those present in the actual analysis of the steam dryer. Specifically, the structure was loaded by its own weight for the static component and subjected to the same harmonic pressure distributions applied to the full dryer. Displacements and stresses were computed in the same way as in the full steam dryer stress evaluation.

To investigate the mesh dependence of stresses and displacements, three different grids were considered.

Content Deleted-
Contains EPRI and Continuum Dynamics Inc. Proprietary Information

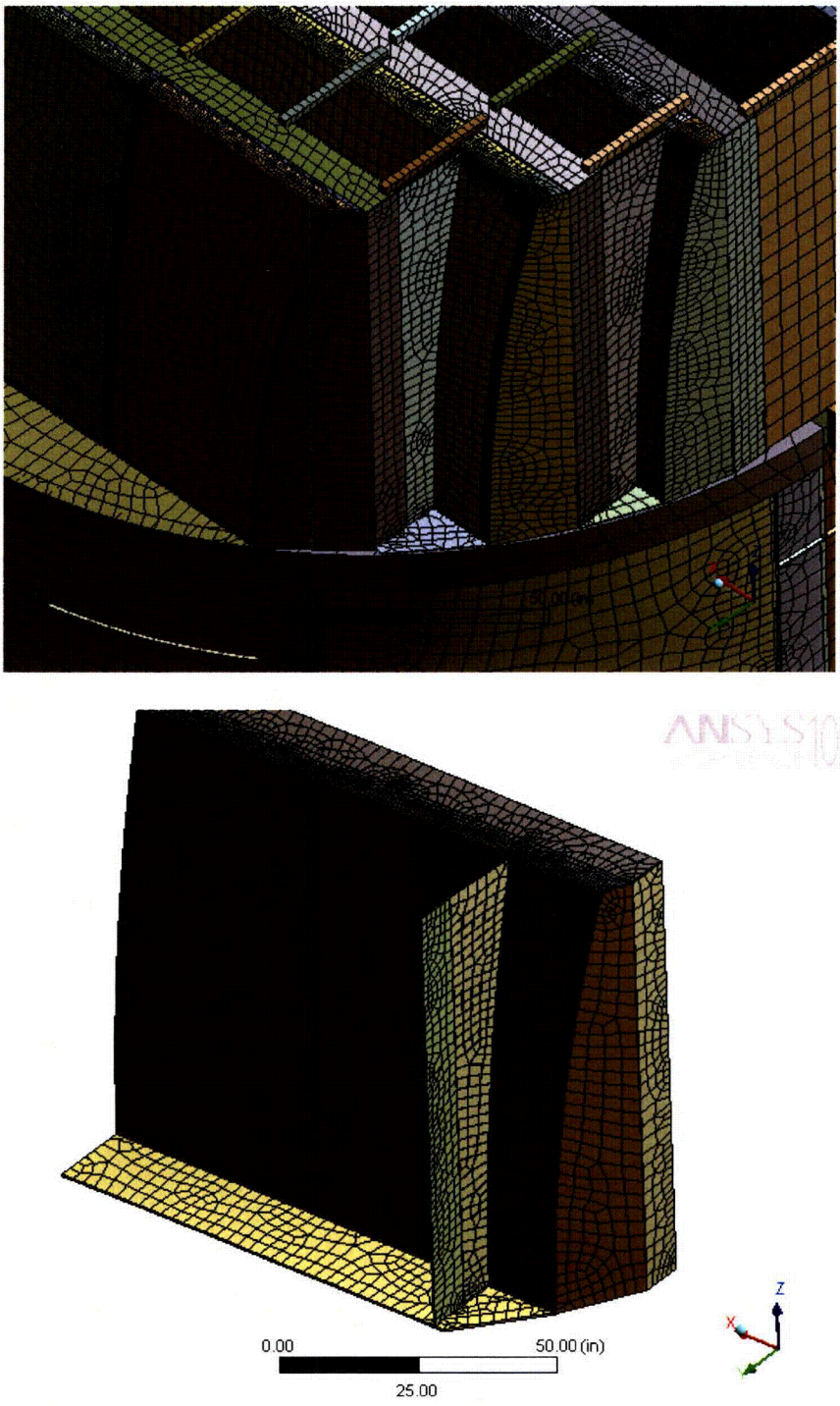

Figure E-68
Mesh used in full steam dryer analysis (top) and the coarsest mesh, Mesh x1, used in the convergence tests (bottom).

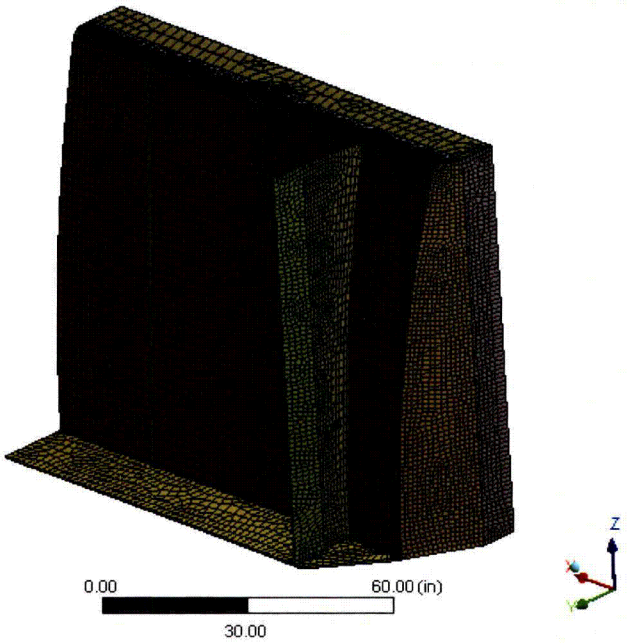

Figure E-69
Refined mesh, Mesh x2, used in the convergence tests.

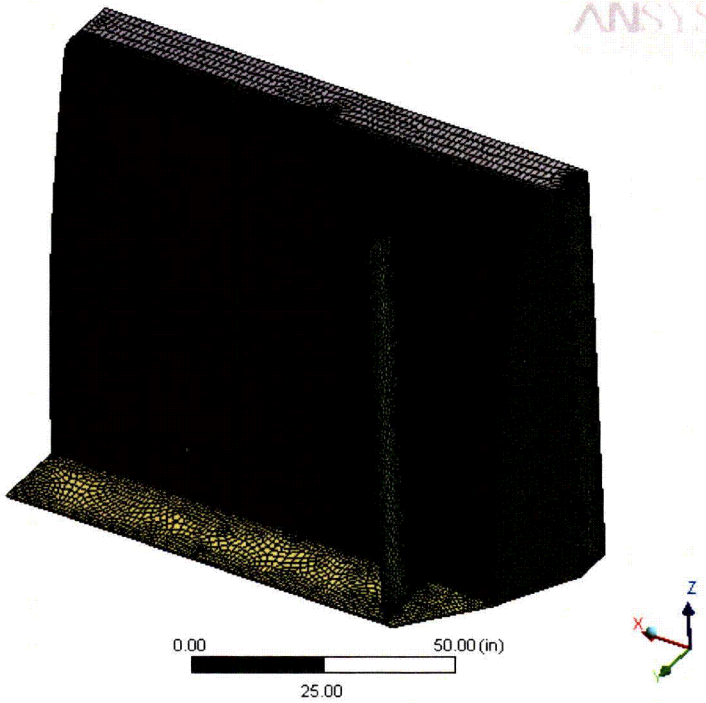

Figure E-70
Further refined mesh, Mesh x4, used in the convergence tests.

E.6.1 Convergence in Static Analysis

The deformations due to gravity were calculated on the three meshes described above. In addition, deflections and stresses were also calculated on grids refined locally using the adaptive meshing capability provided by the ANSYS Simulation module. This adaptive refinement is performed automatically by ANSYS in locations where higher discretization error is detected. This additional refinement was performed on each mesh except Mesh x4, where further adaptive refinement was not needed because the element size was already very small.

The typical convergence behavior for the maximum stress intensity during adaptive mesh refinement is shown in Figure E-71, where the horizontal scale ("Iteration Number") is the number of adaptive mesh refinement steps. The results of adaptive refinement for all three initial grids are summarized in Table E-20. The calculated stresses did not change appreciably during adaptive local mesh refinement. Overall, the range of computed stress intensity values is within

Content Deleted-
Contains EPRI and Continuum Dynamics Inc. Proprietary Information

Content Deleted-
Contains EPRI and Continuum Dynamics Inc. Proprietary Information

Figure E-71
Evolution of stress intensity with adaptive convergence on Mesh x1.

Table E-20
Static solution: structure under its own weight

Content Deleted-
Contains EPRI and Continuum Dynamics Inc. Proprietary Information

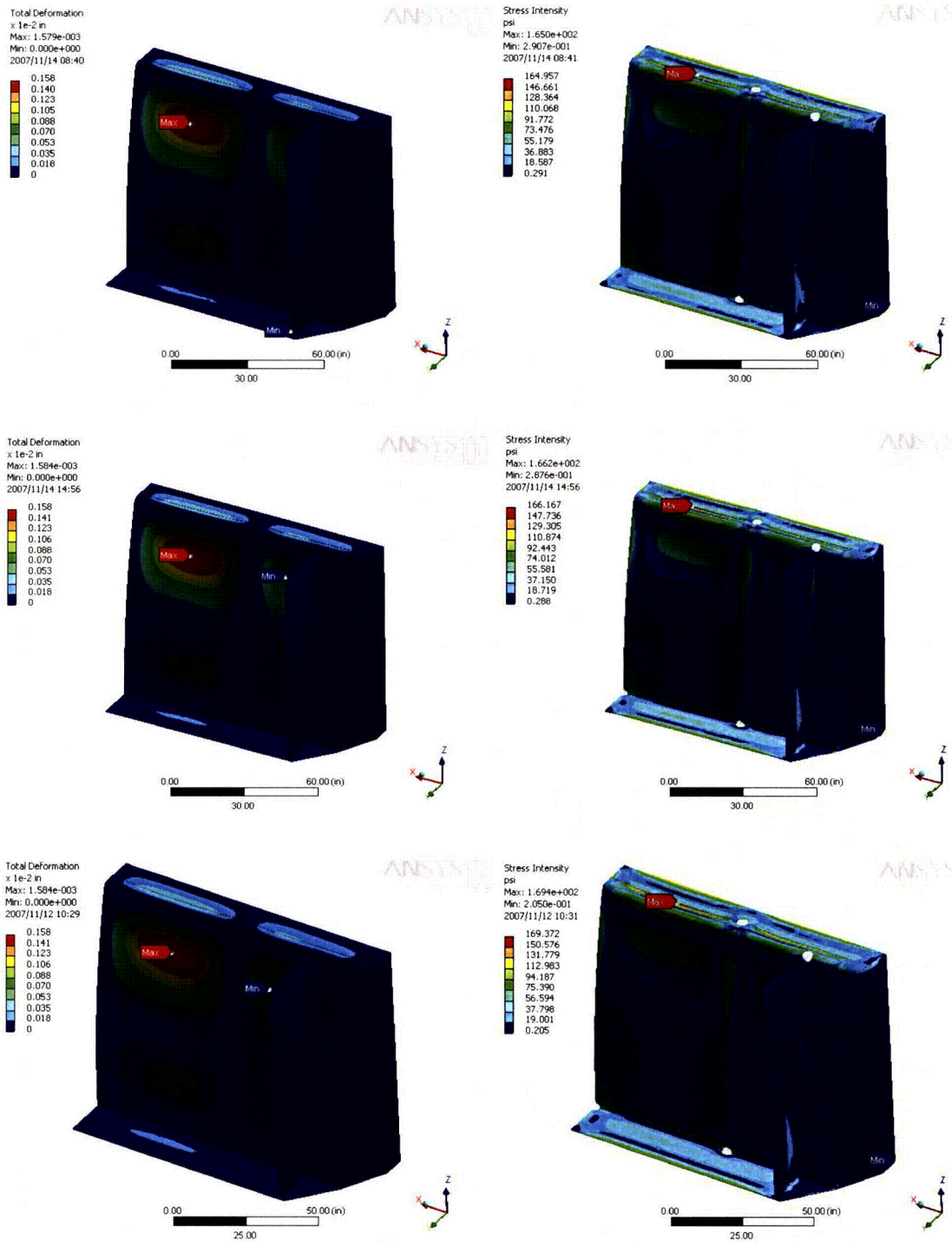

Figure E-72
Comparison of static deflections (left side) and stress intensities (right side) for the grids Mesh x1 (top row), Mesh x2 (middle row), and Mesh x4 (bottom row).

E.6.2 Note on "Hot-Spots"

In the stress convergence results several locations are excluded from the maximum stress evaluation. These locations were identified during adaptive mesh refinement as having non-convergent stress. The typical stress intensity behavior during mesh refinement at these "hot spots" is shown in Figure E-73. A typical stress singularity is shown in Figure E-74 at the re-entrant corner, created by connection of the top of the closure plate to the hood. Note that several plate thicknesses from the junction, the calculated stresses are low and consistent with overall stress distribution. Such "hot spots" can occur at structural discontinuities, such as re-entrant corners, where the stress becomes infinite as the mesh is refined. For example, a re-entrant corner in a continuum element will generally develop infinite stresses. Likewise, the membrane (in-plane) stresses in a shell or plate will become infinite at re-entrant cutouts or cantilever roots when in-plane loads are applied (bending stresses in shells generally converge).

Content Deleted-
Contains EPRI and Continuum Dynamics Inc. Proprietary Information

Figure E-73
Evolution of stress intensity with adaptive convergence at the "hot spot" on Mesh x1.

Content Deleted-
Contains EPRI and Continuum Dynamics Inc. Proprietary Information

Figure E-74
Stress singularity at hood / closure plate junction.

Content Deleted-
Contains EPRI and Continuum Dynamics Inc. Proprietary Information

Content Deleted-
Contains EPRI and Continuum Dynamics Inc. Proprietary Information

In our approach a conservative and computationally practical approximation described in the ASME code is adopted, where the stresses at welded junctions are estimated using weld factors. These factors account for stress concentration as well as weld variability and are determined from collated experience in the design and operation of welded structures.

Content Deleted-
Contains EPRI and Continuum Dynamics Inc. Proprietary Information

E.6.3 Convergence in Harmonic Analysis

The full steam dryer stress analysis proceeds by calculating the harmonic structural response at a number of frequencies. The combination of these harmonics and comparison of these assembled solutions with transient simulations is addressed in [E.16]. Here the accuracy of the harmonic stress solutions is estimated.

Content Deleted-
Contains EPRI and Continuum Dynamics Inc. Proprietary Information

Content Deleted-
Contains EPRI and Continuum Dynamics Inc. Proprietary Information

Figure E-75
Pressure distribution, real part, at 53.863 Hz (top), 101.4 Hz (middle), and 199.61 Hz (bottom).

Content Deleted-
Contains EPRI and Continuum Dynamics Inc. Proprietary Information

Figure E-76
Comparison of the real (left side) and imaginary (right side) components of the stress intensity distribution at 53.863 Hz on Mesh x1 (top), Mesh x2 (middle), and Mesh x4 (bottom).

Content Deleted-
Contains EPRI and Continuum Dynamics Inc. Proprietary Information

Figure E-77
Comparison of the real (left side) and imaginary (right side) components of the stress intensity distribution at 101.4 Hz on Mesh x1 (top), Mesh x2 (middle), and Mesh x4 (bottom).

Content Deleted-
Contains EPRI and Continuum Dynamics Inc. Proprietary Information

Figure E-78
Comparison of the real (left side) and imaginary (right side) components of the stress intensity distribution at 199.61 Hz on Mesh x1 (top), Mesh x2 (middle), and Mesh x4 (bottom).

In

Content Deleted-
Contains EPRI and Continuum Dynamics Inc. Proprietary Information

Table E-21 and Table E-22, quantitative comparisons of the maximum displacement and stress intensity amplitudes on the three meshes are given. Location 1 corresponds to where the real part of the corresponding solution is a maximum; Location 2 corresponds to maximum imaginary part. These tables show that the displacements and stresses are computed to within

Content Deleted-
Contains EPRI and Continuum Dynamics Inc. Proprietary Information

Table E-21
Total displacement amplitudes of the harmonic solution on different resolution meshes

Content Deleted-
Contains EPRI and Continuum Dynamics Inc. Proprietary Information

Table E-22
Total stress intensity amplitudes of the harmonic solution on different resolution meshes

Content Deleted-
Contains EPRI and Continuum Dynamics Inc. Proprietary Information

Content Deleted-
Contains EPRI and Continuum Dynamics Inc. Proprietary Information

Content Deleted-
Contains EPRI and Continuum Dynamics Inc. Proprietary Information

Figure E-79
Stress intensity amplitude vs. frequency for Location 2 in the 100 – 102 Hz frequency range.

Content Deleted-
Contains EPRI and Continuum Dynamics Inc. Proprietary Information

Figure E-80
Extrapolation of the peak stress intensity amplitudes as a function of mesh size. The peak stress amplitudes occur at 100.75 Hz in Figure E-79. The mesh size is normalized by the mesh spacing on Mesh x1.

E.7 References

E.1. Flugge, W. (ed.). 1962. Handbook of Engineering Mechanics. McGraw-Hill, p. 61-62.

E.2. Blevins, R. 1979. Formulas for Natural Frequency and Mode Shape. Van Nostrand-Reinhold Co., p. 261.

E.3. Continuum Dynamics, Inc. 2007. Stress Assessment of Hope Creek Unit 1 Steam Dryer Based on Revision 4 Loads Model. C.D.I. Report No. 07-17 (Rev. 4).

E.4. Continuum Dynamics, Inc. 2007. Stress Analysis of the Hope Creek Unit 1 Steam Dryer at EPU Conditions using One-Eighth Scale Model Pressure Measurement Data. C.D.I. Report No. 06-27 (Rev. 2).

E.5. ASME. 2004, ASME Boiler and Pressure Vessel Code, Section III, Article A-8000, Stresses in Perforated Flat Plates.

E.6. O'Donnell, W. J. 1973. Effective Elastic Constants for the Bending of Thin Perforated Plates with Triangular and Square Penetration Patterns. *ASME Journal of Engineering for Industry* 95: 121-128.

E.7. Continuum Dynamics, Inc. 2007. Finite Element Modeling Bias and Uncertainty Estimates Derived from the Hope Creek Unit 2 Dryer Shaker Test. C.D.I. Report No. 07-27P.

E.8. STI Technologies, Inc. 2007. Hope Creek Steam Dryer Vibration Test. Technical Report No. PA2168 (Rev. 1).

E.9. U. S. Nuclear Regulatory Commission, Regulatory Guide 1.20, Rev. 3. March 2007. Comprehensive Vibration Assessment Program for Reactor Internals During Preoperational and Initial Startup Testing.

E.10. U. S. Nuclear Regulatory Commission, 1973 Regulatory Guide 1.61. October 1973. Damping Values for Seismic Design of Nuclear Power Plants.

E.11. Idel'chik, I., E. and E. Fried. 1989. Flow Resistance, A Design Guide for Engineers. Taylor and Francis: Washington, D.C. p. 260.

E.12. DeSanto, D. F. 1981. Added Mass and Hydrodynamic Damping of Perforated Plates Vibrating in Water. *ASME Journal of Pressure Vessel Technology* 103: 176-182.

E.13. Shapiro, A. 1953 The Dynamics and Thermodynamics of Compressible Fluid Flow. The Ronald Press Company: New York. Vol. 1, p. 85.

E.14. Kayser, C. J. and R. L. Shambaugh. 1991. Discharge Coefficients for Compressible Flow Through Small-Diameter Orifices and Convergent Nozzles. *Chemical Engineering Science* 46:1697-1711.

E.15. Williams, M. L. 1952. Stress Singularities Resulting from Various Boundary Conditions in Angular Corners of Plates in extension. *Journal of Applied Mechanics* 74: 526–528.

E.16. NRC Request for Additional Information on the Hope Creek Generating Station, Extended Power Uprate. 2007. RAI No. 14.110.

F

APPLICATION OF METHODOLOGY TO PREDICT STEAM DRYER FLUCTUATING PRESSURE LOADING FROM IN-PLANT STEAM DRYER PRESSURE MEASUREMENTS

An instrumented dryer, such as the replacement QC2 dryer, offers an alternative way of predicting the pressure loading on the dryer when pressure transducer data are collected at measured power levels. The solution approach includes the use of the **Content Deleted-Contains EPRI and Continuum Dynamics Inc. Proprietary Information** results (discussed in Section 6.3) and a least squares analysis involving applicable data. This appendix summarizes the approach and presents comparisons with the QC2 OLTP data set.

F.1 Approach

Content Deleted-
Contains EPRI and Continuum Dynamics Inc. Proprietary Information

Content Deleted-
Contains EPRI and Continuum Dynamics Inc. Proprietary Information

F.2 Solution

The pressure sensor locations were shown in Figure 6-13 to Figure 6-15. The best representation of the solution uses all of the data at the 27 sensor locations, by minimizing the error

Content Deleted-
Contains EPRI and Continuum Dynamics Inc. Proprietary Information

Content Deleted-
Contains EPRI and Continuum Dynamics Inc. Proprietary Information

Figure F-1
Least squares predictions at 790 MWe at the dryer pressure sensors: peak minimum (top) and peak maximum (bottom) pressure levels, with data (blue) and predictions (red).

Content Deleted-
Contains EPRI and Continuum Dynamics Inc. Proprietary Information

Figure F-2
PSD comparison at 790 MWe for pressure sensor data (blue curves) and least squares prediction (red curves), for P1 (top) and P2 (bottom).

Content Deleted-
Contains EPRI and Continuum Dynamics Inc. Proprietary Information

Figure F-3
PSD comparison at 790 MWe for pressure sensor data (blue curves) and least squares prediction (red curves), for P3 (top) and P4 (bottom).

Content Deleted-
Contains EPRI and Continuum Dynamics Inc. Proprietary Information

Figure F-4
PSD comparison at 790 MWe for pressure sensor data (blue curves) and least squares prediction (red curves), for P5 (top) and P6 (bottom).

Content Deleted-
Contains EPRI and Continuum Dynamics Inc. Proprietary Information

Figure F-5
PSD comparison at 790 MWe for pressure sensor data (blue curves) and least squares prediction (red curves), for P7 (top) and P8 (bottom).

Content Deleted-
Contains EPRI and Continuum Dynamics Inc. Proprietary Information

Figure F-6
PSD comparison at 790 MWe for pressure sensor data (blue curves) and least squares prediction (red curves), for P9 (top) and P10 (bottom).

Content Deleted-
Contains EPRI and Continuum Dynamics Inc. Proprietary Information

Figure F-7
PSD comparison at 790 MWe for pressure sensor data (blue curves) and least squares prediction (red curves), for P11 (top) and P12 (bottom).

Content Deleted-
Contains EPRI and Continuum Dynamics Inc. Proprietary Information

Figure F-8
PSD comparison at 790 MWe for pressure sensor data (blue curves) and least squares prediction (red curves), for P13 (top) and P14 (bottom).

Content Deleted-
Contains EPRI and Continuum Dynamics Inc. Proprietary Information

Figure F-9
PSD comparison at 790 MWe for pressure sensor data (blue curves) and least squares prediction (red curves), for P15 (top) and P16 (bottom).

Content Deleted-
Contains EPRI and Continuum Dynamics Inc. Proprietary Information

Figure F-10
PSD comparison at 790 MWe for pressure sensor data (blue curves) and least squares prediction (red curves), for P17 (top) and P18 (bottom).

Content Deleted-
Contains EPRI and Continuum Dynamics Inc. Proprietary Information

Figure F-11
PSD comparison at 790 MWe for pressure sensor data (blue curves) and least squares prediction (red curves), for P19 (top) and P20 (bottom).

Content Deleted-
Contains EPRI and Continuum Dynamics Inc. Proprietary Information

Figure F-12
PSD comparison at 790 MWe for pressure sensor data (blue curves) and least squares prediction (red curves), for P21 (top) and P22 (bottom).

Content Deleted-
Contains EPRI and Continuum Dynamics Inc. Proprietary Information

Figure F-13
PSD comparison at 790 MWe for pressure sensor data (blue curves) and least squares prediction (red curves), for P23 (top) and P24 (bottom).

Content Deleted-
Contains EPRI and Continuum Dynamics Inc. Proprietary Information

Figure F-14
PSD comparison at 790 MWe for pressure sensor data (blue curves) and least squares prediction (red curves), for P25 (top) and P26 (bottom).

Content Deleted-
Contains EPRI and Continuum Dynamics Inc. Proprietary Information

Figure F-15
PSD comparison at 790 MWe for pressure sensor data (blue curves) and least squares prediction (red curves), for P27.

Content Deleted-
Contains EPRI and Continuum Dynamics Inc. Proprietary Information

Figure F-16
Least squares pressure comparisons (790 MWe) at the six averaged pressure sensors: P1, P2, and P3 (top); P4, P5, and P6 (bottom): data (blue curves), predictions (red curves).

Content Deleted-
Contains EPRI and Continuum Dynamics Inc. Proprietary Information

Figure F-17
Least squares pressure comparisons (790 MWe) at the six averaged pressure sensors: P7, P8, and P9 (top); P10, P11, and P12 (bottom): data (blue curves), predictions (red curves).

Content Deleted-
Contains EPRI and Continuum Dynamics Inc. Proprietary Information

Figure F-18
Least squares pressure comparisons (790 MWe) at the six averaged pressure sensors: P19 and P21 (top); P18 and P20 (bottom): data (blue curves), predictions (red curves).

Table F-1
QC2 bias and uncertainty values for specified frequency intervals

Content Deleted-
Contains EPRI and Continuum Dynamics Inc. Proprietary Information

Content Deleted-
Contains EPRI and Continuum Dynamics Inc. Proprietary Information

Figure F-19
Comparison between measured and least-squares predicted peak pressures at the 27 pressure sensors in QC2 at 790 MWe. The line is the one-to-one boundary.

Content Deleted-
Contains EPRI and Continuum Dynamics Inc. Proprietary Information

Figure F-20
Comparison between measured and least-squares predicted peak pressures at the 27 pressure sensors in QC2 at 790 MWe with overall uncertainty added to the predicted load. The line is the one-to-one boundary.

The Electric Power Research Institute (EPRI), with major locations in Palo Alto, California; Charlotte, North Carolina; and Knoxville, Tennessee, was established in 1973 as an independent, nonprofit center for public interest energy and environmental research. EPRI brings together members, participants, the Institute's scientists and engineers, and other leading experts to work collaboratively on solutions to the challenges of electric power. These solutions span nearly every area of electricity generation, delivery, and use, including health, safety, and environment. EPRI's members represent over 90% of the electricity generated in the United States. International participation represents nearly 15% of EPRI's total research, development, and demonstration program.

Together...Shaping the Future of Electricity

Programs:

Nuclear Power

BWR Vessel and Internals Project

Printed on recycled paper in the United States of America

1016578NP

Electric Power Research Institute
3420 Hillview Avenue, Palo Alto, California 94304-1338 • PO Box 10412, Palo Alto, California 94303-0813 USA
800.313.3774 • 650.855.2121 • askepri@epri.com • www.epri.com